ERDC/GSL TR-09-17

US Army Corps
of Engineers®
Engineer Research and
Development Center

# Laboratory Characterization of Redstone Technical Test Center Brick

Steven S. Graham, Erin M. Williams, and Paul A. Reed

June 2009

Geotechnical and Structures Laboratory

ERDC/GSL TR-09-17
June 2009





# Laboratory Characterization of Redstone Technical Test Center Brick

Steven S. Graham, Erin M. Williams, and Paul A. Reed

*Geotechnical and Structures Laboratory*
*U.S. Army Engineer Research and Development Center*
*3909 Halls Ferry Road*
*Vicksburg, MS 39180-6199*

Final report





Prepared for Headquarters, U.S. Army Corps of Engineers
Washington, DC 20314-1000

Under Hardened Combined Effects Penetrator Warheads Work Package
Penetration Experiments into Urban Materials Work Unit

**Abstract:** Personnel of the Geotechnical and Structures Laboratory, U.S. Army Engineer Research and Development Center, conducted a laboratory investigation to characterize the strength and constitutive property behavior of Redstone Technical Test Center (RTTC) brick. A total of 23 mechanical property tests were successfully completed: two hydrostatic compression tests, three unconfined compression (UC) tests, ten triaxial compression (TXC) tests, three uniaxial strain tests, two uniaxial-strain-load/constant-volumetric-strain-load (UX/CV) tests, and three direct-pull (DP) tests. In addition to the mechanical property tests, nondestructive, pulse-velocity measurements were obtained from each specimen. The TXC tests exhibited a continuous increase in maximum principal stress difference with increasing confining stress. A compression failure surface was developed from the TXC test results at six levels of confining pressure and from the results of the UC tests. The results for the DP tests were used to determine the unconfined tensile strength of RTTC brick. The RTTC brick specimens displayed tensile strengths of less than 10 percent of the unconfined compressive strength. Due to the relatively low initial dry densities of the UX/CV test specimens, the stress path data plot just below the failure surface developed from the TXC tests.

# Contents

# Figures and Tables

## Figures

## Tables

# Preface

This laboratory mechanical property investigation of Redstone Technical Test Center brick was conducted by personnel of the U.S. Army Engineer Research and Development Center (ERDC). The study was conducted with funds provided by the Directorate of Military Programs, Headquarters, U.S. Army Corps of Engineers, under the Research, Development, Test, and Evaluation Program. The investigation reported herein was accomplished under the Hardened Combined Effects Penetrator Warheads Work Package. This study was conducted between April and June 2008 by staff members of the Impact and Explosion Effects Branch (IEEB), Engineering Systems and Materials Division (ESMD), Geotechnical and Structures Laboratory (GSL), ERDC, under the general direction of Henry S. McDevitt, Jr., Chief, IEEB; Dr. Larry N. Lynch, Chief, ESMD; Dr. William P. Grogan, Deputy Director, GSL; and Dr. David W. Pittman, Director, GSL.

The Principal Investigator for this project was Rayment E. Moxley, IEEB. Steven S. Graham and Erin M. Williams, both of IEEB, served as co-investigators for this project. Graham processed the material property data and prepared this report. Laboratory characterization tests were performed by Paul A. Reed, IEEB, under the technical direction of Williams. Instrumentation support was provided by Johnny L. Morrow, Engineering and Informatic Systems Division, ERDC Information Technology Laboratory.

COL Gary E. Johnston was Commander and Executive Director of ERDC. Dr. James R. Houston was Director.

# 1 Introduction

## Background

Personnel of the Geotechnical and Structures Laboratory, U.S. Army Engineer Research and Development Center, conducted a laboratory investigation to characterize the strength and constitutive property behavior of Redstone Technical Test Center (RTTC) brick under the U.S. Army Corps of Engineers' Hardened Combined Effects Penetrator Warheads Work Package, Penetration Experiments into Urban Materials Work Unit. A total of 24 mechanical property tests were conducted, of which 23 were successfully completed. The 23 tests consisted of two hydrostatic compression tests, three unconfined compression tests, ten triaxial compression tests, three uniaxial strain tests, two uniaxial-strain-load/constant-volumetric-strain-load tests, and three direct-pull extension tests. In addition to the mechanical property tests, nondestructive, pulse-velocity measurements were obtained from each specimen.

## Purpose and scope

The purpose of this report is to document the results from the mechanical property tests conducted on the RTTC brick specimens along with the results of nondestructive, pulse-velocity measurements from each specimen. The physical and composition properties, test procedures, and test results are documented in Chapter 2. Comparative plots and analyses of the experimental results are presented in Chapter 3. A summary is provided in Chapter 4.

# 2 Laboratory Tests

## Material description

The test specimens used in this investigation were prepared from samples cored from solid, severe-weather-grade brick pavers provided by RTTC. The brick used for the material property tests was also used to build triple-brick walls at RTTC for penetration experiments. The material properties determined from the characterization of the material will be used to develop mathematical models of the brick's responses for use in numerical simulations of penetration tests.

## Composition property tests

Prior to performing the mechanical property tests, the height, diameter, and weight of each test specimen were obtained. These measurements were used to compute the specimen's wet, bulk, or "as-tested" density. Results from these determinations are provided in Table 1. Measurements of posttest water content[1] were conducted in accordance with procedures given in American Society for Testing and Materials (ASTM) D 2216 (ASTM 2005d). Based on the appropriate values of posttest water content, wet density, and an assumed grain density of 2.68 Mg/m$^3$, values of dry density, porosity, degree of saturation, and volumes of air, water, and solids were calculated (Table 1). Also listed in Table 1 are maximum, minimum, and mean values, as well as the standard deviation about the mean for each quantity. The RTTC brick specimens had a mean wet density of 2.175 Mg/m$^3$, a mean water content of 0.03 percent, and a mean dry density of 2.171 Mg/m$^3$.

## Ultrasonic pulse-velocity determinations

Prior to performing the mechanical property tests, ultrasonic pulse-velocity measurements were obtained from each test specimen. This involved measuring the transit distance and time for each P-wave (compressional) or S-wave (shear) pulse to propagate through a given specimen. The velocity was then computed by dividing the transit distance by the transit time. A matching pair of 1-MHz piezoelectric transducers

[1] Water content is defined as the weight of water removed during drying in a standard oven divided by the weight of dry solids.

were used to transmit and receive the ultrasonic P-waves, while a pair of 2.25-MHz piezoelectric transducers were used to transmit and receive the ultrasonic S-waves. The transit time was measured with a 100-MHz digital oscilloscope, and the transit distance with a digital micrometer. All of the velocity determinations were made under atmospheric conditions, i.e., no pre-stress of any type was applied to the specimen. The tests were conducted in accordance with procedures given in ASTM C 597 (ASTM 2005c).

One compressional-wave and one shear-wave velocity were determined axially through each specimen. Six radial P-wave velocities were determined; two measurements were taken transverse to each other at elevations of 1/4, 1/2, and 3/4 of the specimen height. Two radial S-wave velocities were measured; these determinations were made at approximately 1/4 and 3/4 of the specimen height. The various P- and S-wave velocities determined for the test specimens are provided in Table 1. The radial-wave velocities listed in Table 1 are the average values.

## Mechanical property tests

Twenty-three mechanical property tests were successfully performed on the RTTC brick specimens to characterize the strength and constitutive properties of the material. All of the mechanical property tests were conducted quasi-statically with axial strain rates on the order of $10^{-4}$ to $10^{-5}$ per second and times to peak load on the order of 5 to 30 min. Mechanical property data were obtained under several stress and strain paths. Undrained compressibility data were obtained from two hydrostatic compression (HC) tests and the hydrostatic loading phases of the triaxial compression (TXC) tests. Shear and failure data were obtained from unconfined compression (UC) tests, unconsolidated, undrained TXC tests, and direct-pull (DP) tests. One-dimensional compressibility data were obtained from undrained, uniaxial strain (UX), or $K_0$, tests with lateral stress measurements. One type of undrained, strain path test was conducted during the test program. The strain path tests were initially loaded under uniaxial strain boundary conditions to a prescribed level of stress or strain. At the end of the UX loading, a constant axial-to-radial-strain ratio (ARSR) of -2.0 was applied. The ARSR = -2.0 path is a constant-volumetric-strain loading path, and these tests are referred to as UX/CV. The terms undrained and unconsolidated signify that no pore fluid (liquid or gas) was allowed to escape or drain from the membrane-enclosed specimens. The completed test matrix is presented in Table 2. Table 2 lists the

test types, number of tests, test numbers for each test type, and the nominal, peak radial stress applied to specimens prior to shear loading or during the HC, UX, or strain-path loading.

### Specimen preparation

The mechanical property test specimens were cut from solid RTTC bricks using a diamond-bit core barrel following the procedures provided in ASTM C 42 (ASTM 2005b). Once the test specimens were cut to the correct length, the ends were ground flat and parallel to each other and perpendicular to the sides of the core in accordance with procedures in ASTM D 4543 (ASTM 2005e). The prepared test specimens had a mean diameter of 50 mm and a mean height of 113 mm.

Prior to testing, each specimen was placed between hardened steel top and base caps. With the exception of the UC and the DP test specimens, two 0.6-mm-thick membranes were placed around each specimen, and the exterior of the outer membrane was coated with a liquid synthetic rubber to inhibit deterioration caused by the confining fluid (Figure 1). The confining fluid used was a mixture of kerosene and hydraulic oil. Finally, the specimen, along with its top and base cap assembly, was placed on the instrumentation stand of the test apparatus, and the instrumentation setup was initiated.

### Test devices

Three sets of test devices were used in this test program. The axial load for all of the UC tests was provided by a 3.3 MN (750,000-lb) loader. The application of load was manually controlled with this test device. No pressure vessel was required for the UC tests; only a base, load cell, vertical and radial deformeters were necessary.

Direct-pull tests were performed by using the direct-pull apparatus in which end caps were attached to unconfined specimens with a high-modulus, high-strength epoxy. A manually operated hydraulic pump was used to pressurize the direct-pull chamber. When the chamber was pressurized, the piston retracted and produced tensile loading on the test specimens. Measurements of the loading of the specimen were recorded from the output of the load cell.

All of the remaining tests were conducted in a 600-MPa-capacity pressure vessel (Figure 2), and the axial load was provided by an 8.9-MN loader. With this loader, the application of load, pressure, and axial displacement were regulated by a servo-controlled data acquisition system. This servo-controlled system allowed the user to program rates of load, pressure, and axial displacement in order to achieve the desired stress or strain path. Confining pressure was measured externally to the pressure vessel by a pressure transducer mounted in the confining fluid line. A load cell mounted in the base of the specimen pedestal was used to measure the applied axial loads inside the pressure vessel (Figure 1).

Outputs from the various instrumentation sensors were electronically amplified and filtered, and the conditioned signals were recorded by computer-controlled, 16-bit, analog-to-digital converters. The data acquisition system was programmed to sample the data channels every 1 to 5 seconds, convert the measured voltages to engineering units, and store the data for further processing.

### Test instrumentation

The vertical deflection measurement system used for all tests, except for the direct-pull tests, consisted of two linear variable differential transformers (LVDTs) mounted vertically on the instrumentation stand and positioned 180 deg (3.14 rad) apart. They were oriented to measure the displacement between the top and base caps, thus providing a measure of the axial deformation of the specimen. For the confined tests, a linear potentiometer was mounted externally to the pressure vessel to measure the displacement of the piston through which axial loads were applied. This provided a backup to the vertical LVDTs in the event they exceeded their calibrated range or malfunctioned.

Two types of radial deflection measurement systems (lateral deformeters) were used in this test program. The output of each deformeter was calibrated to the radial displacement of the two footings glued to the sides of the test specimen (Figure 1). These two small, steel footings were placed 180 deg apart at the specimen's mid-height and were glued directly to the specimen. The footing faces were machined to match the curvature of the test specimen. A threaded post extended from each footing and protruded through the membranes. Once the membranes were in place, steel caps were screwed onto the threaded posts to seal the membranes to each footing. The lateral deformeter ring was then attached to these steel caps

with set screws. The completed specimen lateral deformeter setup is shown in Figure 3.

One of the two types of lateral deformeters used consisted of an LVDT mounted on a hinged ring; the LVDT measured the expansion or contraction of the ring. This lateral deformeter was used over smaller ranges of radial deformation, when the greatest measurement accuracy was required. This lateral deformeter was used for all of the HC, UC, UX, and strain-path tests. This design is similar to the radial deformeter design provided by Bishop and Henkel (1962). When the specimen expanded (or contracted), the hinged-deformeter ring opened (or closed) causing a change in the electrical output of the horizontally mounted LVDT.

The second type of lateral deformeter, used for all of the TXC tests, consisted of two strain-gaged spring-steel arms mounted on a double-hinged ring; the strain-gaged arms deflected as the ring expanded or contracted. When the specimen expanded or contracted laterally, the rigid deformeter ring flexed about its hinge, causing a change in the electrical output of the strain-gaged arm. This deformeter was used when the greatest radial deformation range was required and was slightly less accurate than the LVDT-type deformeter. The output of the strain gages was calibrated to measure the specimen's lateral deformation. Radial strain measurements were not recorded during the direct-pull tests.

### Test descriptions

The TXC tests were conducted in two phases. During the initial or hydrostatic-compression phase, the cylindrical test specimen was subjected to an increase in hydrostatic pressure while measurements of the specimen's height and diameter changes were recorded. The data from this phase are typically plotted as pressure versus volumetric strain, the slope of which, assuming elastic theory, is the bulk modulus, $K$. The second phase of the TXC test, the shear-loading phase, was conducted after the desired confining pressure was reached during the HC phase. While holding the desired confining pressure constant, axial load was increased, and measurements of the changes in the specimen's height and diameter were made. The axial (compressive) load was increased until the specimen failed. The shear data are generally plotted as principal stress difference versus axial strain, the slope of which represents Young's modulus, $E$. The maximum principal stress difference that a given specimen can support or the principal stress

difference at 15 percent axial strain during shear, whichever occurs first, is defined as the peak strength of the material.

The UC tests were performed in accordance with ASTM C 39 (ASTM 2005a). The UC test is a type of TXC test in which no confining pressure is applied. The maximum principal stress difference observed during a UC test is defined as the unconfined compressive strength of the material.

Extension shear data for the brick were obtained by performing direct-pull (DP) tests. Similar to the UC tests, no confining pressure was applied during the DP tests. To conduct the DP tests, end caps were attached to the specimen with epoxy. The end caps were screwed into the direct-pull apparatus, and the specimen was pulled apart vertically when pressure was applied to the piston. Extension shear data for the material is generally plotted as principal stress difference versus mean normal stress.

Uniaxial strain (UX) tests were conducted by applying axial load and confining pressure simultaneously so that as the cylindrical specimen shortened, its diameter remained unchanged; i.e., zero radial strain boundary conditions were maintained. The data are generally plotted as axial stress versus axial strain, the slope of which is the constrained modulus, $M$. The data are also plotted as principal stress difference versus mean normal stress, the slope of which is twice the shear modulus, G, divided by the bulk modulus, $K$ , i.e., $2G/K$, or, in terms of Poisson's ratio $\nu$, $3(1-2\nu)/(1+\nu)$.

The strain-path tests in this program were conducted in two phases. Initially, the specimen was subjected to uniaxial-strain loading up to a desired level of mean normal, radial, or axial stress. At the end of the UX loading, a constant axial-to-radial-strain ratio of -2.0 was applied; these tests were identified earlier as UX/CV tests. In order to conduct these tests, the software controlling the servo-controls had to correct the measured inputs for system compressibility and for the nonlinear calibrations of specific transducers.

### Definition of stresses and strains

During the mechanical property tests, measurements were typically made of the axial and radial deformations of the specimen as confining pressure and/or axial load was applied or removed. These measurements along with the pretest measurements of the height and diameter of the specimen

were used to convert the measured test data to true stresses and engineering strains.[1]

Axial strain, $\varepsilon_a$, was computed by dividing the measured axial deformation, $\Delta h$ (change in height), by the original height, $h_o$, i.e., $\varepsilon_a = \Delta h/h_o$. Similarly, radial strain, $\varepsilon_r$, was computed by dividing the measured radial deformation, $\Delta d$ (change in diameter), by the original diameter, $d_o$, i.e., $\varepsilon_r = \Delta d/d_o$. For this report, volumetric strain, $\varepsilon_v$, was assumed to be the sum of the axial strain and twice the radial strain, i.e., $\varepsilon_v = \varepsilon_a + 2\varepsilon_r$.

The principal stress difference, $q$, was calculated by dividing the axial load by the cross-sectional area of the specimen $A$, which is equal to the original cross-sectional area, $A_o$, multiplied by $(1 - \varepsilon_r)^2$. In equation form,

$$q = (\sigma_a - \sigma_r) = \frac{\text{Axial Load}}{A_o(1-\varepsilon_r)^2} \quad (1)$$

where $\sigma_a$ is the axial stress, and $\sigma_r$ is the radial stress. The axial stress is related to the confining pressure and the principal stress difference by

$$\sigma_a = q + \sigma_r \quad (2)$$

The mean normal stress, $p$, is the average of the applied principal stresses. In cylindrical geometry,

$$p = \frac{(\sigma_a + 2\sigma_r)}{3} \quad (3)$$

## Results

Results from all the mechanical property tests, except the direct-pull tests, are presented in Plates 1-20. One data plate is presented for each test with reliable results. Results from the HC tests are presented in the plates in four plots, i.e., (a) mean normal stress versus volumetric strain, (b) mean normal stress versus axial strain, (c) radial versus axial strain, and (d) mean normal stress versus radial strain. Each plate for the UC, TXC, UX, and strain-path tests also displays four plots, i.e., (a) principal stress

[1] Compressive stresses and strains are positive in this report.

difference versus mean normal stress, (b) principal stress difference versus axial strain, (c) volumetric strain versus mean normal stress, and (d) volumetric strain versus axial strain.

Table 1. Physical and composition properties of RTTC brick.

| Test number | Type of test | Plate no. | Wet Density $Mg/m^3$ | Posttest water content % | Dry density $Mg/m^3$ | Porosity % | Degree of saturation % | Volume of air % | Volume of water % | Volume of solids % | Axial P-wave velocity km/s | Radial P-wave velocity km/s | Axial S-wave velocity km/s | Radial S-wave velocity km/s |
|---|---|---|---|---|---|---|---|---|---|---|---|---|---|---|
| 1 | UC | 3 | 2.164 | 0.05 | 2.163 | 19.29 | 0.56 | 19.18 | 0.11 | 80.71 | 3.34 | 3.38 | 2.30 | 2.36 |
| 2 | UC | 4 | 2.202 | 0.04 | 2.201 | 17.87 | 0.49 | 17.79 | 0.09 | 82.13 | 3.61 | 3.56 | 2.44 | 2.44 |
| 3 | UC | 5 | 2.159 | 0.06 | 2.158 | 19.47 | 0.67 | 19.34 | 0.13 | 80.53 | 3.34 | 3.32 | 2.28 | 2.21 |
| 4 | HC | 1 | 2.151 | 0.04 | 2.150 | 19.78 | 0.43 | 19.69 | 0.09 | 80.22 | 3.29 | 3.27 | 2.26 | 2.14 |
| 5 | HC | 2 | 2.190 | 0.04 | 2.189 | 18.31 | 0.48 | 18.22 | 0.09 | 81.69 | 3.50 | 3.49 | 2.35 | 2.25 |
| 6 | UX | 16 | 2.181 | 0.00 | 2.181 | 18.62 | 0.00 | 18.62 | 0.00 | 81.38 | 3.55 | 3.50 | 2.38 | 2.28 |
| 7 | UX | 17 | 2.160 | 0.01 | 2.160 | 19.40 | 0.11 | 19.38 | 0.02 | 80.60 | 3.36 | 3.41 | 2.29 | 2.23 |
| 8 | UX | 18 | 2.145 | 0.00 | 2.145 | 19.97 | 0.02 | 19.97 | 0.00 | 80.03 | 3.24 | 3.24 | 2.23 | 2.04 |
| 9 | TXC/10 | 6 | 2.200 | | | | | | | | 3.60 | 3.57 | 2.44 | 2.50 |
| 10 | TXC/10 | 7 | 2.153 | 0.07 | 2.151 | 19.72 | 0.76 | 19.57 | 0.15 | 80.28 | 3.26 | 3.26 | 2.23 | 2.36 |
| 11 | TXC/35 | 8 | 2.156 | 0.05 | 2.155 | 19.58 | 0.55 | 19.47 | 0.11 | 80.42 | 3.32 | 3.36 | 2.25 | 2.13 |
| 12 | TXC/35 | 9 | 2.183 | 0.04 | 2.182 | 18.58 | 0.47 | 18.49 | 0.09 | 81.42 | 3.55 | 3.49 | 2.40 | 2.39 |
| 13 | TXC/50 | 10 | 2.175 | 0.03 | 2.174 | 18.87 | 0.35 | 18.81 | 0.07 | 81.13 | 3.45 | 3.40 | 2.33 | 2.35 |
| 14 | TXC/50 | 11 | 2.219 | 0.02 | 2.218 | 17.24 | 0.26 | 17.19 | 0.04 | 82.76 | 3.68 | 3.70 | 2.48 | 2.49 |
| 15 | TXC/100 | 12 | 2.185 | 0.01 | 2.185 | 18.48 | 0.12 | 18.46 | 0.02 | 81.52 | 3.43 | 3.49 | 2.36 | 2.32 |
| 16 | TXC/100 | 13 | 2.156 | 0.01 | 2.155 | 19.57 | 0.11 | 19.55 | 0.02 | 80.43 | 3.29 | 3.36 | 2.26 | 2.16 |
| 17 | TXC/200 | 14 | 2.193 | 0.00 | 2.193 | 18.17 | 0.00 | 18.17 | 0.00 | 81.83 | 3.56 | 3.59 | 2.43 | 2.28 |
| 18 | TXC/200 | 15 | 2.182 | 0.00 | 2.182 | 18.58 | 0.00 | 18.58 | 0.00 | 81.42 | 3.56 | 3.47 | 2.39 | 2.28 |
| 20 | UX/CV/50 | 19 | 2.148 | 0.05 | 2.147 | 19.90 | 0.54 | 19.79 | 0.11 | 80.10 | 3.25 | 3.21 | 2.27 | 2.06 |

(*continued*)

Table 1. (*concluded*)

| Test number | Type of test | Plate no. | Wet density Mg/m$^3$ | Posttest water content % | Dry density Mg/m$^3$ | Porosity % | Degree of saturation % | Volume of air % | Volume of water % | Volume of solids % | Axial P-wave velocity km/s | Radial P-wave velocity km/s | Axial S-wave velocity km/s | Radial S-wave velocity km/s |
|---|---|---|---|---|---|---|---|---|---|---|---|---|---|---|
| 21 | UX/CV/100 | 20 | 2.145 | 0.01 | 2.145 | 19.97 | 0.11 | 19.95 | 0.02 | 80.03 | 3.30 | 3.32 | 2.28 | 2.10 |
| 22 | DP | | 2.180 | 0.06 | 2.179 | 18.70 | 0.70 | 18.57 | 0.13 | 81.30 | 3.45 | 3.53 | 2.35 | 2.26 |
| 23 | DP | | 2.191 | 0.06 | 2.190 | 18.29 | 0.72 | 18.16 | 0.13 | 81.71 | 3.50 | 3.60 | 2.38 | 2.25 |
| 24 | DP | | 2.198 | 0.05 | 2.197 | 18.01 | 0.61 | 17.90 | 0.11 | 81.99 | 3.56 | 3.50 | 2.42 | 2.47 |
| | | | | | | | | | | | | | | |
| N | | | 23 | 22 | 22 | 22 | 22 | 22 | 22 | 22 | 23 | 23 | 23 | 23 |
| Mean | | | 2.175 | 0.03 | 2.171 | 19.00 | 0.42 | 18.92 | 0.08 | 81.00 | 3.43 | 3.44 | 2.34 | 2.28 |
| Stdv | | | 0.021 | 0.02 | 0.022 | 0.81 | 0.24 | 0.82 | 0.05 | 0.81 | 0.13 | 0.13 | 0.07 | 0.13 |
| Max | | | 2.219 | 0.07 | 2.218 | 19.97 | 0.76 | 19.97 | 0.15 | 82.76 | 3.68 | 3.70 | 2.48 | 2.50 |
| Min | | | 2.145 | 0.00 | 2.145 | 17.24 | 0.02 | 17.19 | 0.00 | 80.03 | 3.24 | 3.21 | 2.23 | 2.04 |

Table 2. Completed RTTC brick test matrix.

| Type of test | No. of tests | Test nos. | Nominal peak radial stress, MPa |
|---|---|---|---|
| Hydrostatic compression | 2 | 4,5 | 510 |
| Triaxial compression | 3 | 1,2,3 | 0 |
| | 2 | 9,10 | 10 |
| | 2 | 11,12 | 35 |
| | 2 | 13,14 | 50 |
| | 2 | 15,16 | 100 |
| | 2 | 17,18 | 200 |
| UX strain | 3 | 6,7,8 | 510 |
| UX/CV | 1 | 20 | 50 |
| | 1 | 21 | 100 |
| Direct pull | 3 | 22,23,24 | 0 |
| Total no. of tests | 23 | | |

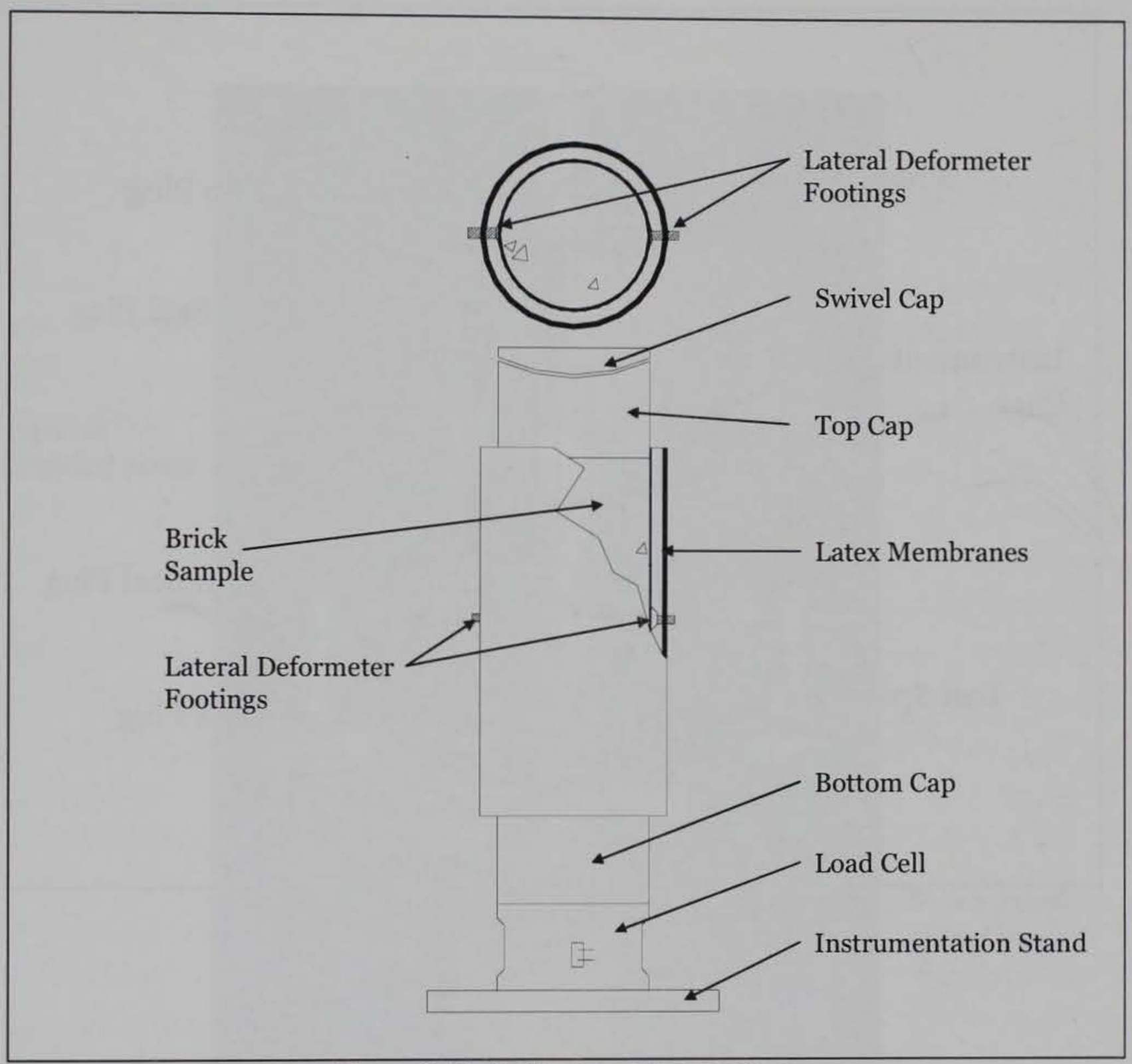


Figure 1. Typical test specimen setup.

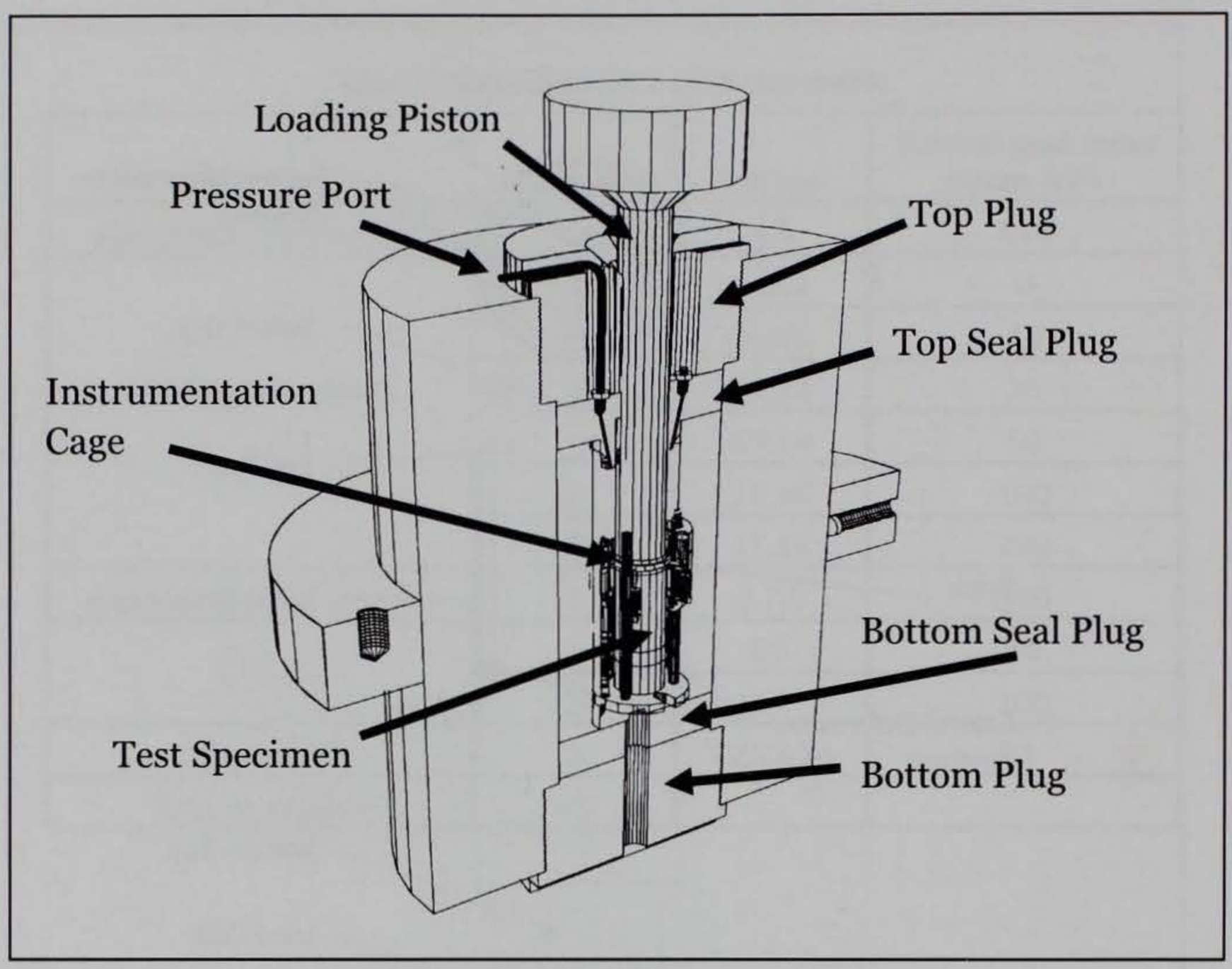


Figure 2. 600-MPa pressure vessel details.

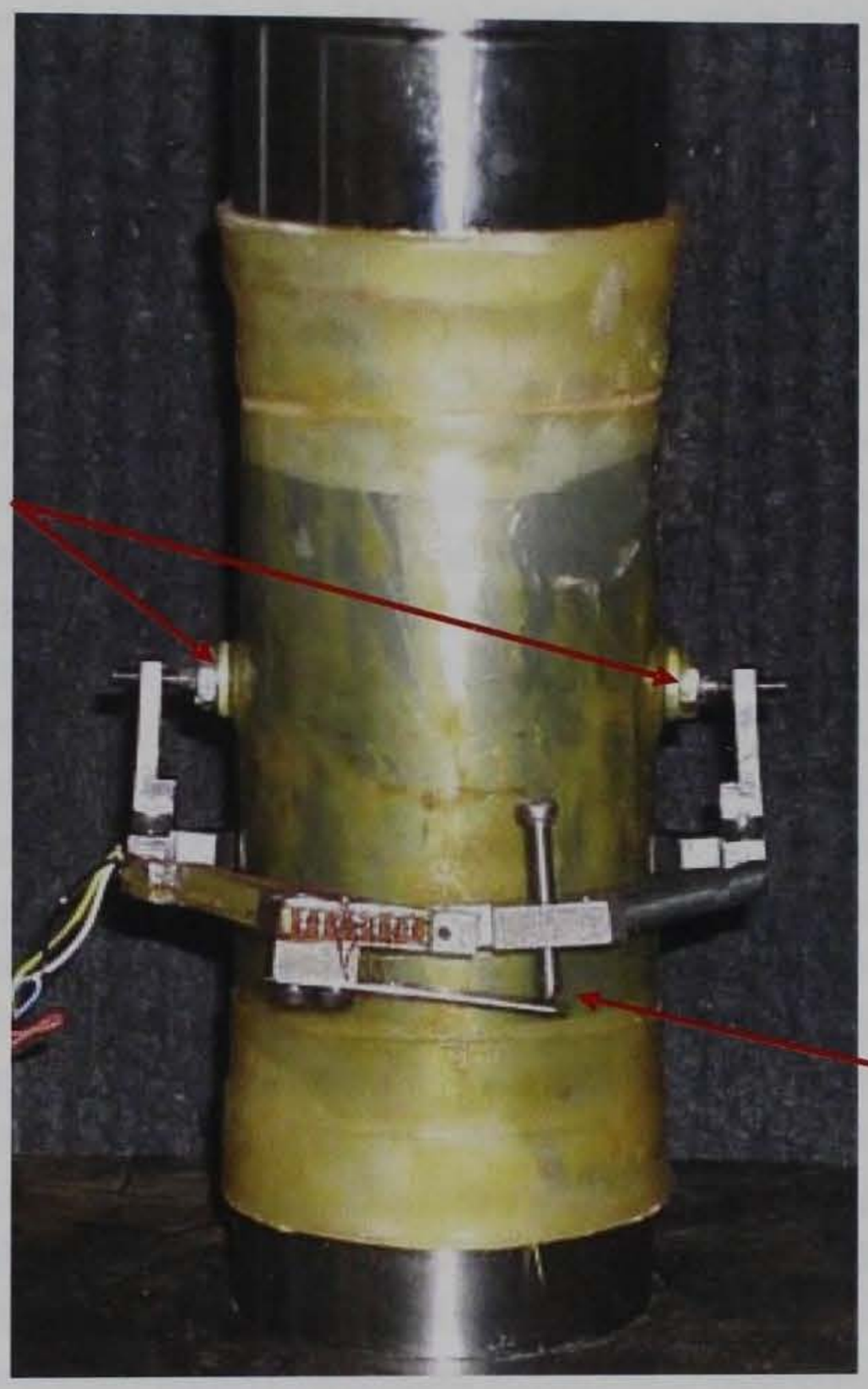


Figure 3. Spring-arm lateral deformeter mounted on test specimen.

# 3 Analysis of Test Results

## Hydrostatic compression tests

Undrained compressibility data were obtained from two HC tests and from the hydrostatic loading phases of the ten TXC tests. The pressure-volume data from the two HC tests are plotted in Figure 4. The initial dry densities of HC test specimens 4 and 5 were 2.150 and 2.189 Mg/m$^3$, respectively. Figure 5 presents the pressure-time histories for the HC tests. Once each HC test reached the maximum prescribed pressure, the pressure was intentionally held constant for a period of time. During the pressure hold, the volumetric strains continued to increase, indicating that RTTC brick is susceptible to creep (Figures 4 and 5). The pressure for test specimen 4 was held at 510 MPa for 139 sec, during which time a volumetric strain of 0.12 percent occurred. For test specimen 5, the pressure was held at 510 MPa for 148 sec, during which time a volumetric strain of 0.12 percent occurred. The brick displays a stiffening of the initial bulk modulus until approximately 1 percent volumetric strain, after which the bulk modulus remains relatively constant for the remainder of each test (Figure 4).

Pressure-volume data were also obtained during the hydrostatic loading phases of the TXC tests (Figure 6). Pressure-volume data from all of the TXC tests and the HC data from Figure 4 are plotted in Figure 7. The TXC test data display slight differences from the HC test data during the initial hydrostatic loading phases. The differences are due to the lower accuracy of the strain-gaged lateral deformeter used during the TXC tests; small inaccuracies in the initial radial strain measurements caused the initial volumetric strains to be calculated as greater than the initial volumetric strains obtained with the LVDT lateral deformeter. Based on the data from the HC tests, the initial elastic bulk modulus, $K$, for RTTC brick is approximately 9.7 GPa.

## Triaxial compression tests

Shear and failure data were successfully obtained from three unconfined compression tests and ten unconsolidated, undrained TXC tests. Recall from Chapter 2 that the second phase of the TXC test, the shear-loading phase, was conducted after the desired confining pressure was applied during the HC phase. The UC tests are a special type of TXC test without

the application of confining pressure. Results from the UC tests are plotted in Figures 8 and 9, and results from the TXC tests are plotted in Figures 10 through 19. In all figures, the axial and volumetric strains were set to zero at the start of the shear phase; i.e., only the strains during shear are plotted.

Stress-strain data from the three UC tests in Figures 8 and 9 are plotted as principal stress difference versus axial strain during shear and as principal stress difference versus volumetric strain during shear. Deformeters instead of strain gages were used to measure the axial and radial strains of the UC test specimens. During the UC tests, no attempt was made to capture the post-peak (or softening) stress-strain behavior of this material. The mean unconfined compressive strength of RTTC brick determined from the three UC tests was 87.7 MPa. The dry densities of the specimens ranged from 2.158 Mg/m$^3$ to 2.201 Mg/m$^3$. The results of these three tests indicate increasing strength with increasing initial dry density.

Figures 10 through 19 present the results from the TXC tests conducted at nominal confining pressures of 10, 35, 50, 100, and 200 MPa. The TXC test results are plotted as principal stress difference versus axial strain during shear and as principal stress difference versus volumetric strain during shear. The results are very good, considering the inherent variations in the initial wet and dry densities and water contents of the specimens. The wet densities of the TXC specimens ranged from 2.153 to 2.219 Mg/m$^3$; the dry densities ranged from 2.151 to 2.218 Mg/m$^3$, and the water contents ranged from 0.00 to 0.07 percent.

Results of TXC tests conducted at a constant confining pressure of 10 MPa are shown in Figures 10 and 11. The initial dry density of specimen 10 was 2.151 Mg/m$^3$. Due to post-peak contamination by the confining fluid, the initial dry density of specimen 9 could not be determined. However, since RTTC brick is an extremely dry material, it can be assumed that the initial wet density of each test specimen is essentially equal to its initial dry density. The initial wet densities of specimens 9 and 10 were 2.200 and 2.153 Mg/m$^3$, respectively. This difference in initial wet density explains the higher peak principal stress difference reached by specimen 9 (Figure 10). The volumetric responses of test specimens 9 and 10 display compressive volumetric strains prior to dilating (Figure 11).

Results of TXC tests conducted at a constant confining pressure of 35 MPa are shown in Figures 12 and 13. The initial dry densities for specimens 11 and 12 were 2.155 and 2.182 Mg/m$^3$, respectively. The data indicate a higher peak strength and smaller axial strain at failure for the denser test specimen (Figure 12). The volumetric response data in Figure 13 indicate that at 35 MPa confining pressure, both specimens initially experienced compressive volumetric strain before dilating.

Results of TXC tests conducted at a constant confining pressure of 50 MPa are shown in Figures 14 and 15. The initial dry densities for specimens 13 and 14 were 2.174 and 2.218 Mg/m$^3$, respectively. Figure 14 displays post-peak softening in both specimens. The volumetric responses in Figure 15 indicate that the specimens compacted until just before the peak principal stress difference, then the specimens dilated. The denser test specimen (specimen 14) exhibited a higher strength and a smaller strain at failure.

Results of TXC tests conducted at a constant confining pressure of 100 MPa are shown in Figures 16 and 17. The initial dry densities for specimens 15 and 16 were 2.185 and 2.155 Mg/m$^3$, respectively. The data exhibited post-peak softening and only a minor difference in peak principal stress difference (Figure 16). The reader should note the decrease in variations in the stress-strain data with increasing pressure even with the slightly varying dry densities of the test specimens. The UC tests are very sensitive to small differences in dry density and specimen structure (Figures 8 and 9), which results in variations in the initial loading data and peak strength values. The variations are less pronounced as the confining pressure increases. This is a result of the confining pressure reducing the differences in the initial properties of the test specimens. The volumetric response data in Figure 17 indicate that at 100-MPa confining pressure, the test specimens experienced initial compressive volumetric strain. The post-peak unloading data for specimen 15 is not shown due to a lateral deformeter malfunction during that portion of the test. Again, the denser of the two test specimens (specimen 15) achieved a higher peak strength and a smaller strain at failure.

Test results for TXC tests conducted at a constant confining pressure of 200 MPa are shown in Figures 18 and 19. The initial dry densities for specimens 17 and 18 were 2.193 and 2.182 Mg/m$^3$, respectively. At this confining pressure, the data exhibited very little difference in peak strength with some strain softening (Figure 18). The volumetric response

data in Figure 19 exhibit initial compaction at the start of shear. The specimens begin dilating just prior to reaching the peak principal stress difference, and both show approximately 5 percent dilation after reaching the peak compressive volumetric strain.

Upon completion of the TXC tests, it was determined that none of the specimens reached full saturation during the shear loading, since the stress-strain data continued to exhibit increases in principal stress difference over the entire range of applied confining stresses.

For comparison purposes, stress-strain data from selected TXC tests are plotted in Figure 20 as principal stress difference versus axial strain during shear. In this figure, the results of all tests conducted at and above 50 MPa confining pressure display post-peak softening, while the tests at 35 MPa confining pressure and below were limited to the peak strength of the specimen. The post-peak softening is a result of the frictional strength along the failure plane developed after failure of the test specimen. Higher confining pressures would be necessary for defining the transition of the brittle-to-ductile failure mode of the brick. An attempt was made to acquire data at higher confining pressures. However, the strength of the brick exceeded that of the load cell being used to perform the tests, and no failure data was obtained.

Stress-strain data from the selected TXC tests in Figure 20 are plotted in Figure 21 as principal stress difference versus volumetric strain during shear. The initial stress-strain loadings of the TXC tests are a function of the material's volume changes during shear, and thus are dependent on the magnitude of the applied confining pressure and the position on the material's pressure-volume response curve. In Figure 21, the compressive volumetric strain during shear loading increased with each increase in confining pressure. The increases in volumetric strain with increasing confining pressure are due to the material's nearly linear pressure-volume relation at high confining stresses (Figure 4). Figure 21 also shows that all the test specimens initially compacted during the shear loading then began to dilate just prior to achieving peak strength.

Results from TXC tests conducted at confining pressures from 10 to 200 MPa are plotted in Figure 22 as radial strain versus axial strain during shear. A contour of zero volumetric strain during shear is also shown in this figure. When the instantaneous slope of a curve is shallower than the

contour of zero volumetric strain, the specimen is in a state of volumetric compression; when steeper, the specimen is in a state of dilation or volumetric expansion. Data points plotting below the contour signify that a test specimen has dilated, and the current volume of the specimen is greater than the volume at the start of shear.

The stress paths and failure data from all the UC and TXC tests are plotted in Figure 23 as principal stress difference versus mean normal stress. In Figure 24, a recommended failure surface is plotted with the failure data from Figure 23. The quality of the failure data is very good and exhibits very little scatter. Test specimen 14 had the highest dry density (2.218 $Mg/m^3$), which explains its failure point well above the failure surface. It is important to note that the failure points exhibited a continuous increase in principal stress difference with increasing values of mean normal stress. The response data from the TXC tests indicate that at a mean normal stress of approximately 420 MPa, the brick still has not yet reached void closure. Materials such as concrete and brick can continue to gain strength with increasing pressure until all of the specimen's air porosity is forced out.

### Direct-pull tests

Extension failure data were successfully obtained from three direct-pull (DP) tests. To prepare these specimens for testing, threaded caps are attached to the ends of the sample with a high-strength epoxy and allowed to cure for several days. Once the specimen was mounted into the direct-pull apparatus, tensile stress was applied axially by a manually operated hydraulic pump until failure of the sample occurred. These tests were performed without any application of confining pressure. The stress paths and failure data from the three direct-pull tests are plotted in Figure 25 as principal stress difference versus mean normal stress. The average tensile strength of the DP test specimens occurred at an approximate principal stress difference of -6.3 MPa and at a mean normal stress of -2.1 MPa. The absolute value of the tensile strength of the brick is 7.2 percent of its unconfined compressive strength.

### Uniaxial strain tests

One-dimensional compressibility data were obtained from three undrained, uniaxial strain (UX) tests with lateral stress measurements. Data from the tests are plotted in Figures 26 through 28. The stress-strain

data from the UX tests are plotted in Figure 26, the pressure-volume data in Figure 27, and the stress paths with the failure surface data in Figure 28. The UX responses indicate that the test specimens did not approach a saturated state, i.e., the volumetric strains achieved during the tests were far less than the volumes of air in the specimens.

From the UX stress-strain loading data (Figure 26), an initial constrained modulus, $M$, of 19.5 GPa was calculated. The UX test data may also be plotted as principal stress difference versus mean normal stress (Figure 28), the slope of which is twice the shear modulus divided by the bulk modulus, $2G/K$. An initial shear modulus of 7.4 GPa was calculated from the constrained modulus and the initial elastic bulk modulus, $K$ (9.7 GPa) determined from the HC tests. These two values may be used to calculate other elastic constants, such as an initial Young's modulus of 17.6 GPa and a Poisson's ratio of 0.20.

The stress paths from the UX tests and the failure surface are plotted in Figure 28. The UX stress paths almost reach the recommended TXC failure surface at low stresses before the paths soften slightly. The stress paths soften after the ceramic bonds begin to crush, causing the data to plot below the failure surface. The initial dry densities for test specimens 6, 7, and 8 were 2.181, 2.160, and 2.145 Mg/m$^3$, respectively. The pressure-volume responses from the HC and UX tests are compared in Figure 29. The HC test specimens display much stiffer loading responses than the UX test specimens. The greater volumetric strains and the softer loading responses of the UX test specimens indicate shear-induced compaction during the UX loading.

## Strain path tests

One special type of strain-path test was conducted during this test program. UX/CV refers to tests with uniaxial-strain loading followed by constant-volumetric-strain loading with an axial-to-radial-strain ratio (ARSR) of -2.0. Results from two UX/CV tests conducted at two levels of peak radial stress during the initial UX phase are shown in Figures 30 through 33. The stress-strain data from the UX/CV tests are plotted in Figure 30, the pressure-volume data in Figure 31, the stress paths with the TXC failure surface data in Figure 32, and the strain paths in Figure 33.

When loading along the constant-volume strain path, the specimens tend to increase in volume due to the material's inherent shear-induced dilation

characteristics near the failure surface. Increasing levels of pressure are required to maintain constant-volume boundary conditions (Figure 31). The CV portions of the stress path data in Figure 32 initially exhibit an increase in principal stress difference with a slight decrease in mean normal stress followed by an increase in both principal stress difference and mean normal stress. During the CV loading, the data plot just below the failure surface developed from the TXC tests. This is mostly due to the lower initial dry densities of the UX/CV specimens. The average initial dry density of the TXC specimens was 2.177 Mg/m$^3$, whereas the initial dry densities of test specimens 20 and 21 were 2.147 and 2.145 Mg/m$^3$, respectively. These differences in the initial dry densities explain the UX/CV stress paths plotting just below the failure surface. Typically, the limiting surface for the UX/CV stress paths will be the TXC failure surface, assuming the initial dry densities of the UX/CV specimens are similar in value to the average initial dry density of the TXC specimens.

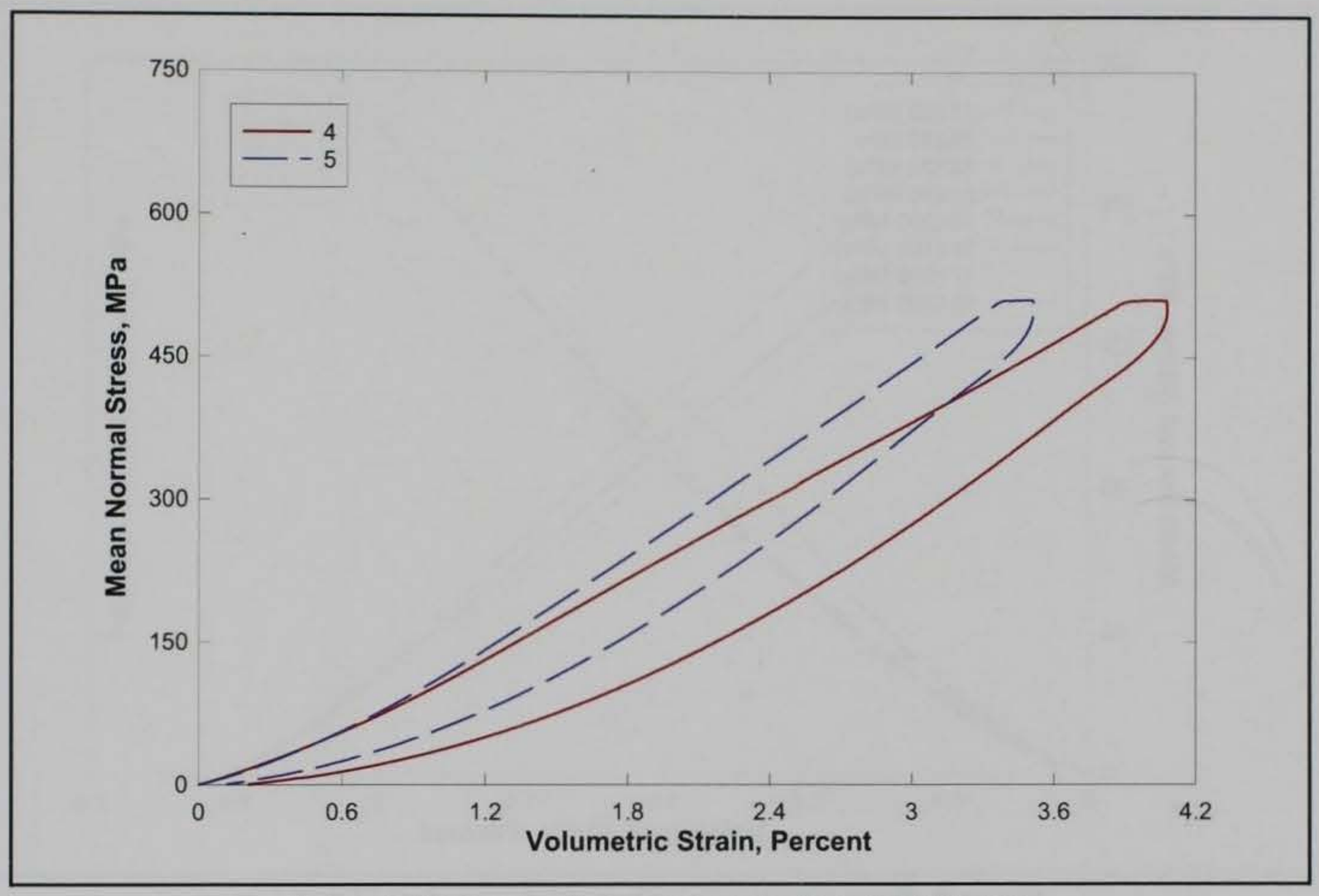


Figure 4. Pressure-volume responses from the HC tests.

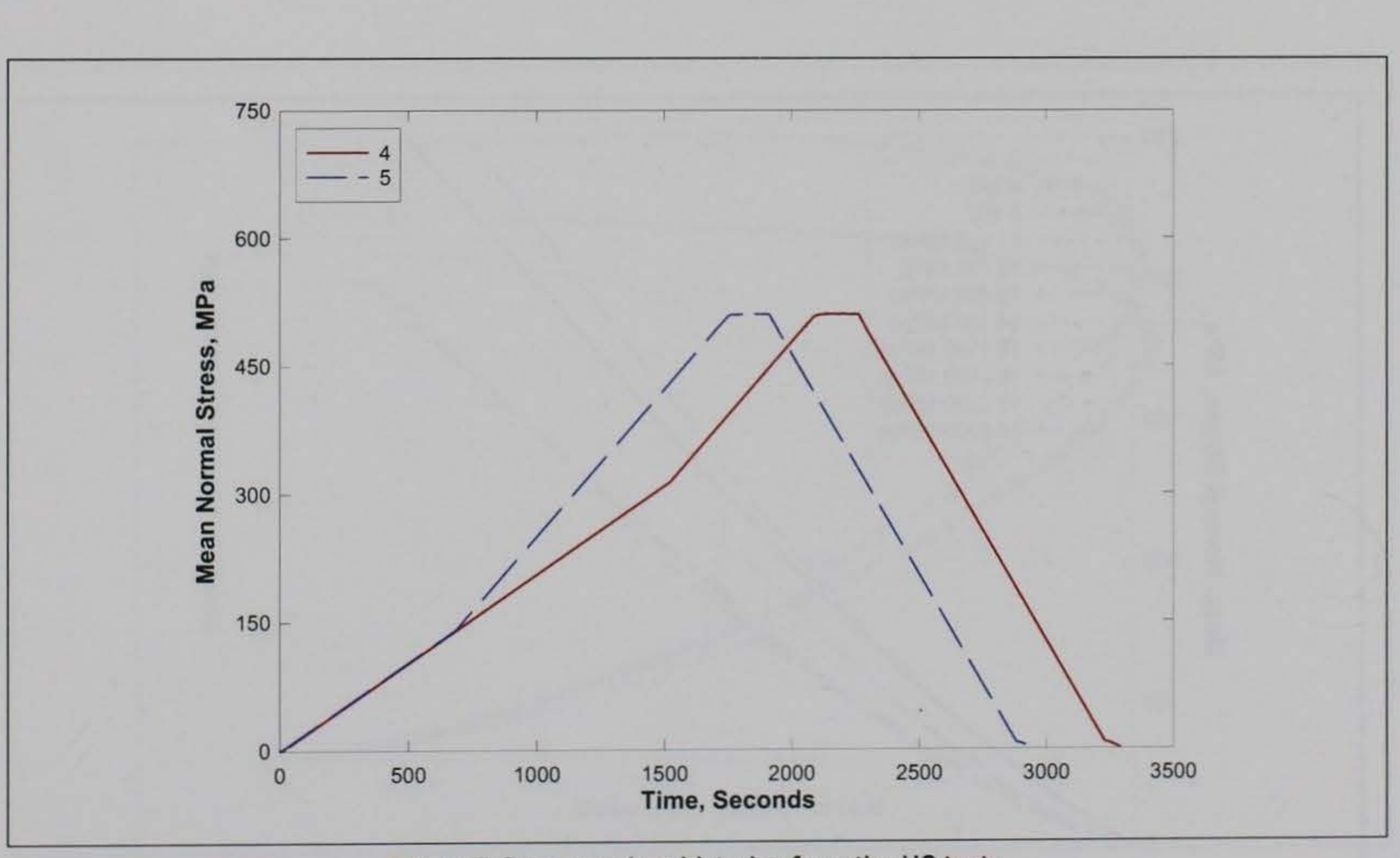


Figure 5. Pressure-time histories from the HC tests.

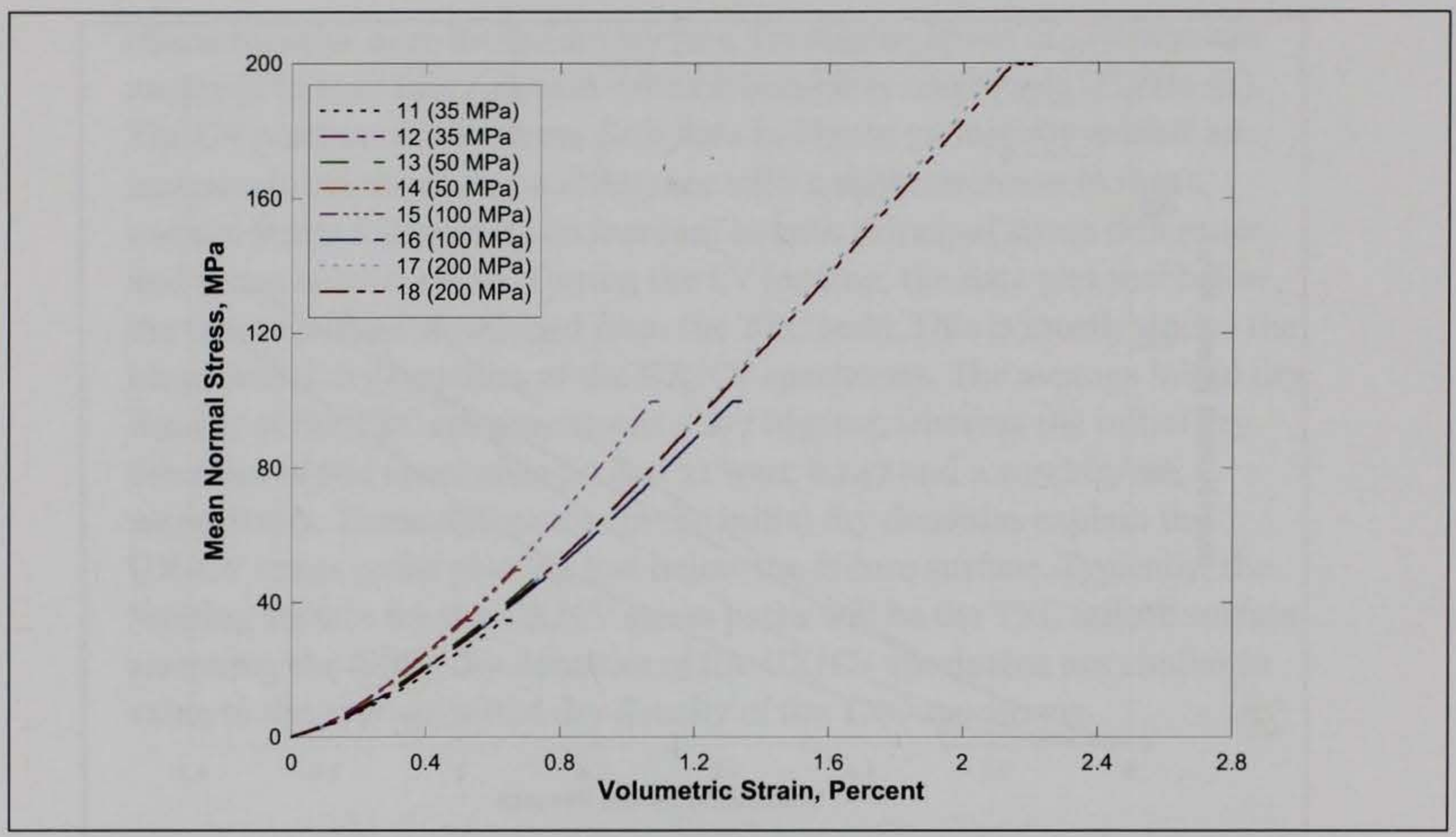


Figure 6. Pressure-volume responses from selected TXC tests.

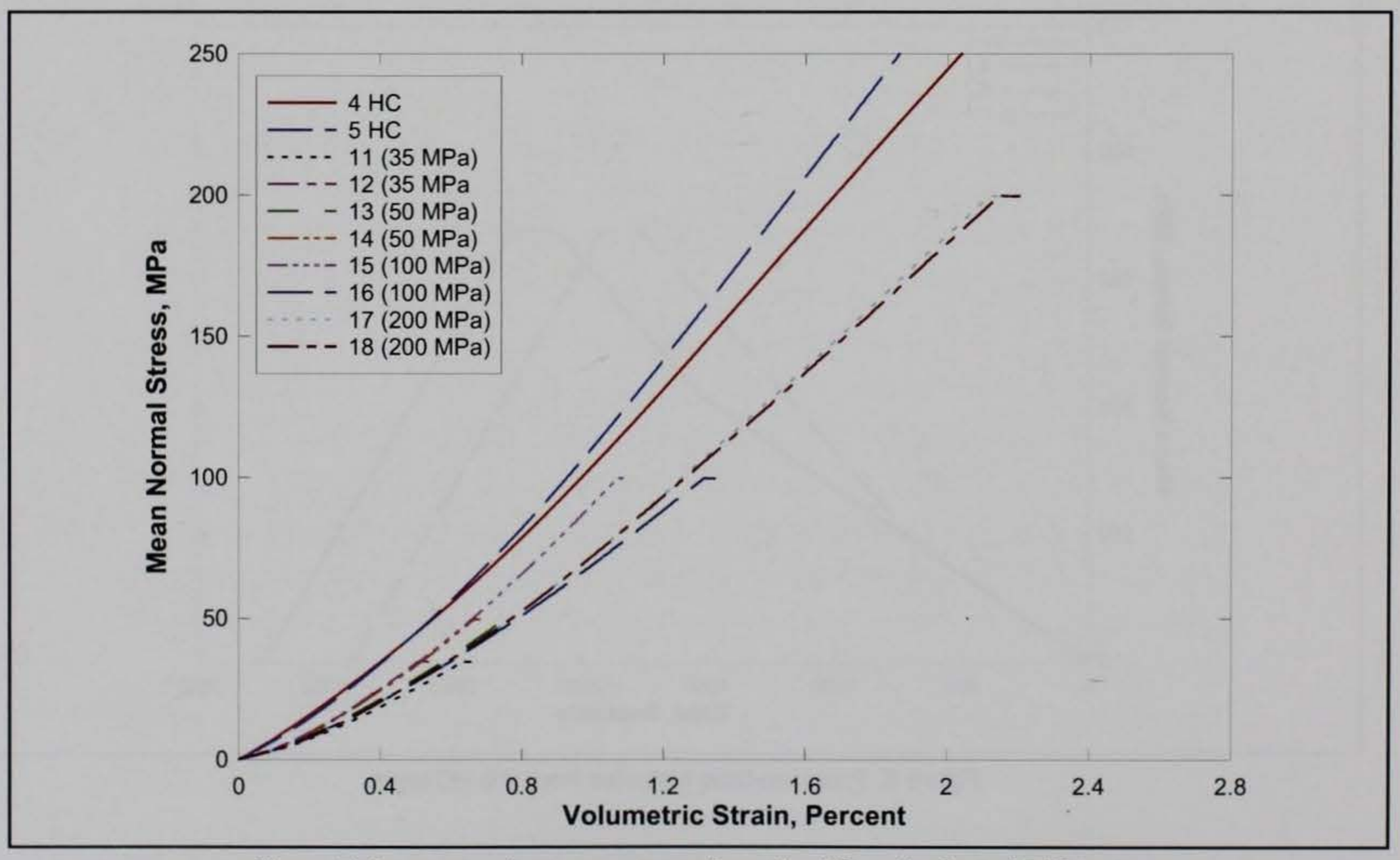


Figure 7. Pressure-volume responses from the HC and selected TXC tests.

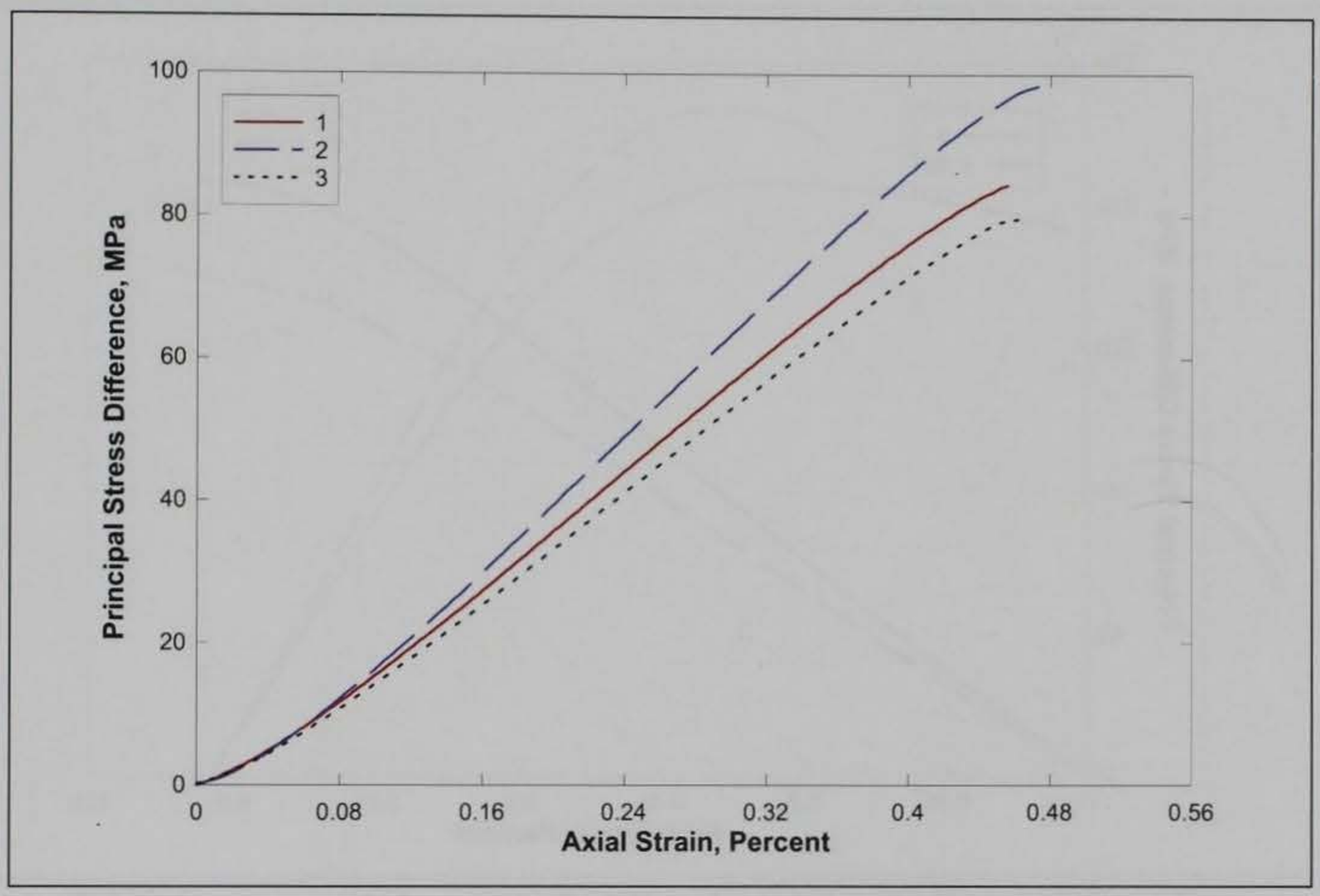


Figure 8. Stress-strain responses from UC tests.

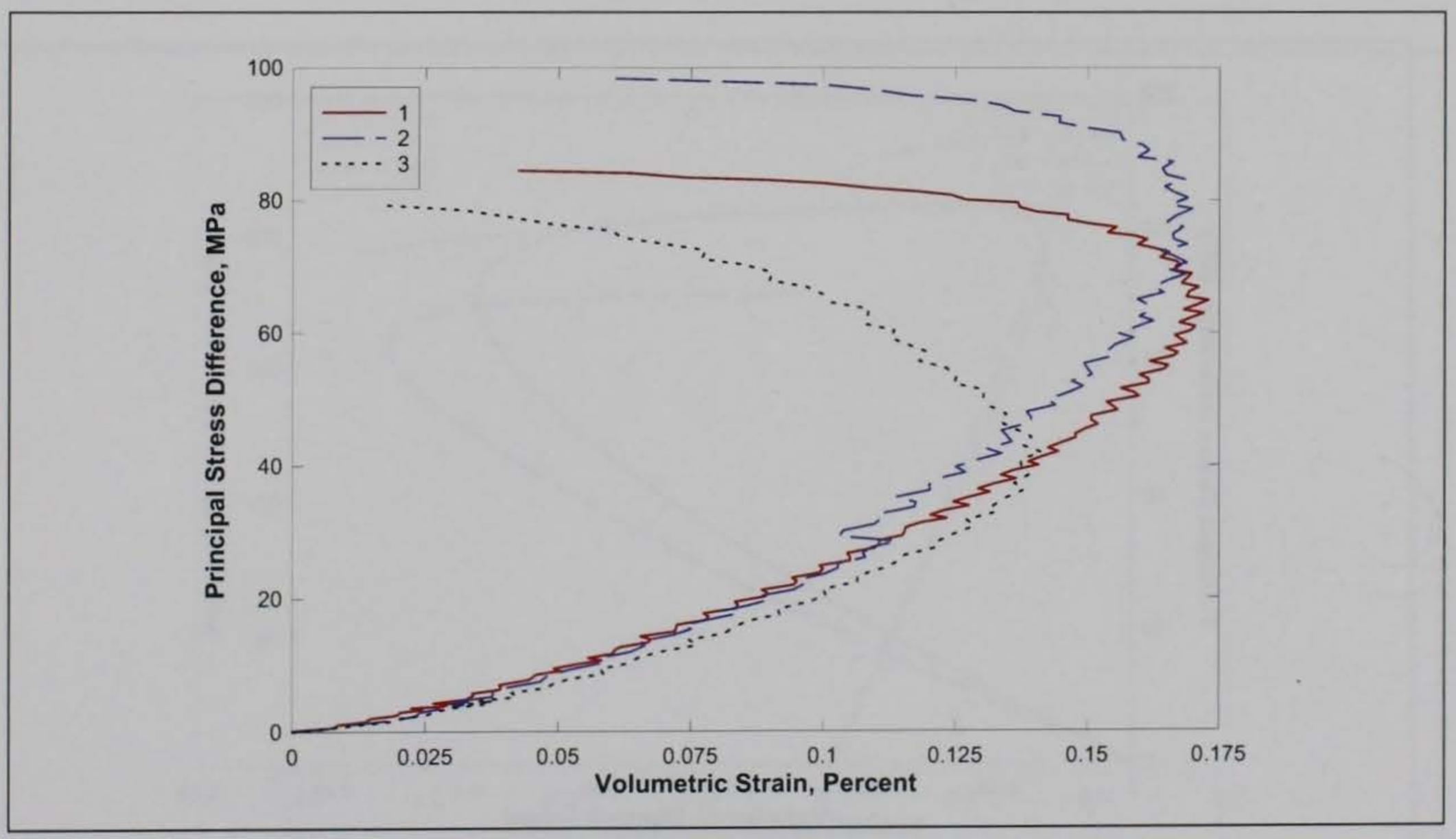


Figure 9. Stress difference-volumetric strain during shear from UC tests.

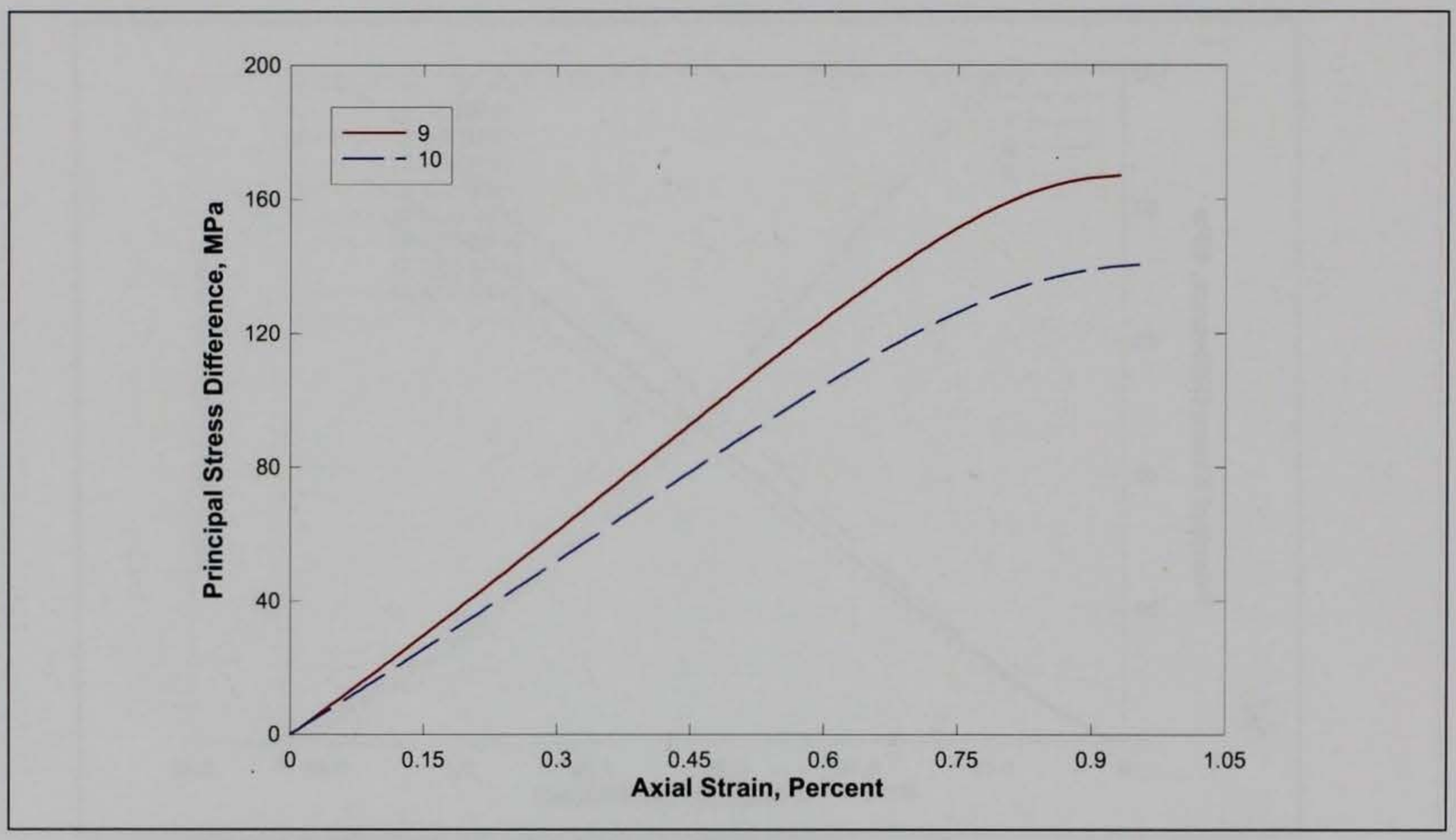


Figure 10. Stress-strain responses from TXC tests at a confining pressure of 10 MPa.

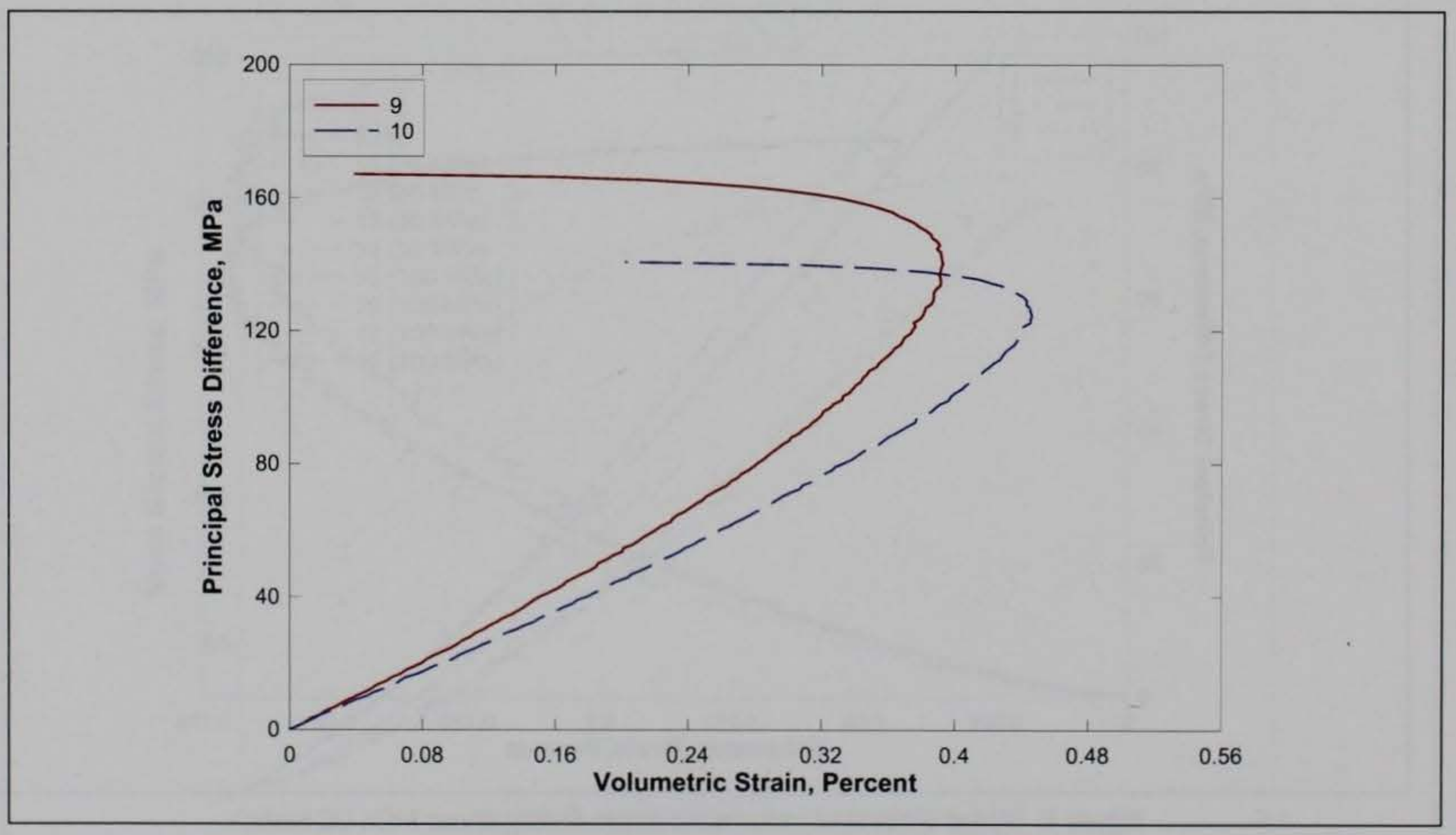


Figure 11. Stress difference-volumetric strain during shear from TXC tests at a confining pressure of 10 MPa.

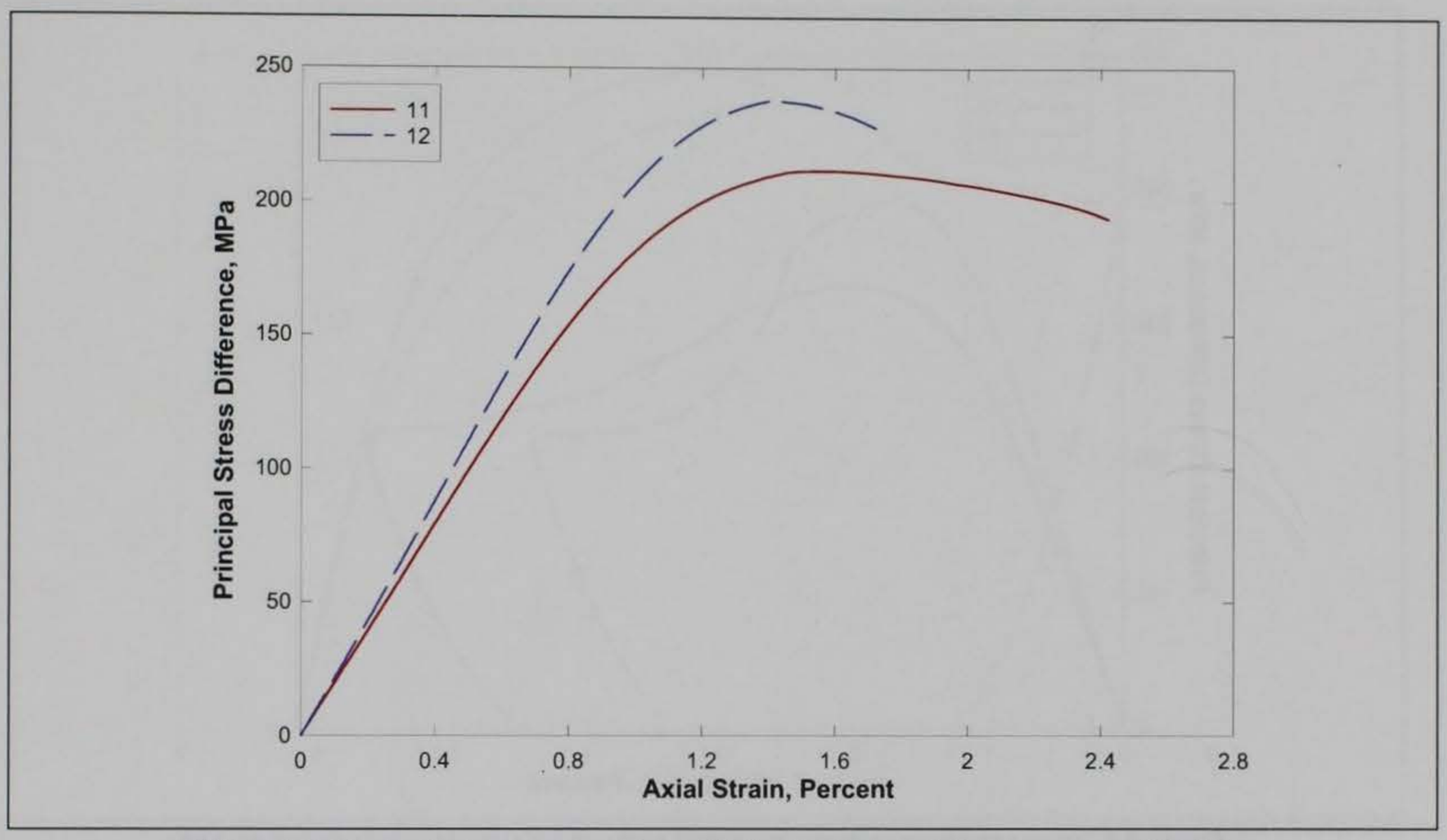


Figure 12. Stress-strain responses from TXC tests at a confining pressure of 35 MPa.

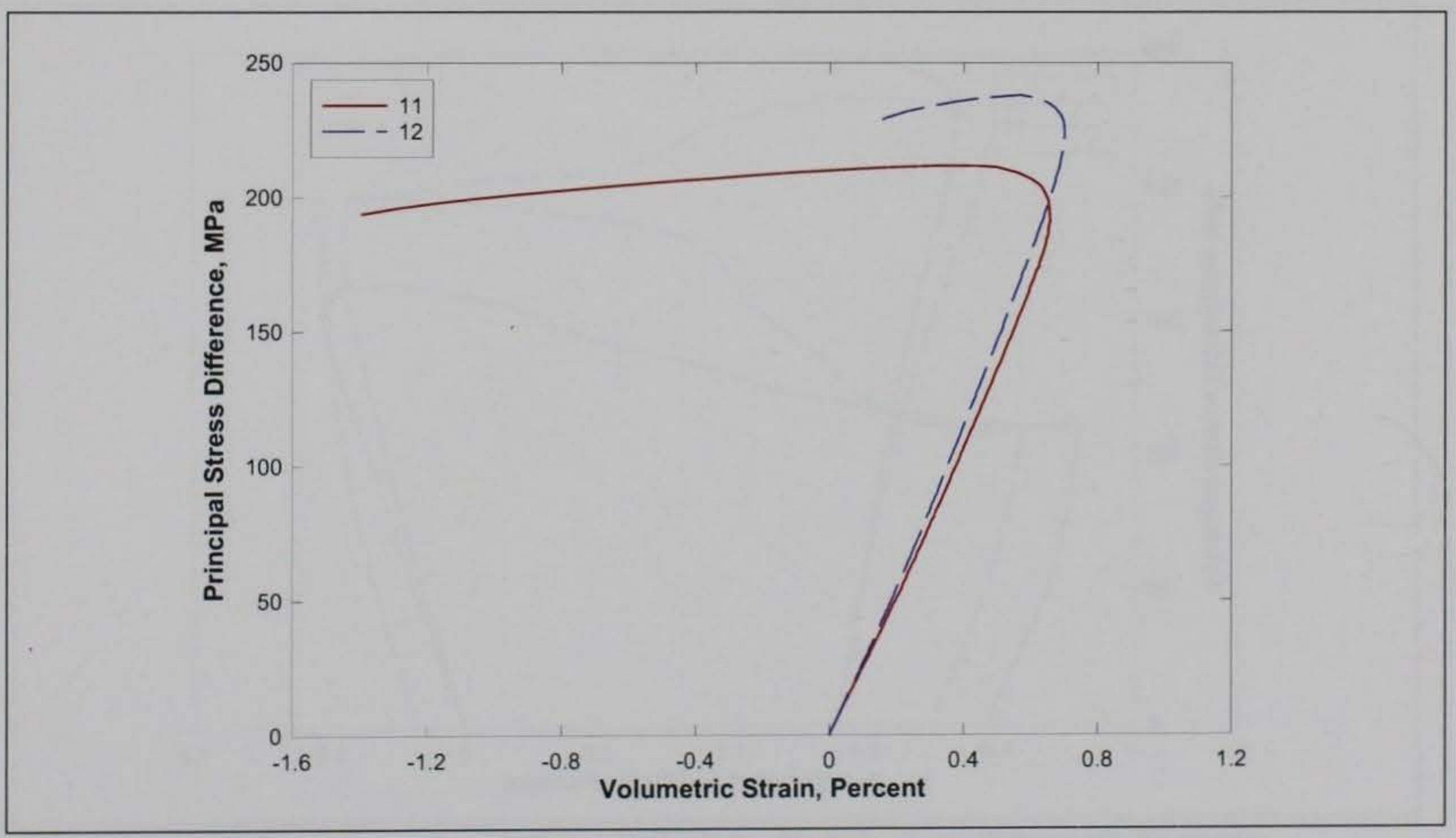


Figure 13. Stress difference-volumetric strain during shear from TXC tests at a confining pressure of 35 MPa.

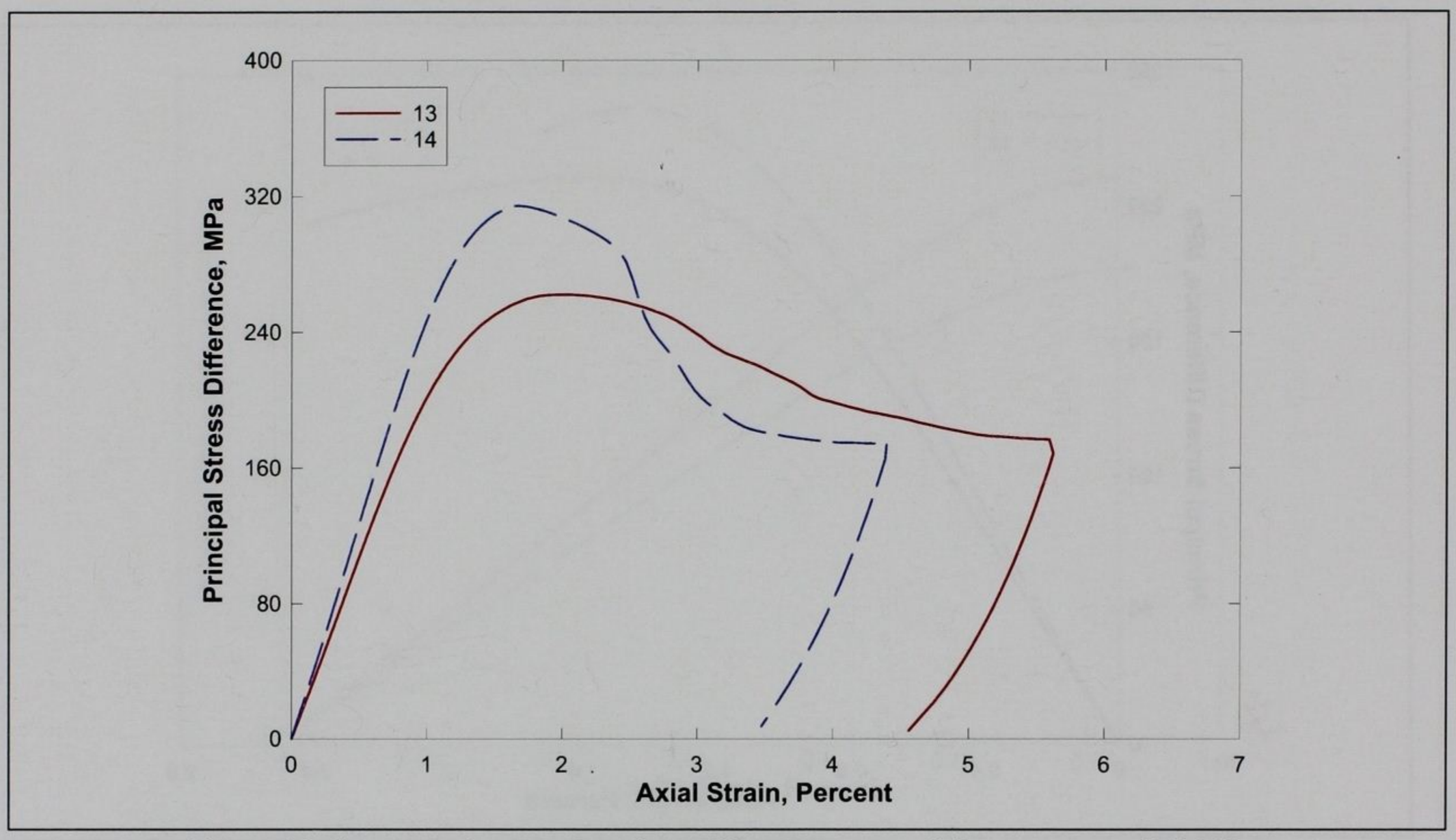


Figure 14. Stress-strain responses from TXC tests at a confining pressure of 50 MPa.

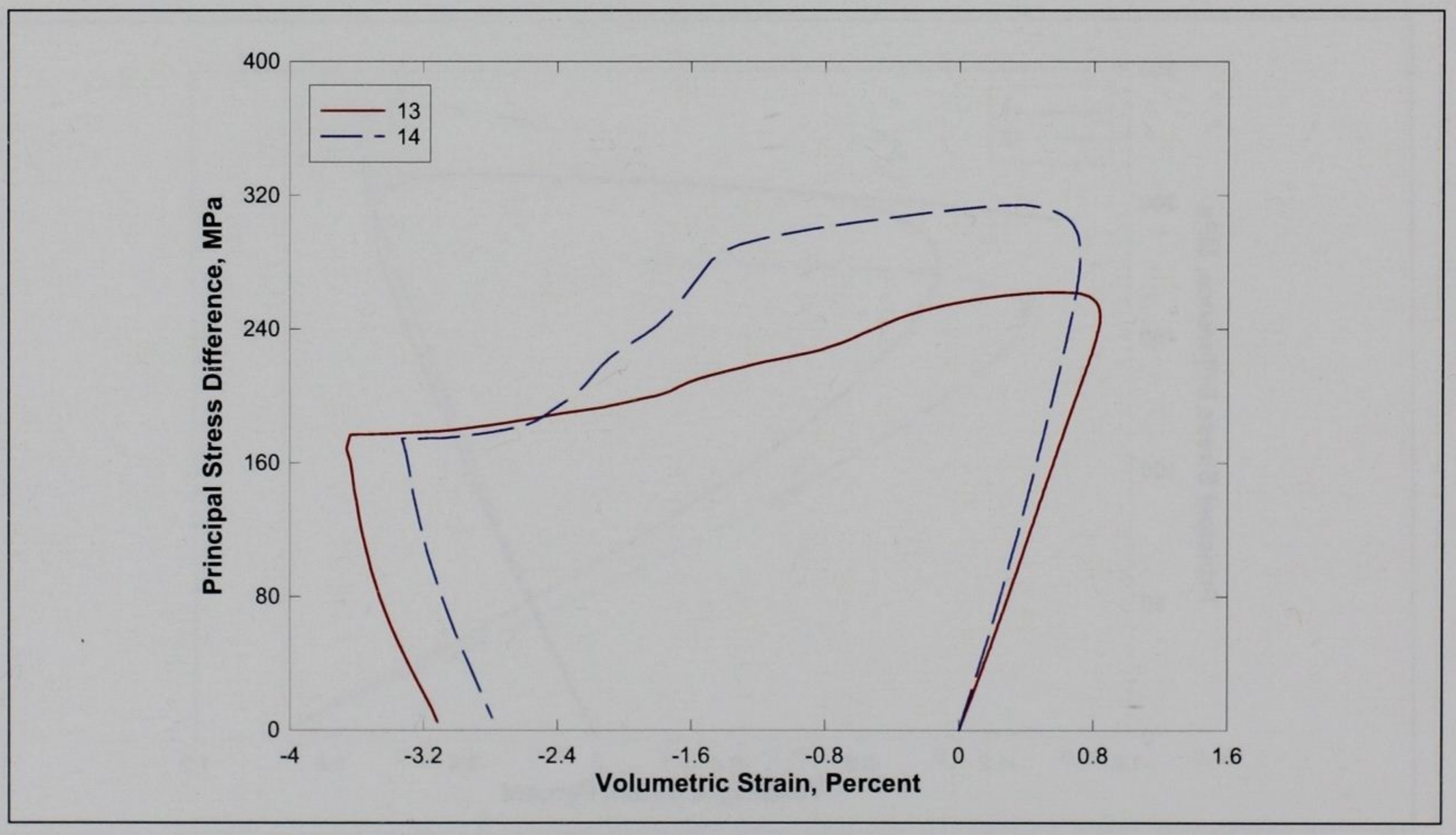


Figure 15. Stress difference-volumetric strain during shear from TXC tests at a confining pressure of 50 MPa.

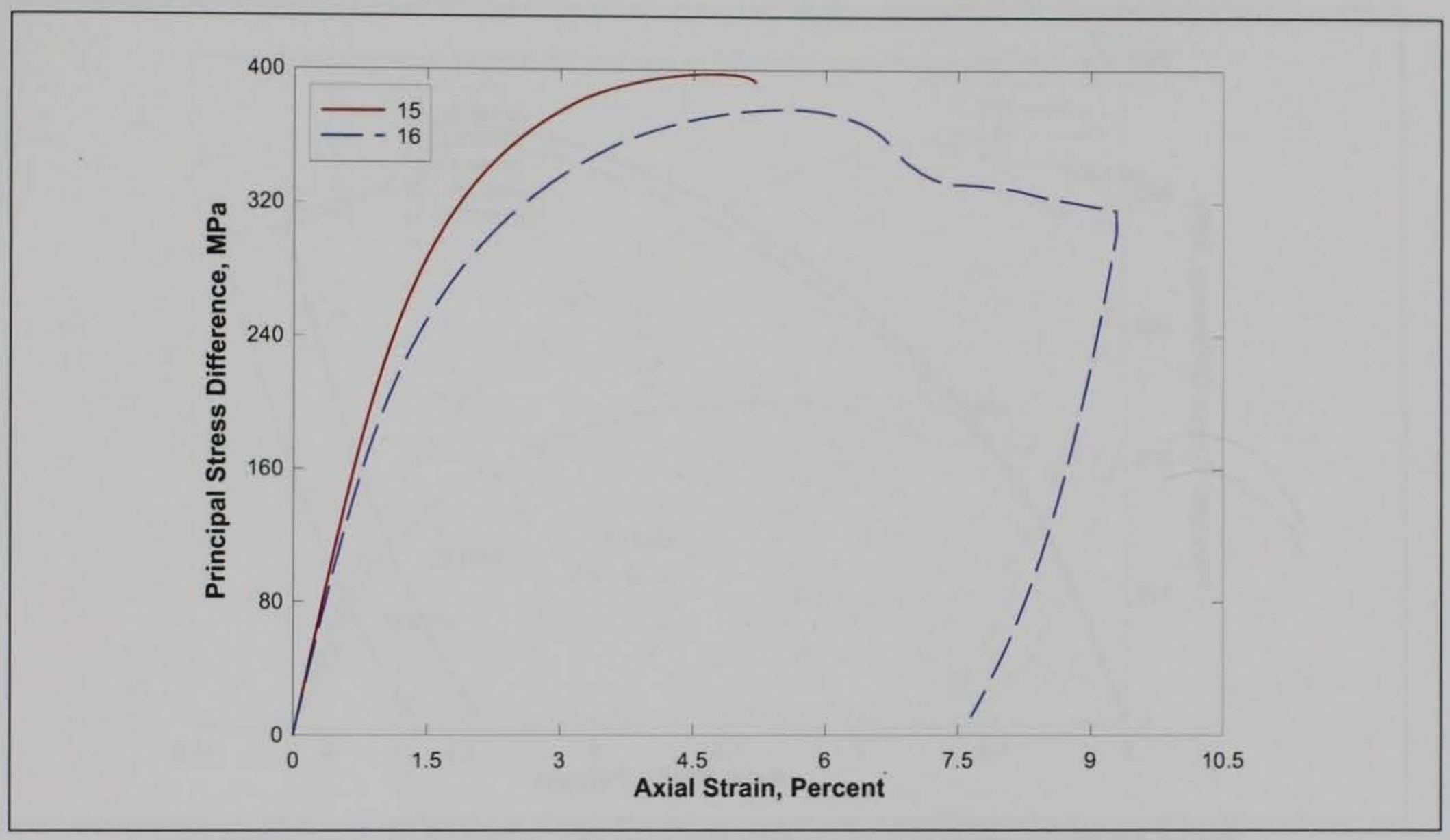


Figure 16. Stress-strain responses from TXC tests at a confining pressure of 100 MPa.

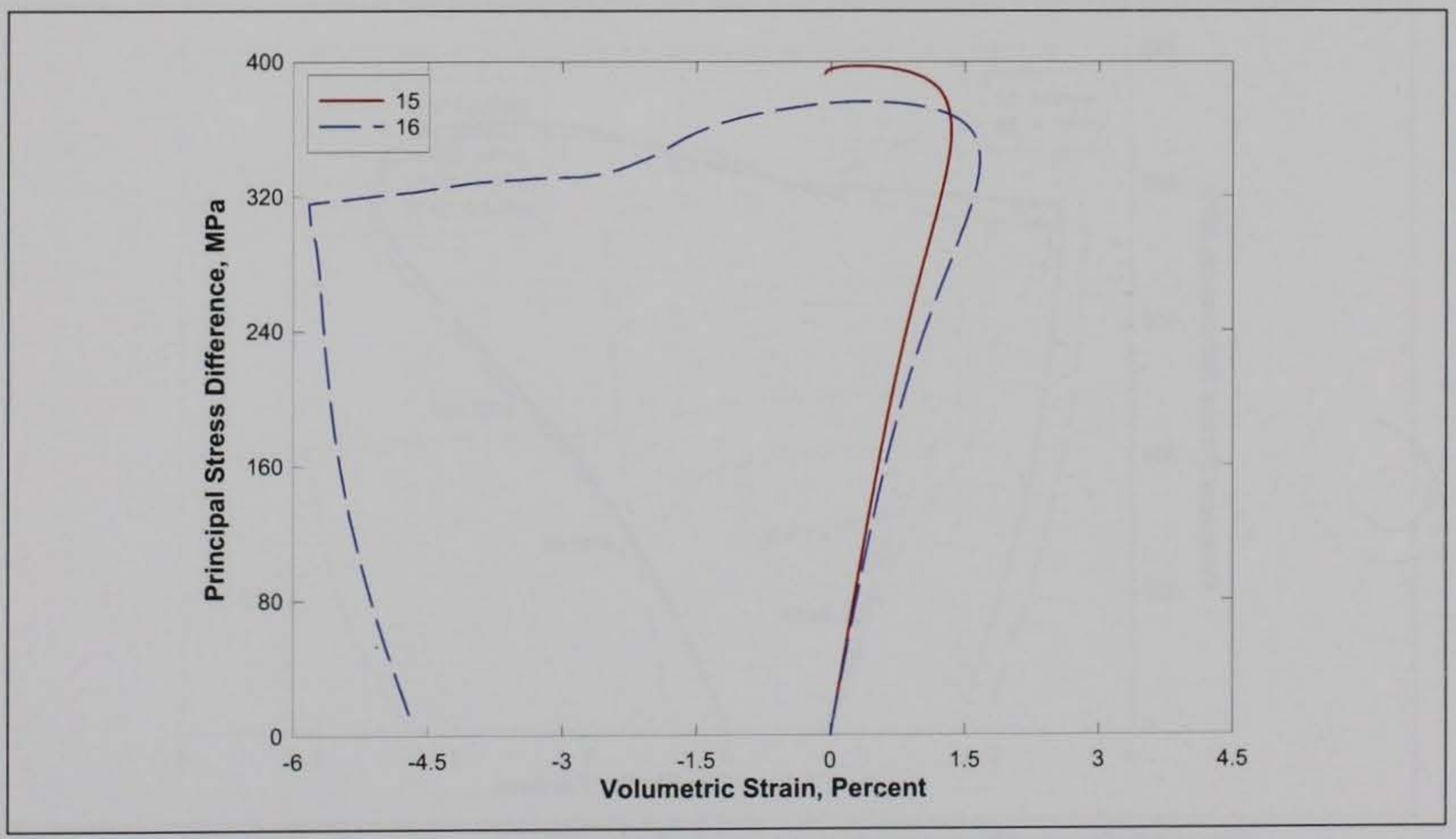


Figure 17. Stress difference-volumetric strain during shear from TXC tests at a confining pressure of 100 MPa.

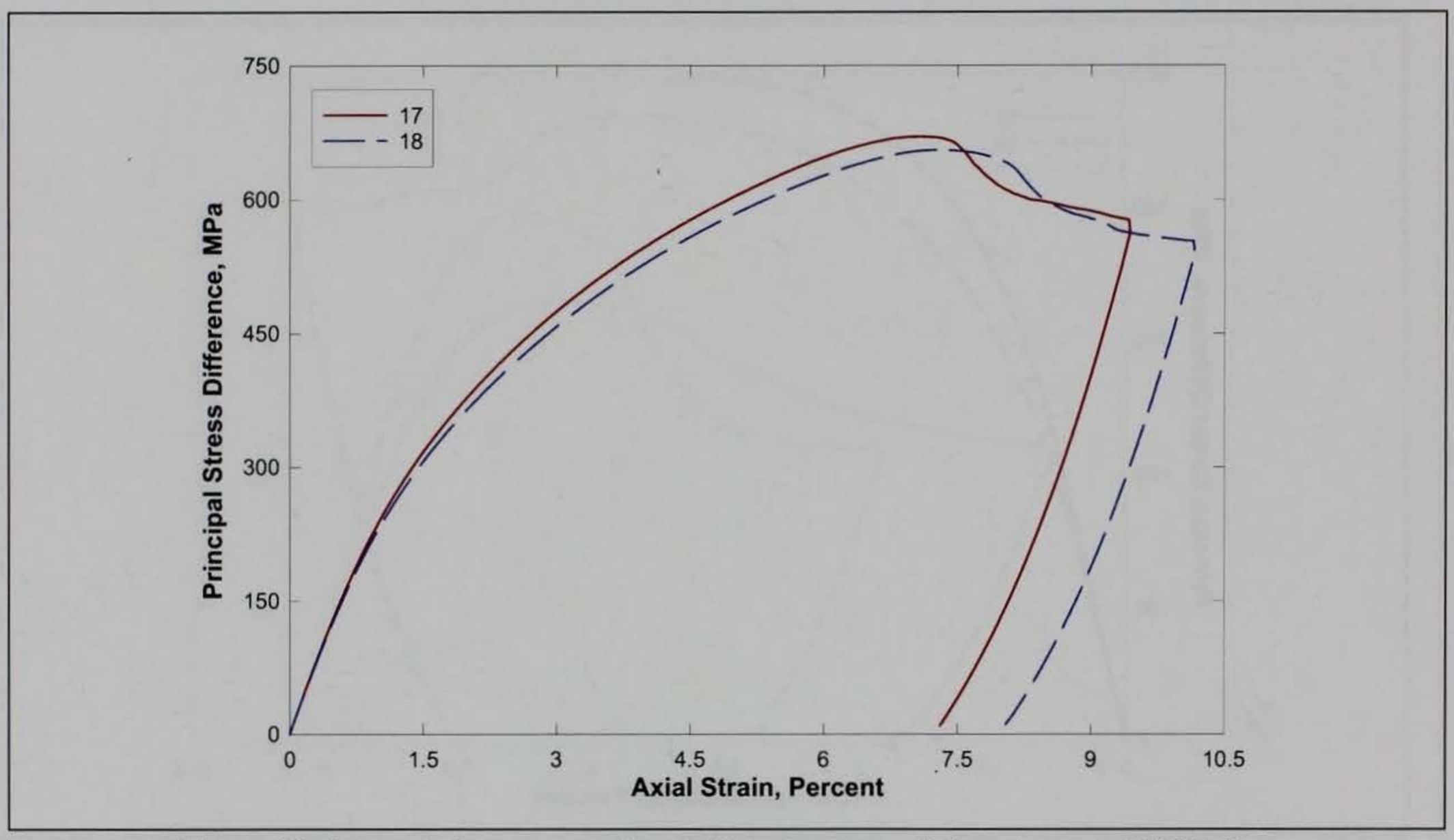


Figure 18. Stress-strain responses from TXC tests at a confining pressure of 200 MPa.

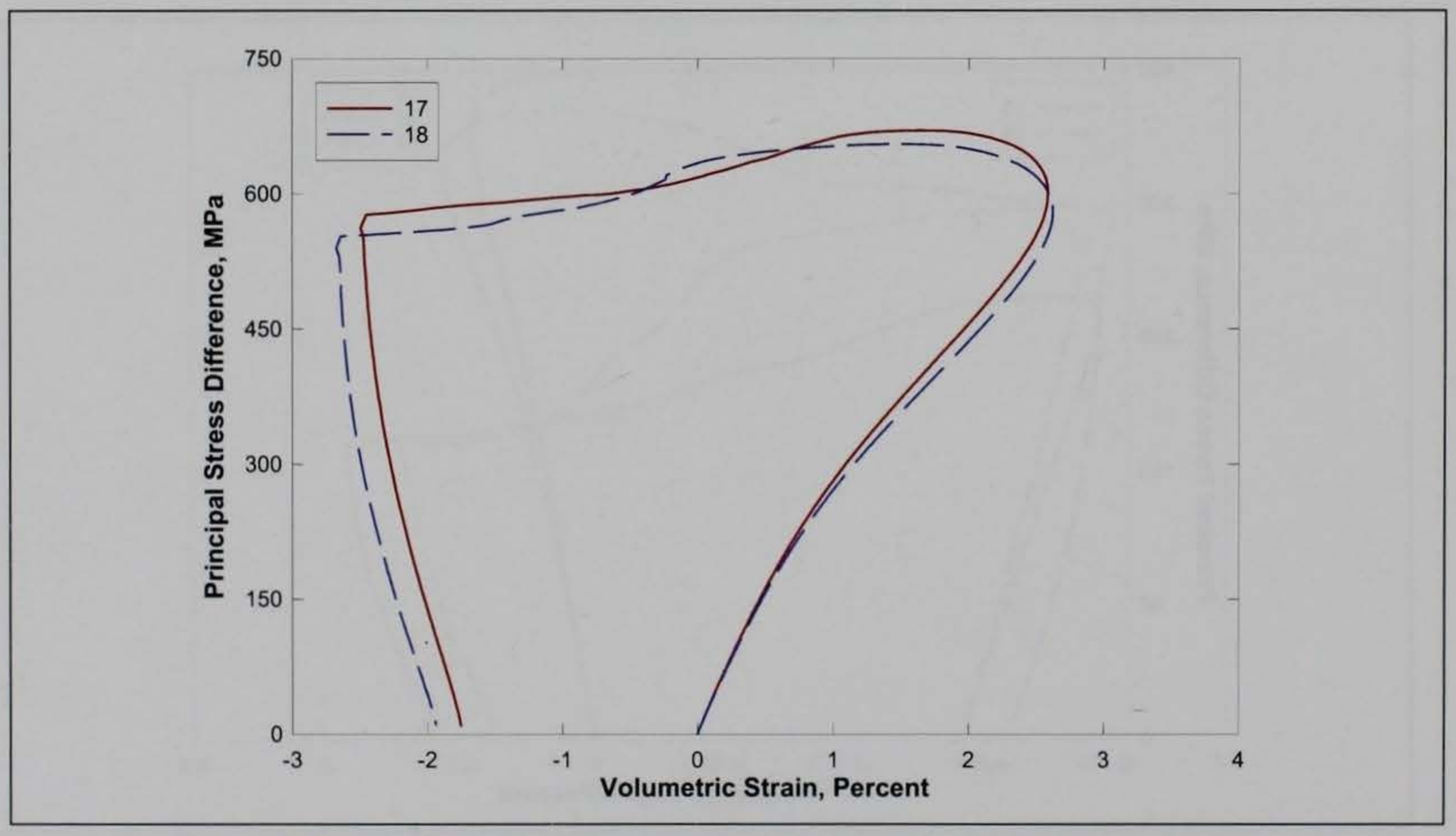


Figure 19. Stress difference-volumetric strain during shear from TXC tests at a confining pressure of 200 MPa.

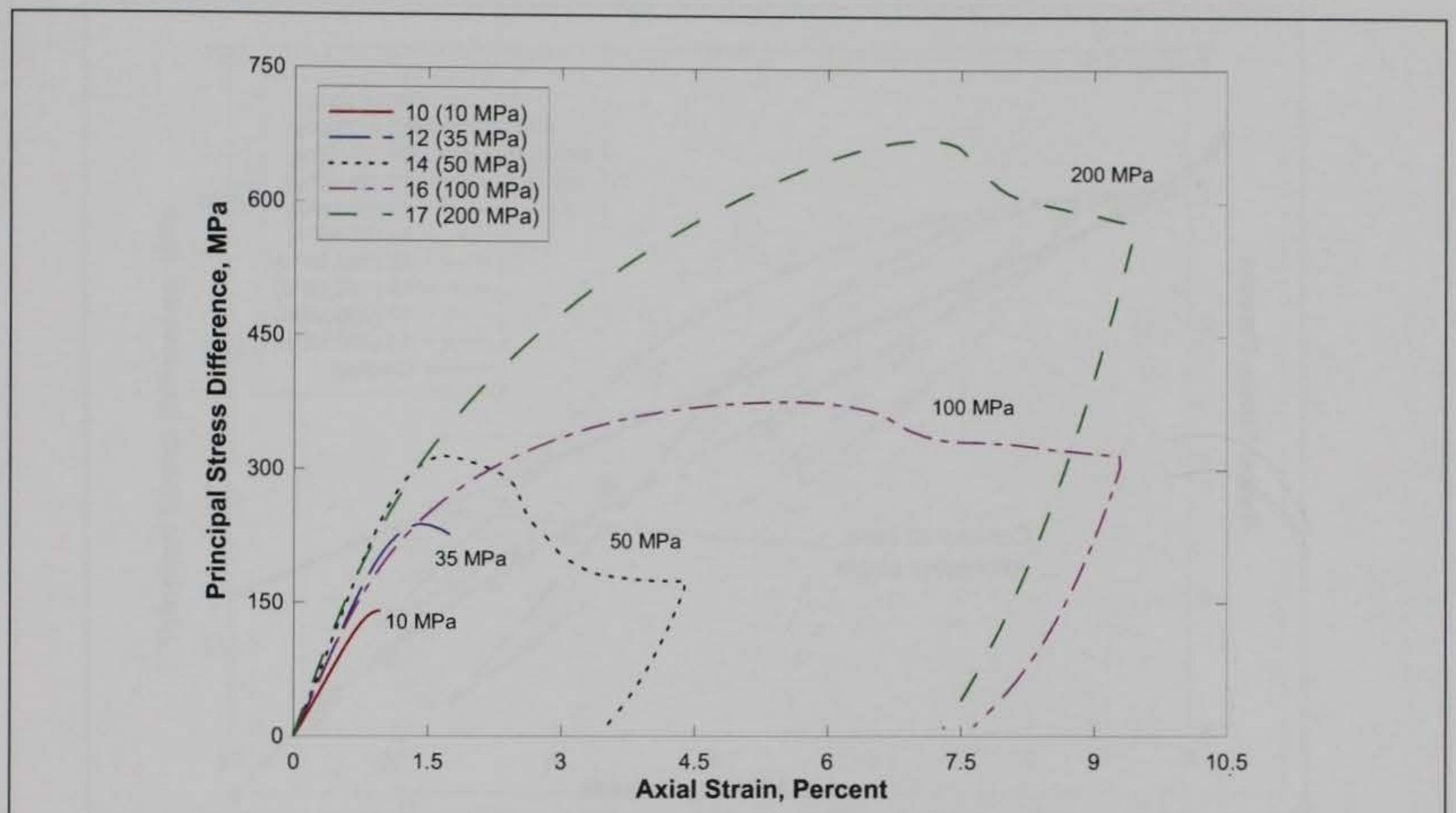


Figure 20. Stress-strain responses from TXC tests at confining pressures between 10 and 200 MPa.

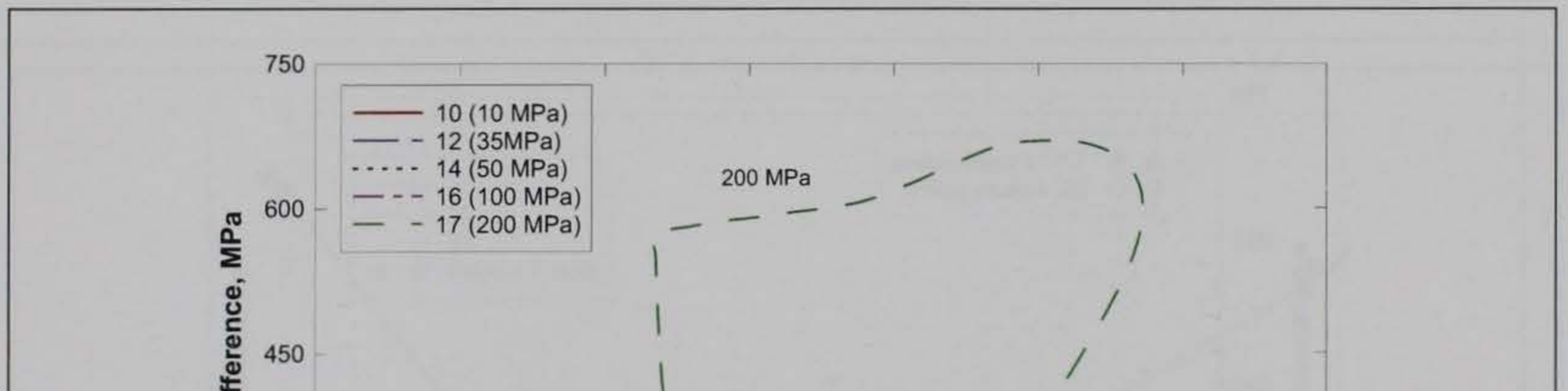


Figure 21. Stress difference-volumetric strain during shear from TXC tests at confining pressures between 10 and 200 MPa.

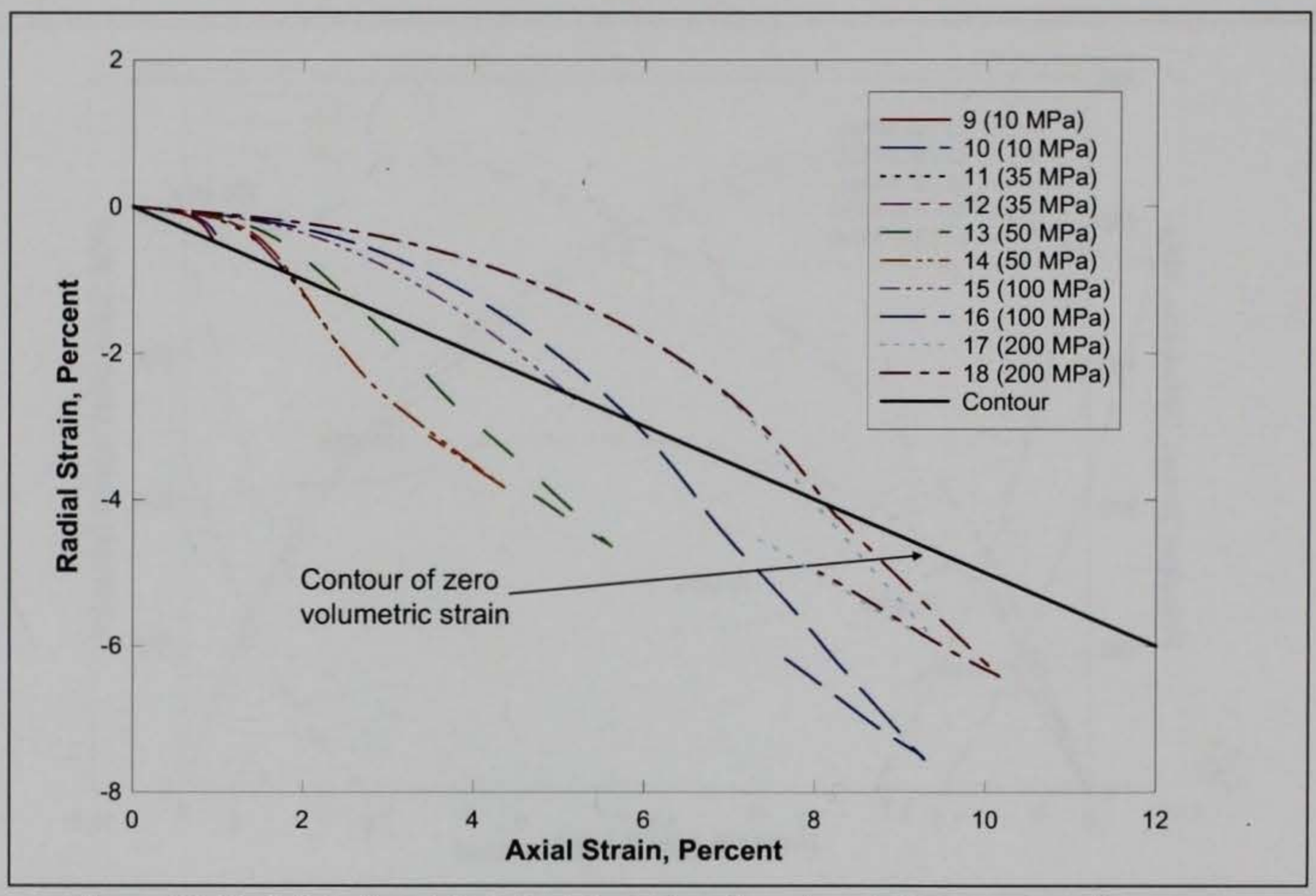


Figure 22. Radial strain-axial strain data during shear from TXC tests at confining pressures between 10 and 200 MPa.

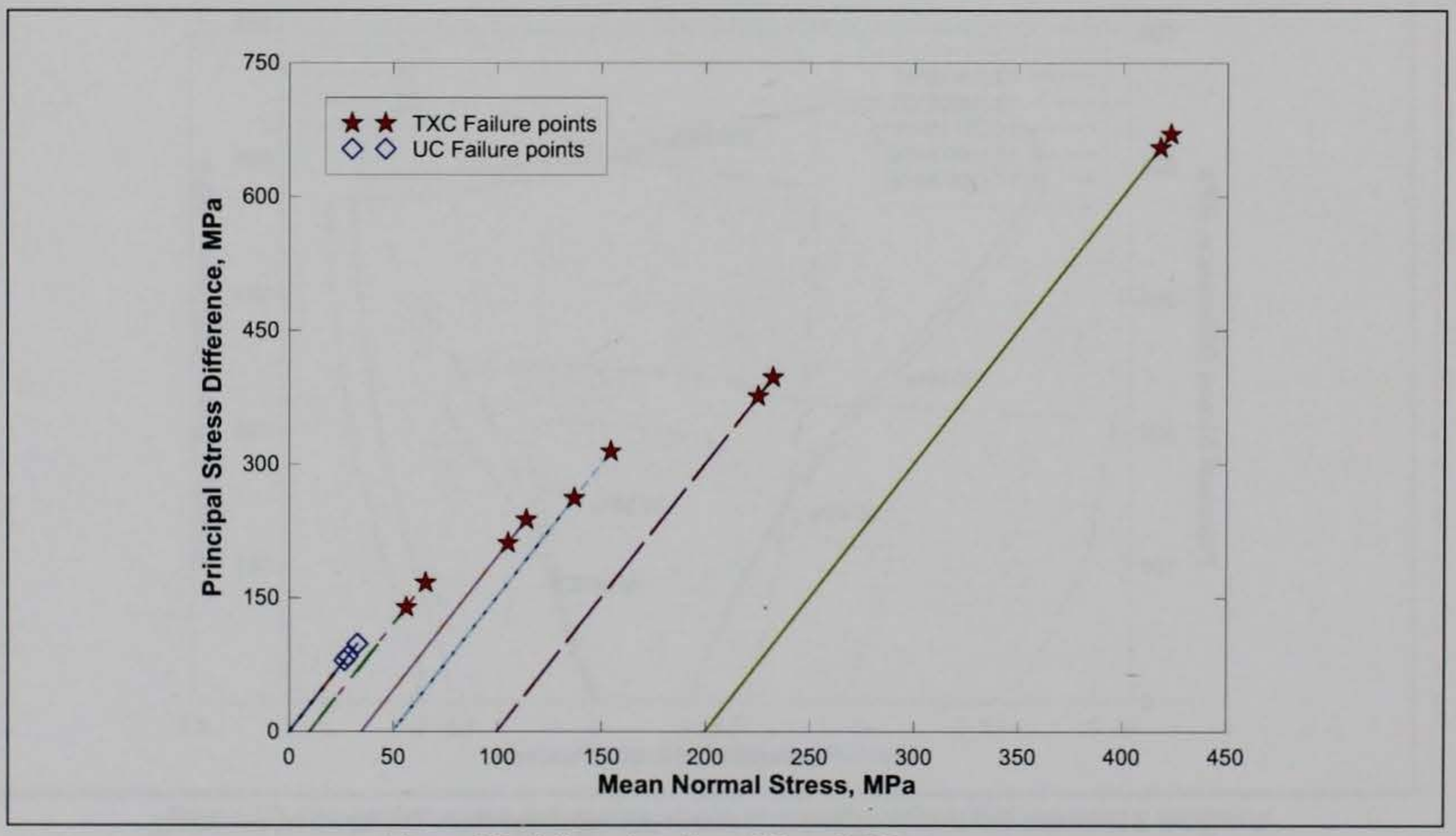


Figure 23. Failure data from UC and TXC tests.

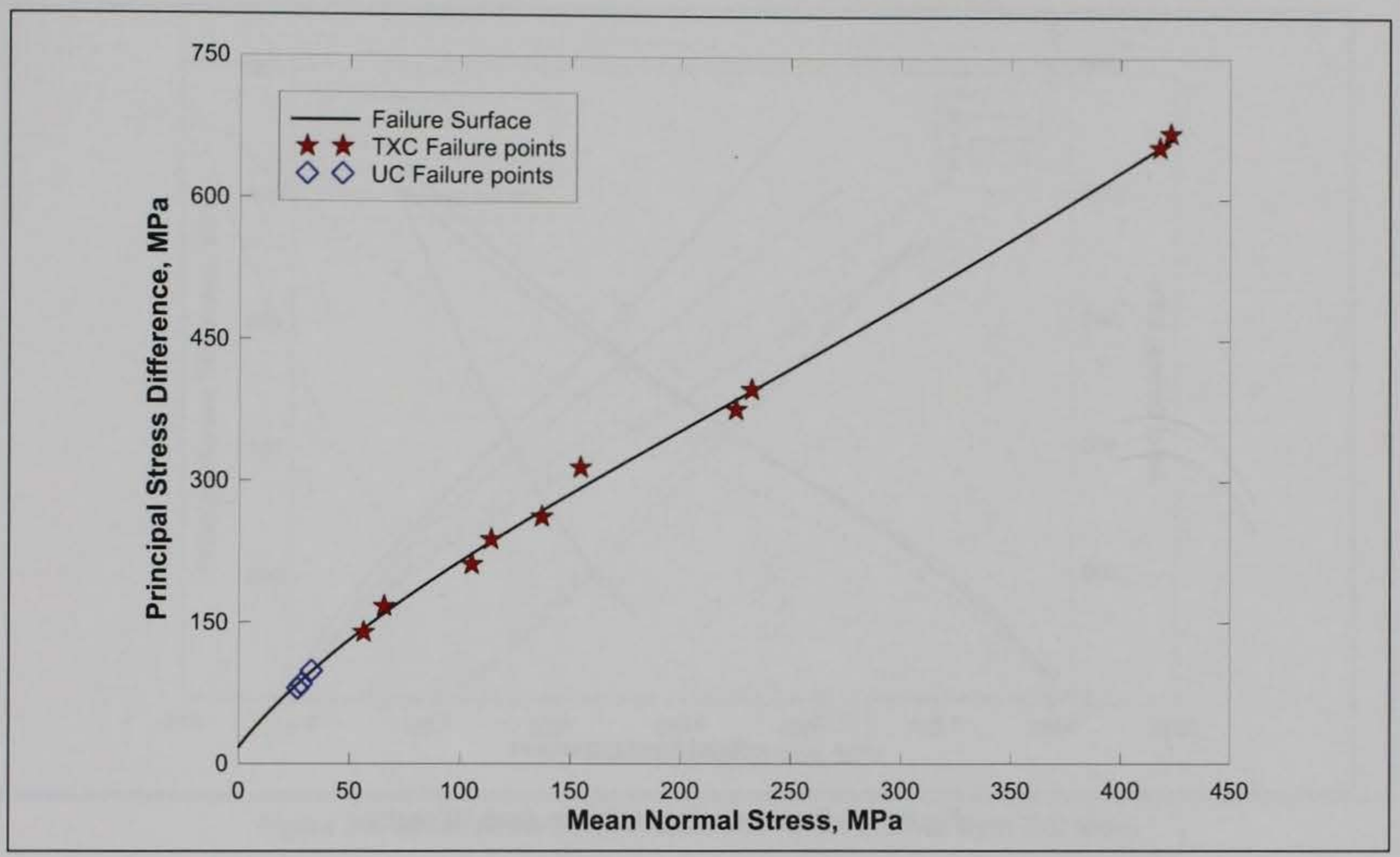


Figure 24. Failure data from UC and TXC tests and recommended failure surface.

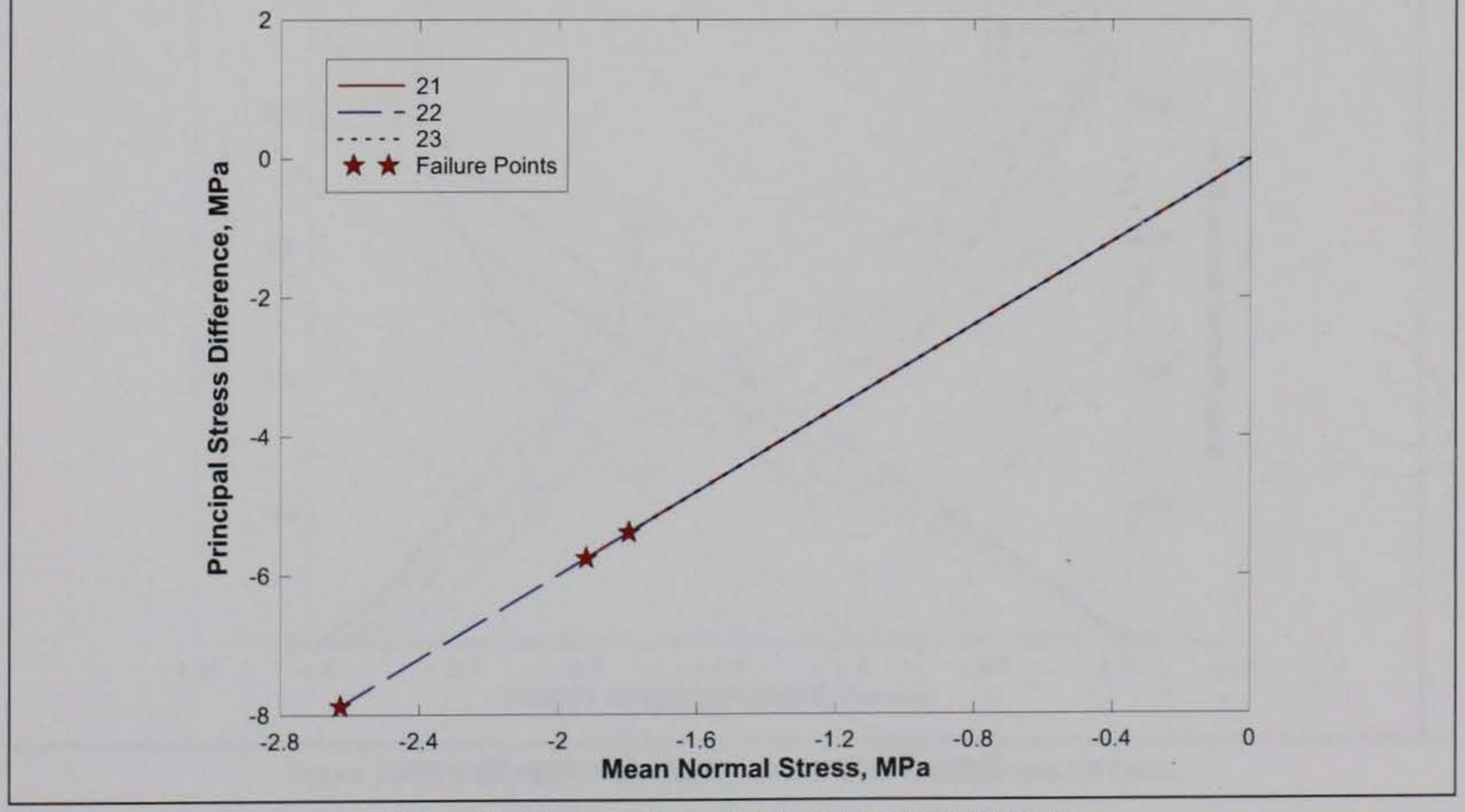


Figure 25. Stress paths and failure data from DP tests.

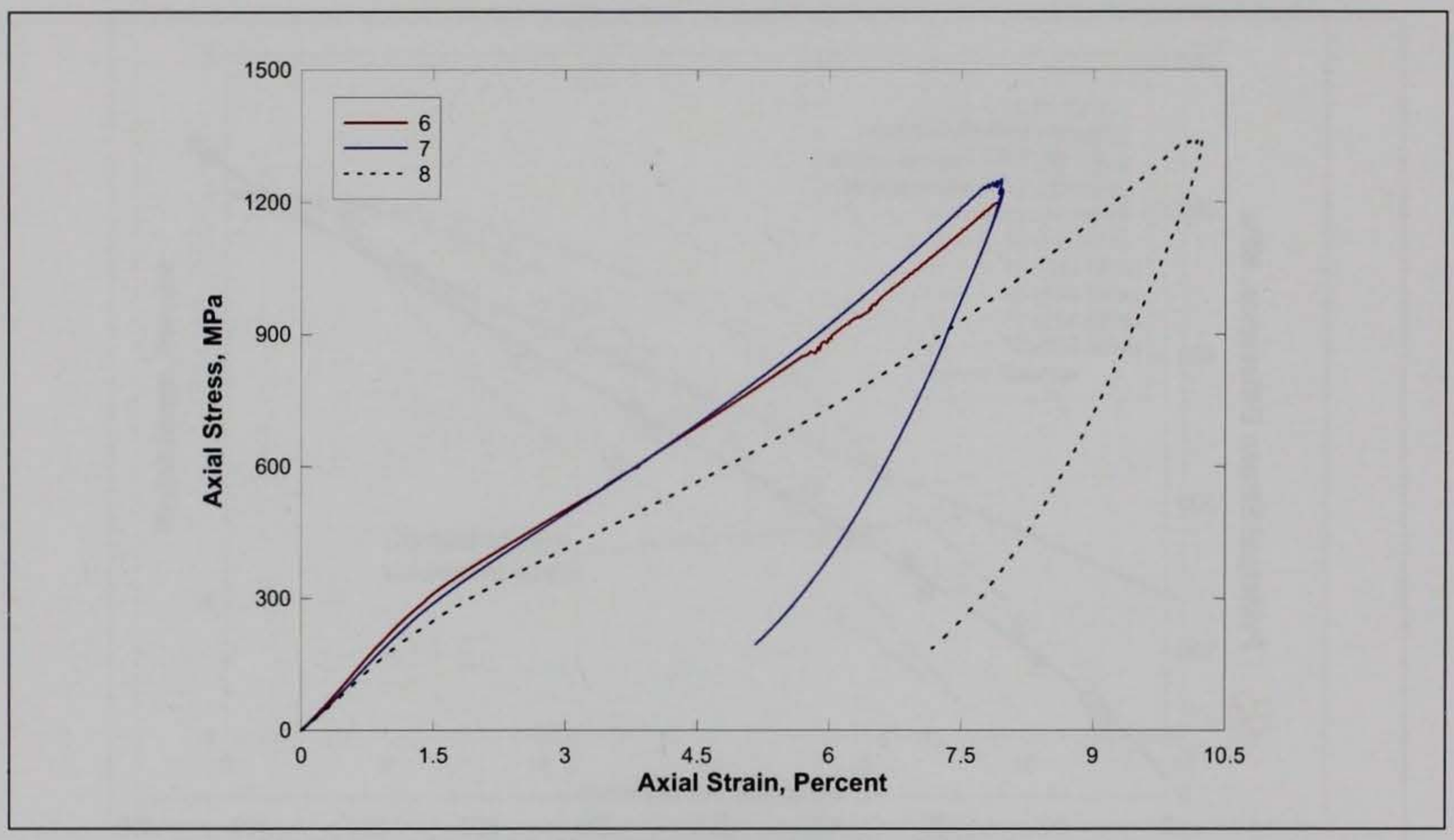


Figure 26. Stress-strain responses from UX tests.

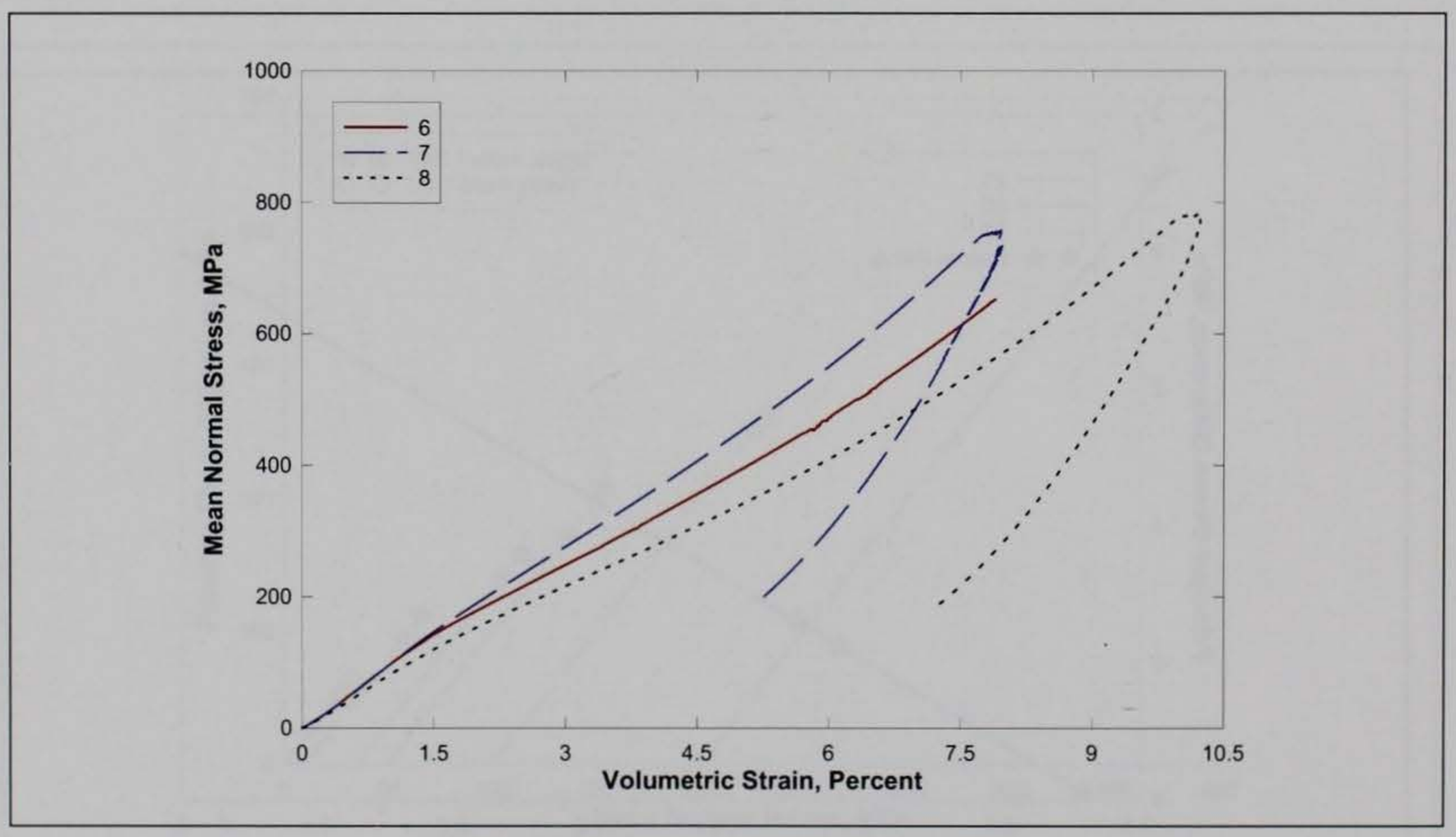


Figure 27. Pressure-volume data from UX tests.

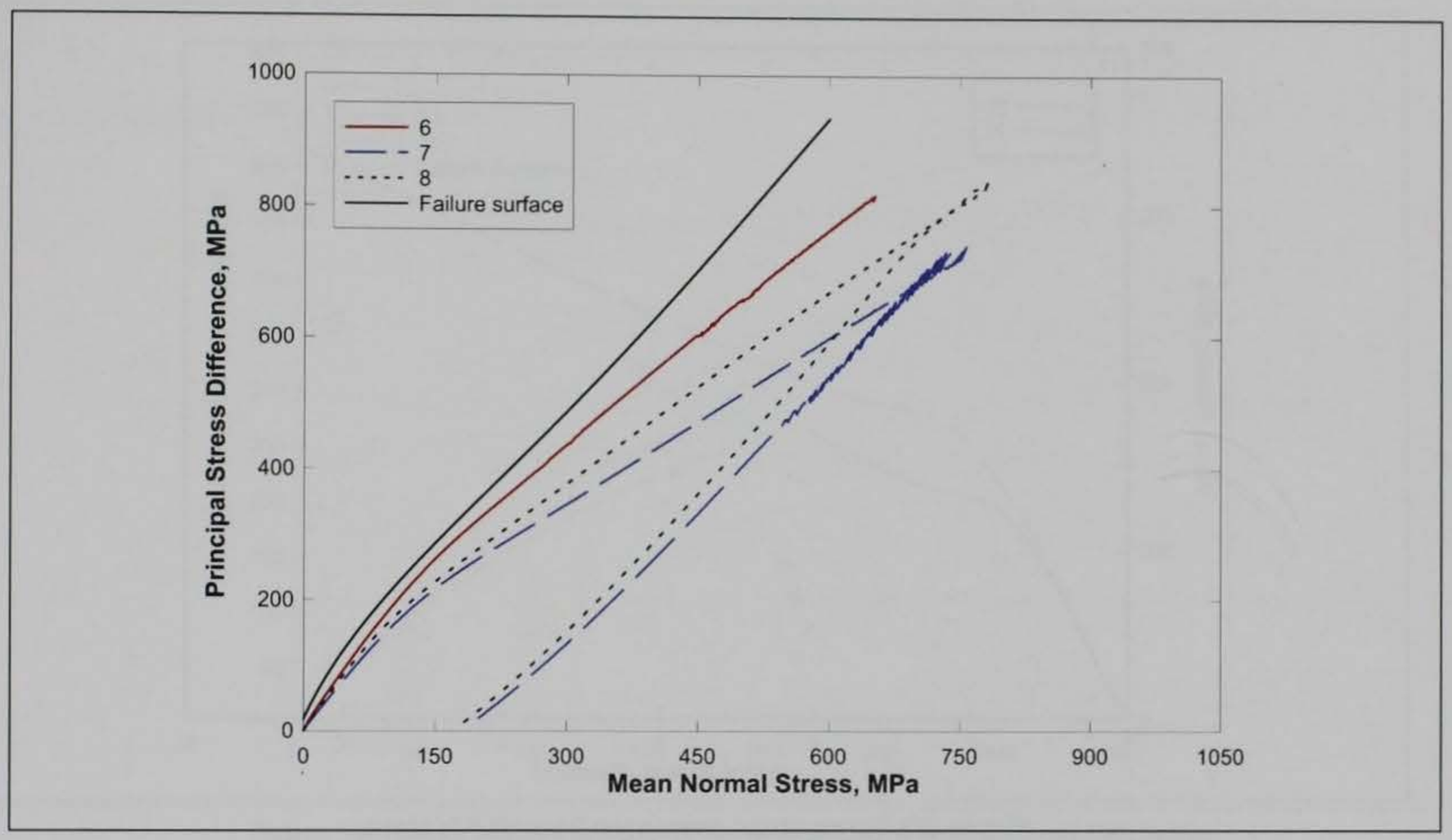


Figure 28. Stress paths from UX tests and failure surface from TXC tests.




Figure 29. Comparison of pressure-volume data from HC and UX tests.

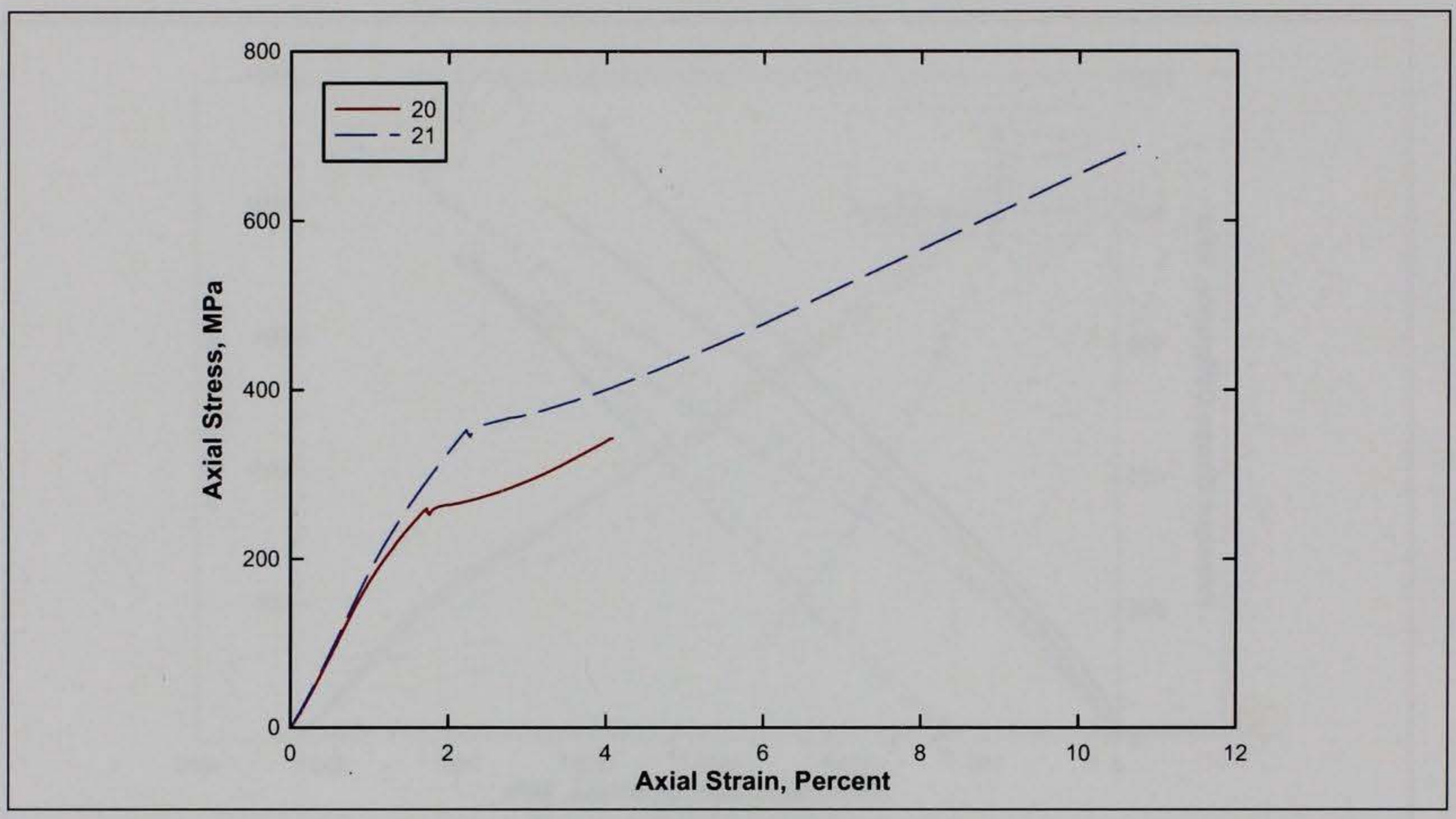


Figure 30. Stress-strain responses from UX/CV tests.

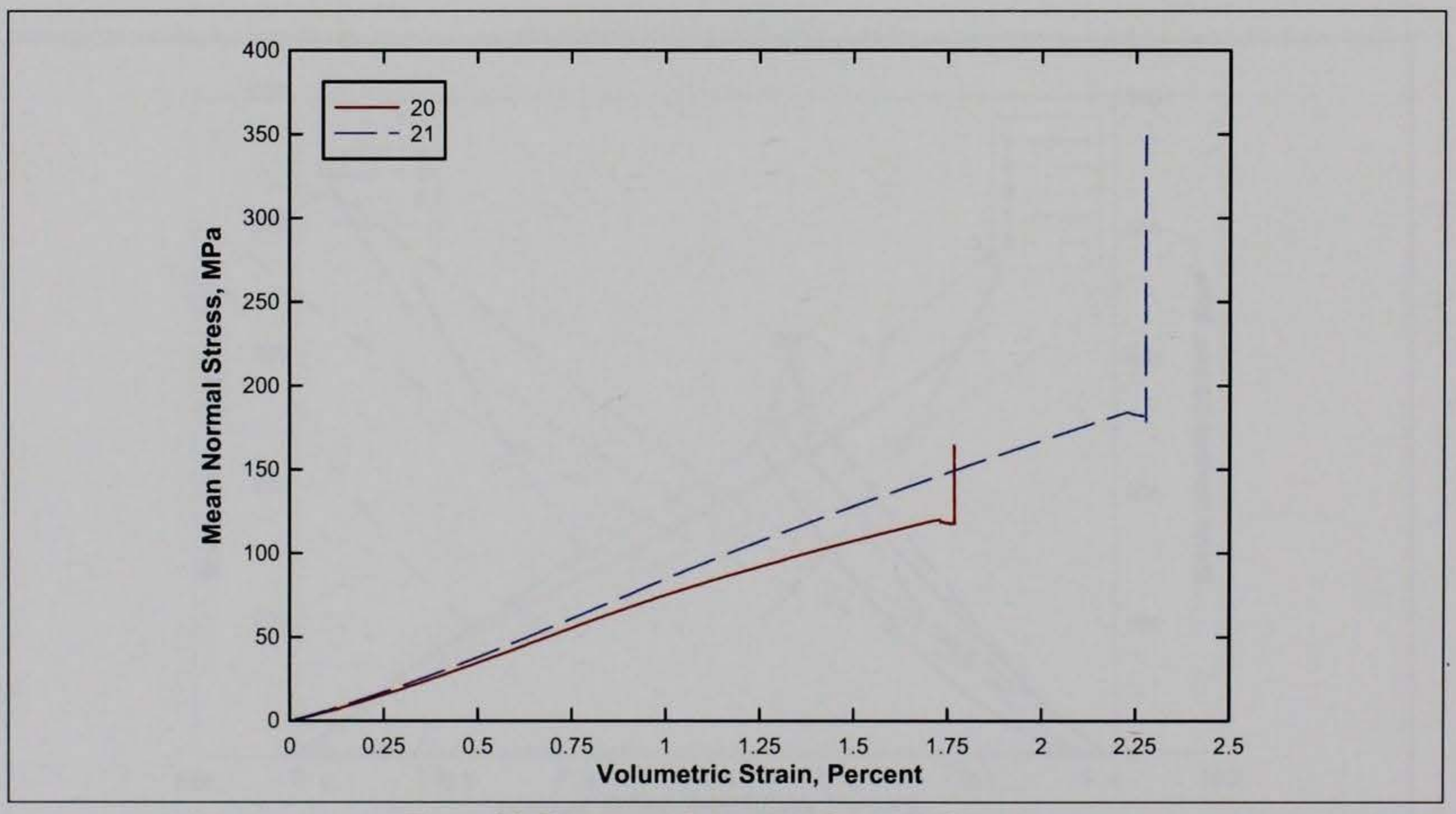


Figure 31. Pressure-volume data from UX/CV tests.

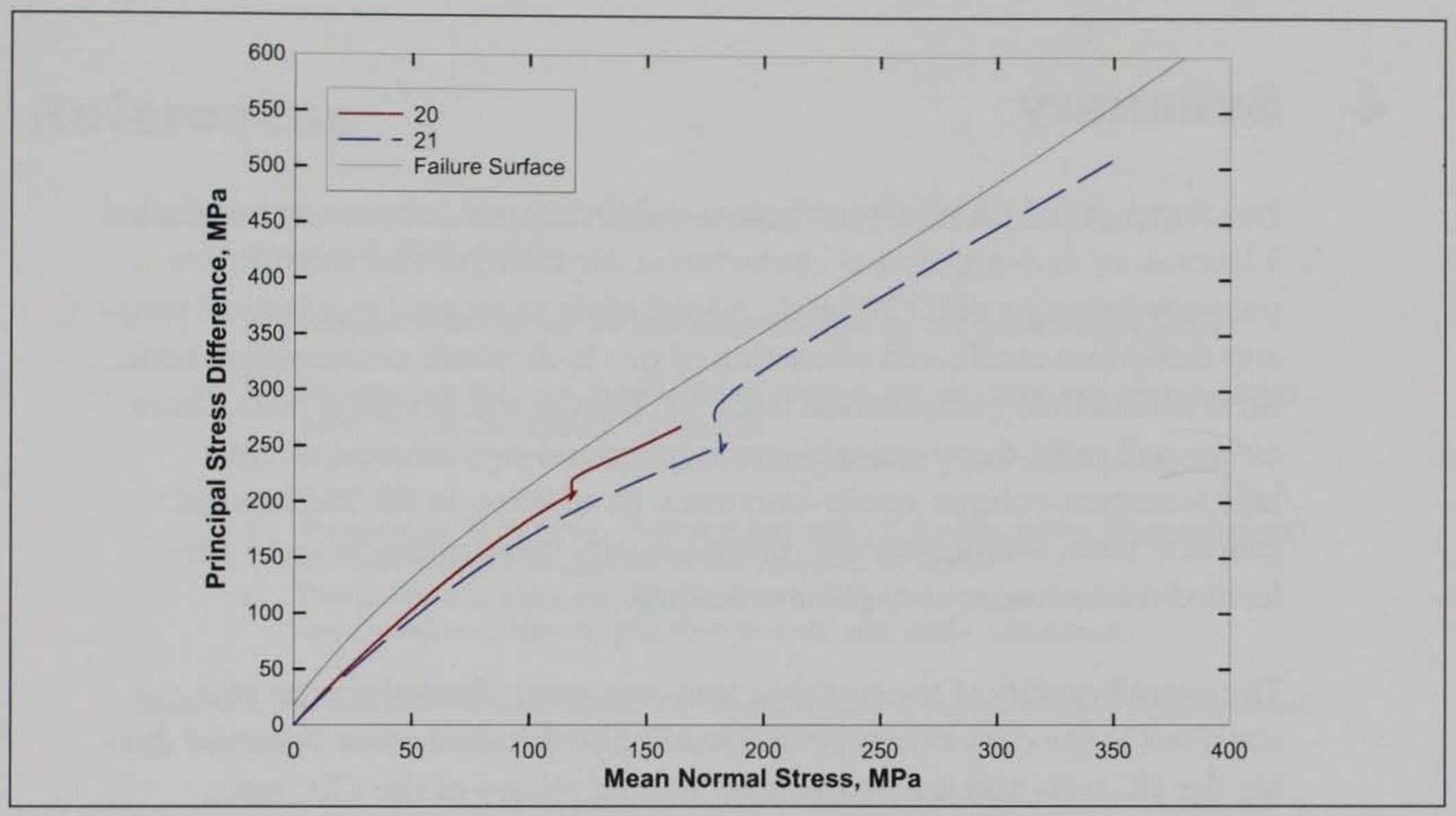


Figure 32. Stress paths from UX/CV tests and failure surface from TXC tests.

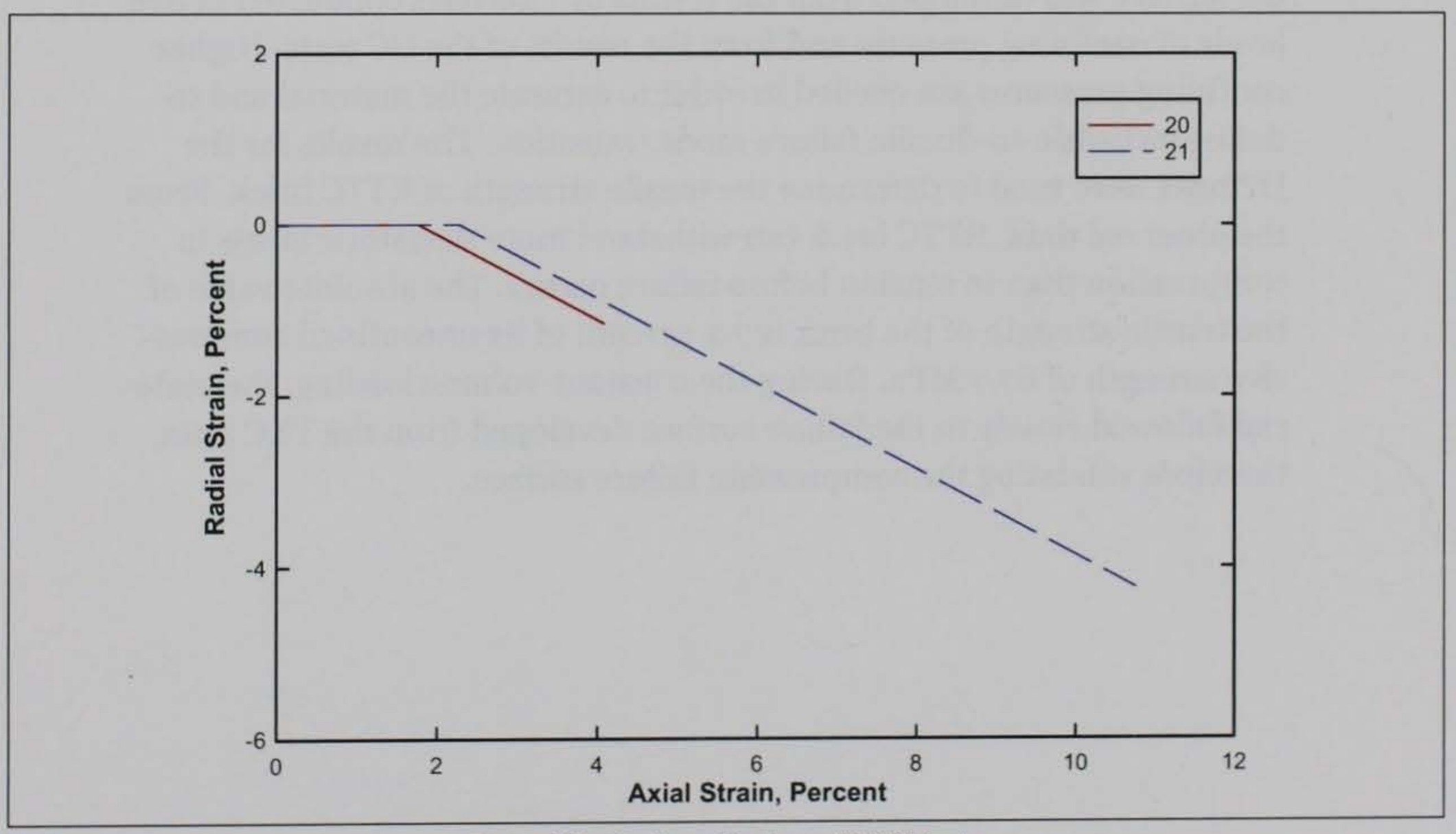


Figure 33. Strain paths from UX/CV tests.

# 4 Summary

Personnel of the ERDC Geotechnical and Structures Laboratory conducted a laboratory investigation to characterize the strength and constitutive property behavior of RTTC brick. A total of 23 successful mechanical property tests were conducted consisting of two hydrostatic compression tests, three unconfined compression tests, ten triaxial compression tests, three direct-pull tests, three uniaxial strain tests, and two uniaxial-strain-load/constant-volume-strain-load tests. In addition to the mechanical property tests, nondestructive, pulse-velocity measurements were performed on each specimen prior to testing.

The overall quality of the test data was very good; limited scatter was observed in the data over repeated loading paths. Creep was observed during the HC tests and the hydrostatic loading phases of the TXC tests. Results from the TXC tests exhibited a continuous increase in principal stress difference with corresponding increases in confining stress, indicating that the brick did not reach a fully saturated state. A compression failure surface was developed from the results of TXC tests conducted at five levels of confining pressure and from the results of the UC tests. Higher confining pressures are needed in order to saturate the material and to define its brittle-to-ductile failure mode transition. The results for the DP tests were used to determine the tensile strength of RTTC brick. From the observed data, RTTC brick can withstand more deviatoric stress in compression than in tension before failure occurs. The absolute value of the tensile strength of the brick is 7.2 percent of its unconfined compressive strength of 87.7 MPa. During the constant-volume loading, the material followed closely to the failure surface developed from the TXC tests, therefore validating the compression failure surface.

# References

American Society for Testing and Materials. 2005. *2005 Annual Book of ASTM Standards*. Philadelphia, PA.

a. Designation C 39-05. Standard test method for compressive strength of concrete specimens.
b. Designation C 42-04. Standard test method for obtaining and testing drilled cores and sawed beams of concrete.
c. Designation C 597-02. Standard test method for pulse velocity through concrete.
d. Designation D 2216-05. Standard test method for laboratory determination of water (moisture) content of soil and rock by mass.
e. Designation D 4543-04. Standard test method for preparing rock core specimens and determining dimensional and shape tolerances.

Bishop, A. W., and D. J. Henkel. 1962. *The measurement of soil properties in the triaxial test*. London: Edward Arnold, Ltd. 72–74.

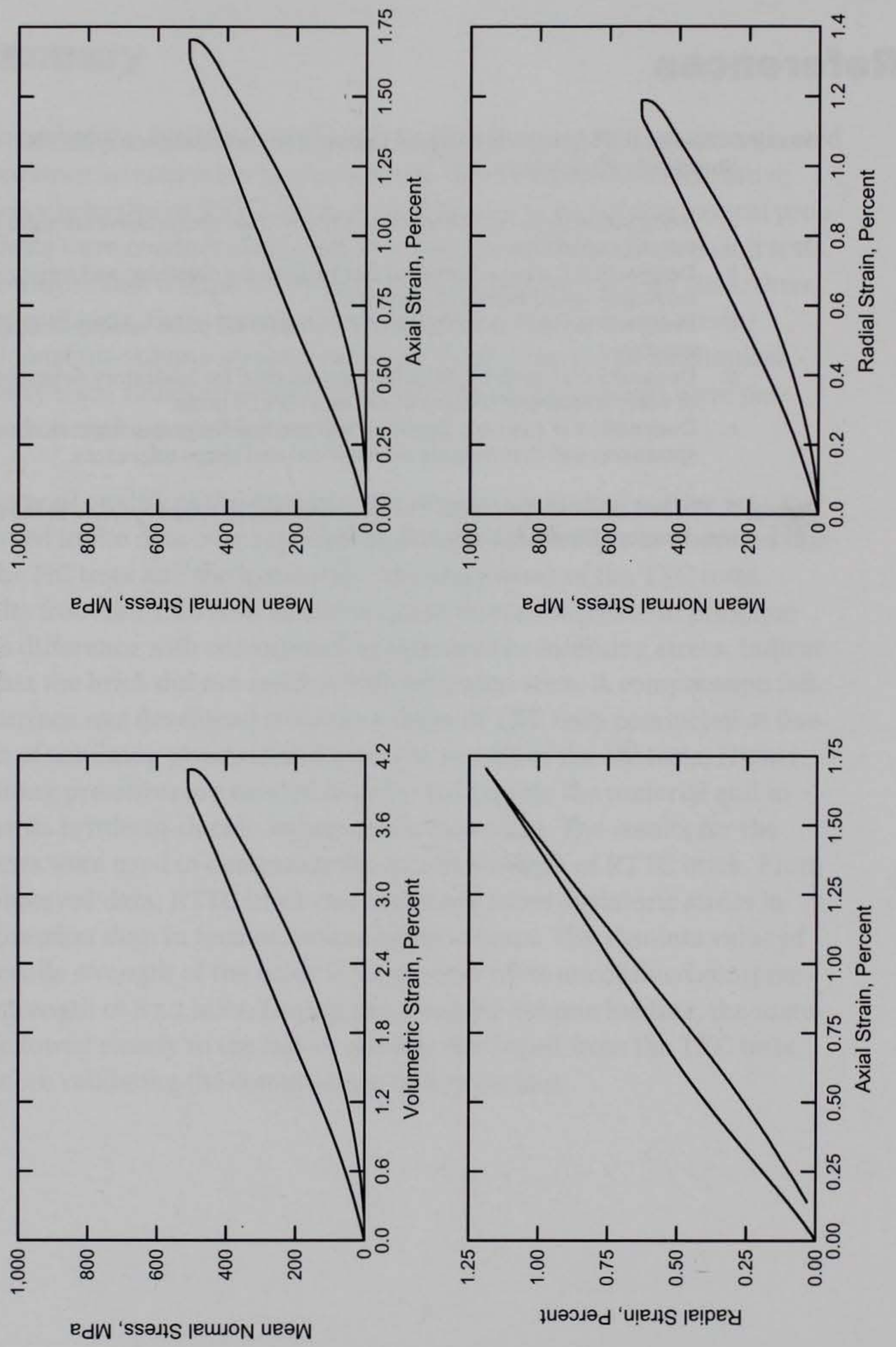
RTTC BRICK
Test. No. 4
Mean Normal Stress, MPa
1,000
800
600
400
200
0
0.00 0.25 0.50 0.75 1.00 1.25 1.50 1.75
Axial Strain, Percent
Mean Normal Stress, MPa
1,000
800
600
400
200
0
0.0 0.2 0.4 0.6 0.8 1.0 1.2 1.4
Radial Strain, Percent
Mean Normal Stress, MPa
1,000
800
600
400
200
0
0.0 0.6 1.2 1.8 2.4 3.0 3.6 4.2
Volumetric Strain, Percent
Radial Strain, Percent
1.25
1.00
0.75
0.50
0.25
0.00
0.00 0.25 0.50 0.75 1.00 1.25 1.50 1.75
Axial Strain, Percent

Plate 1

RTTC BRICK
Test. No. 5

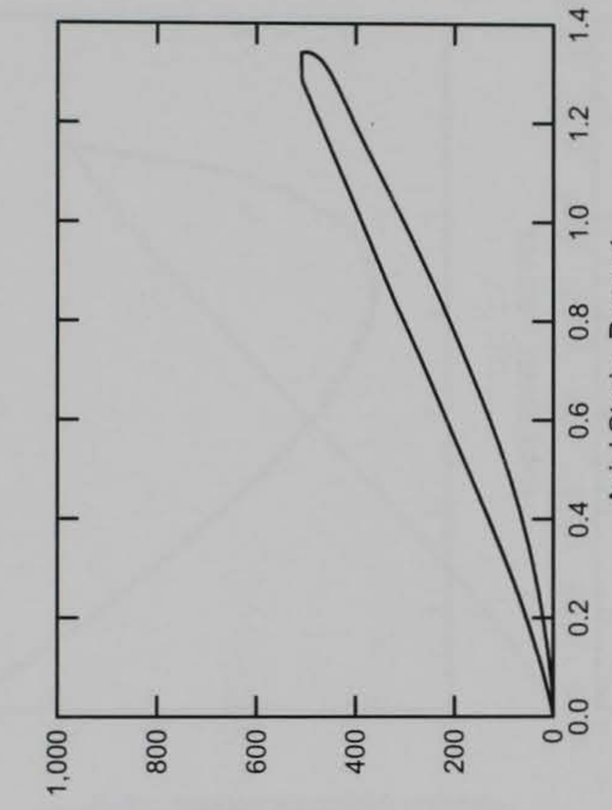


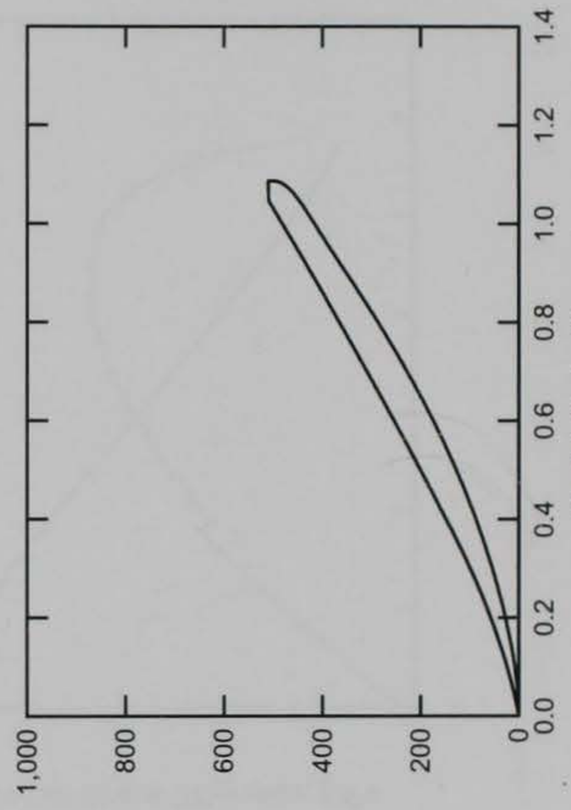


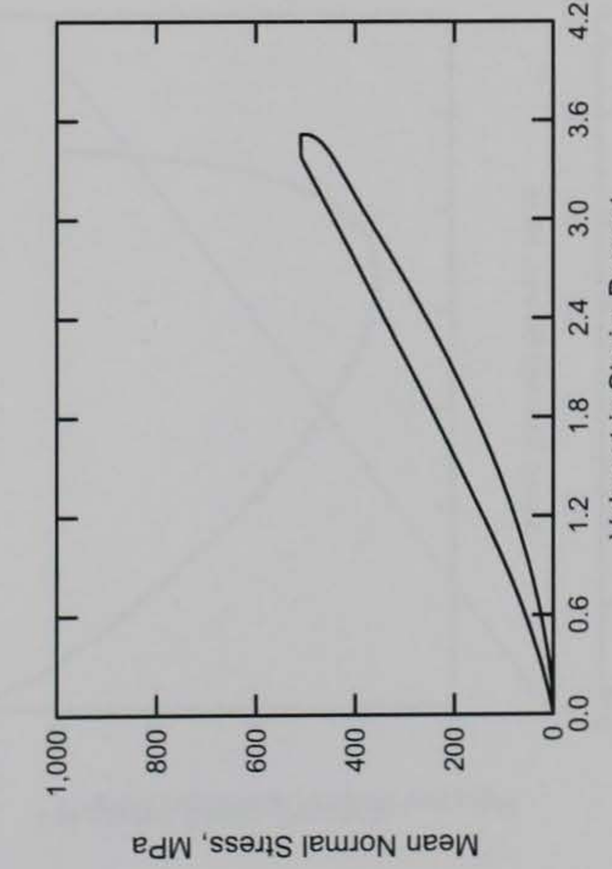


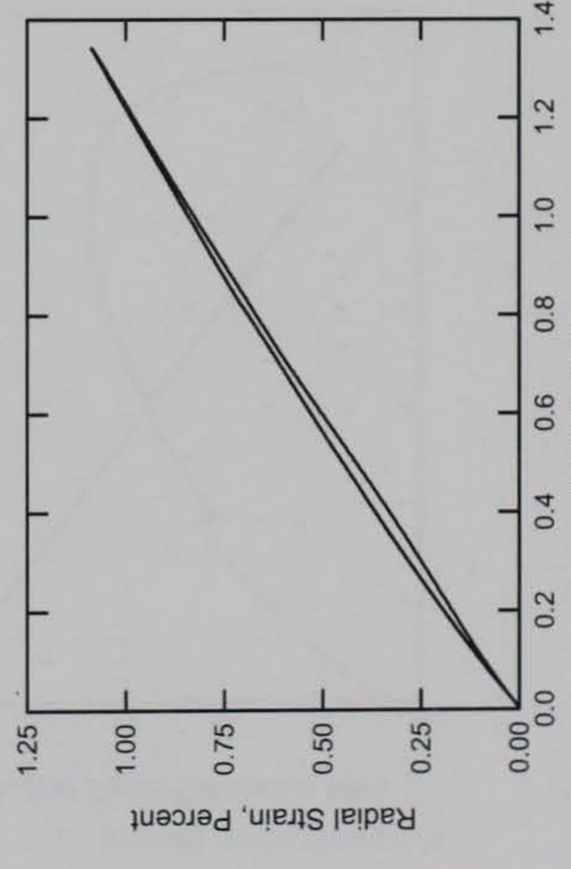


Plate 2

RTTC BRICK
Test No. 1

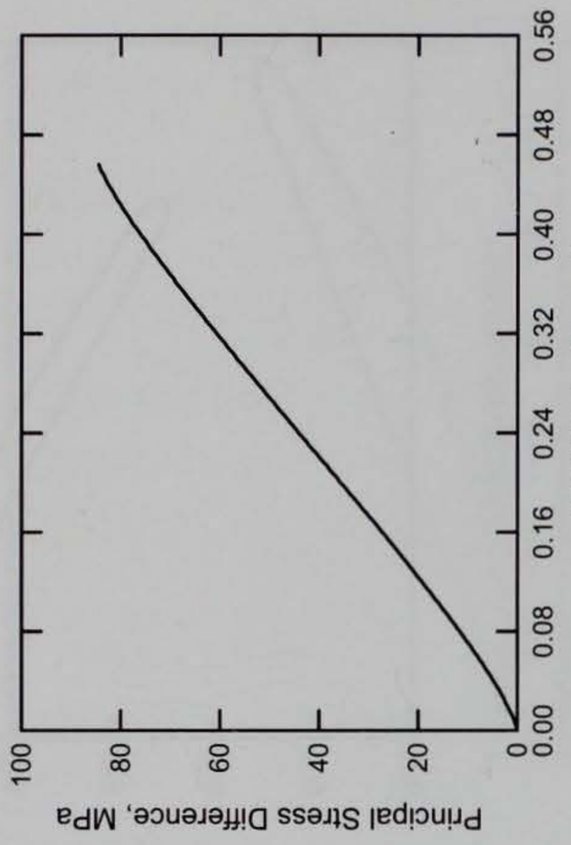


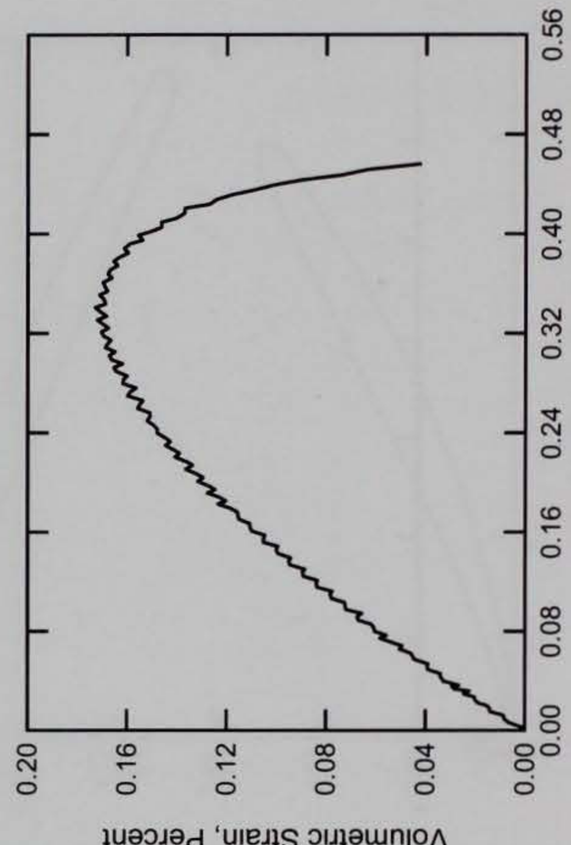


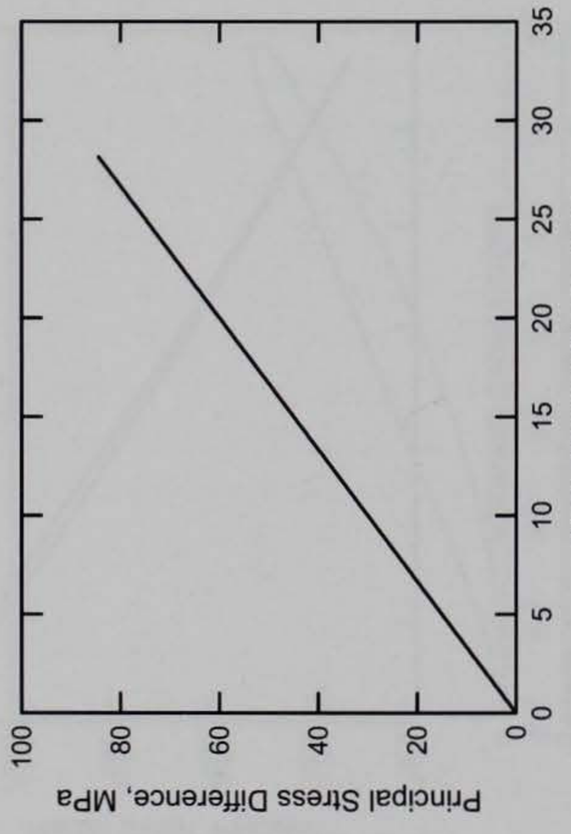


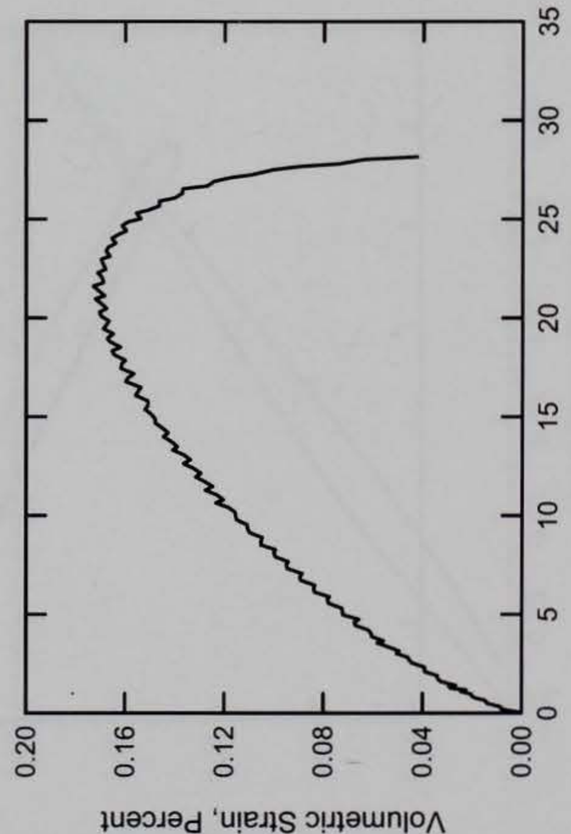


Plate 3

RTTC BRICK
Test No. 2

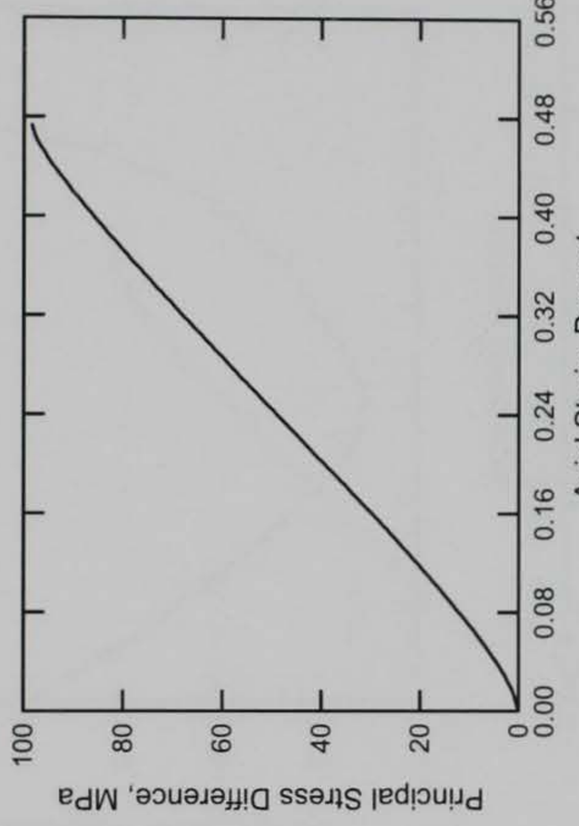


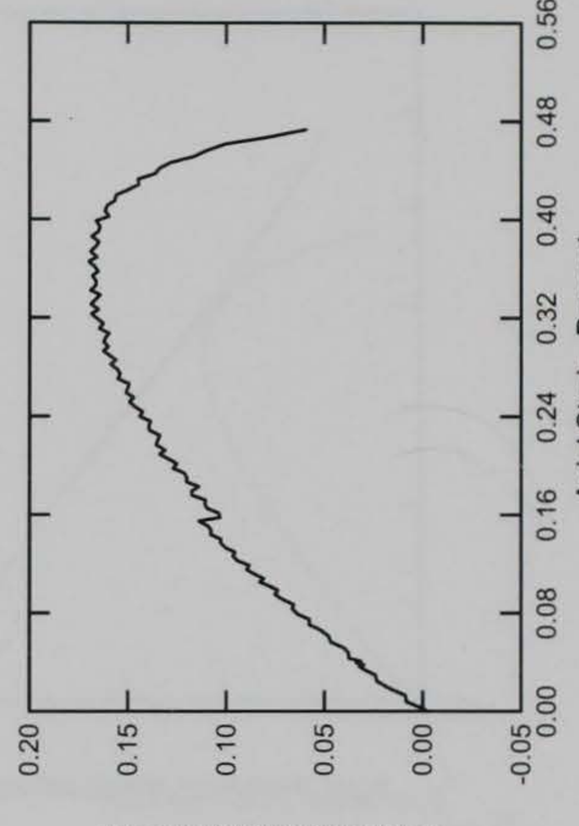


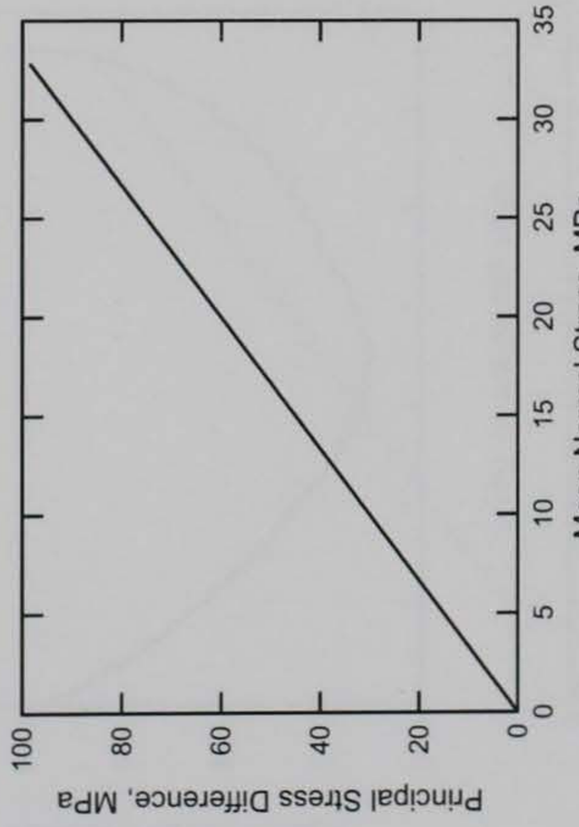


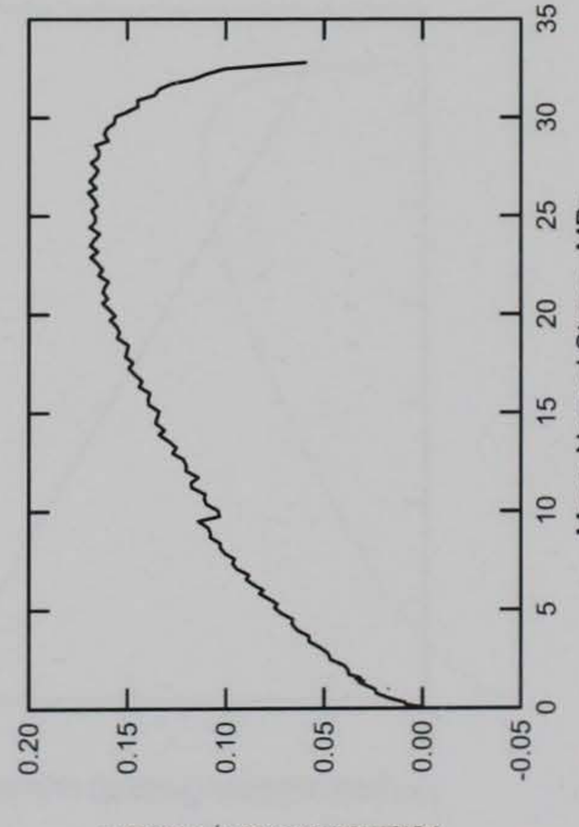


Plate 4

RTTC BRICK
Test No. 3

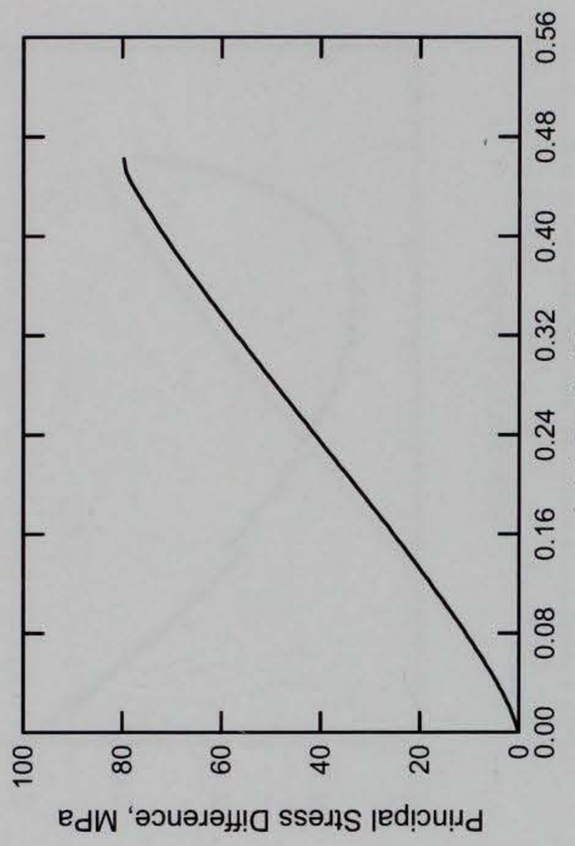


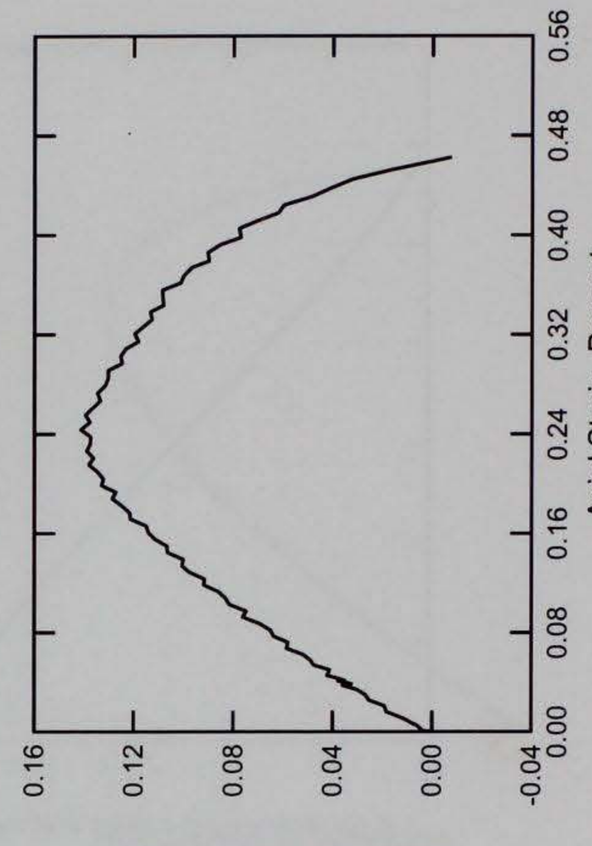


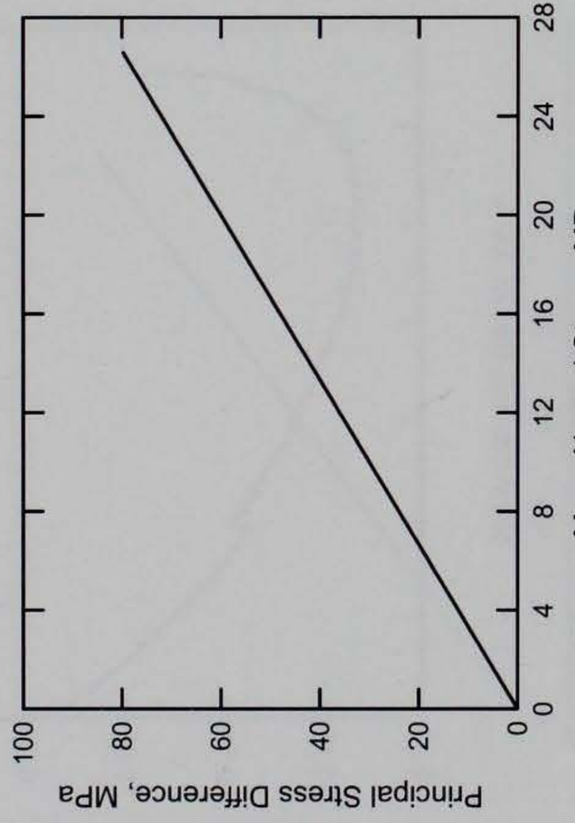


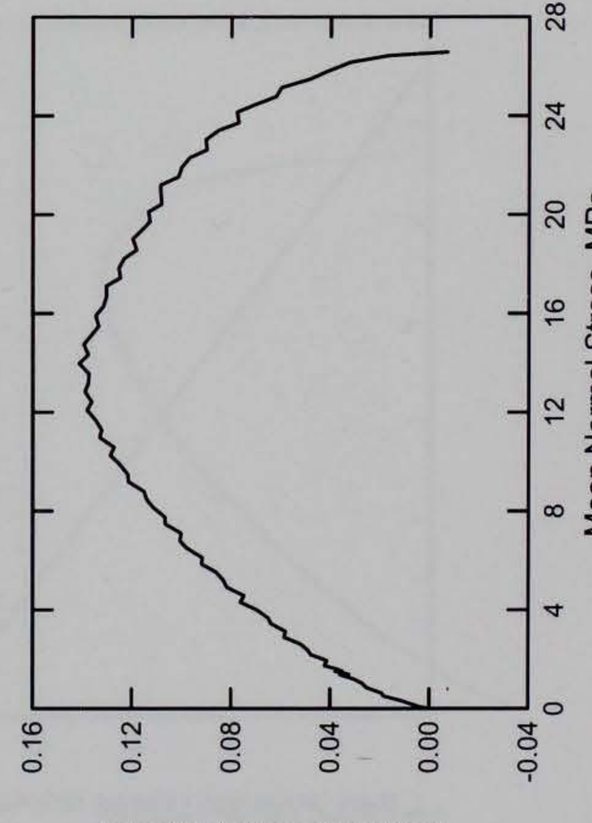


Plate 5

RTTC BRICK
Test No. 9

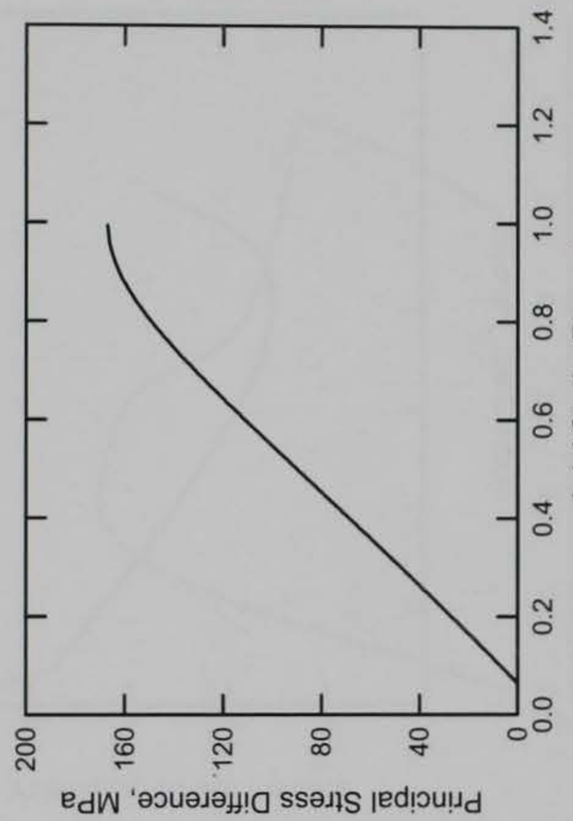


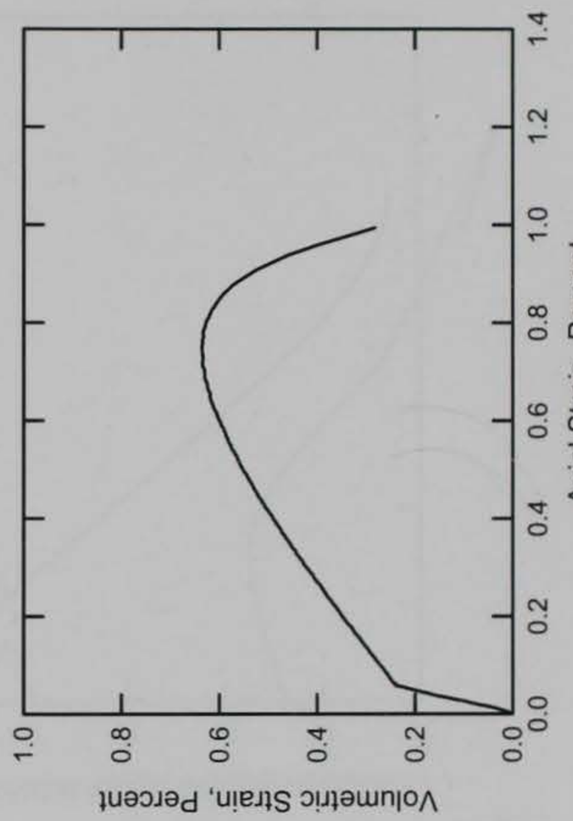


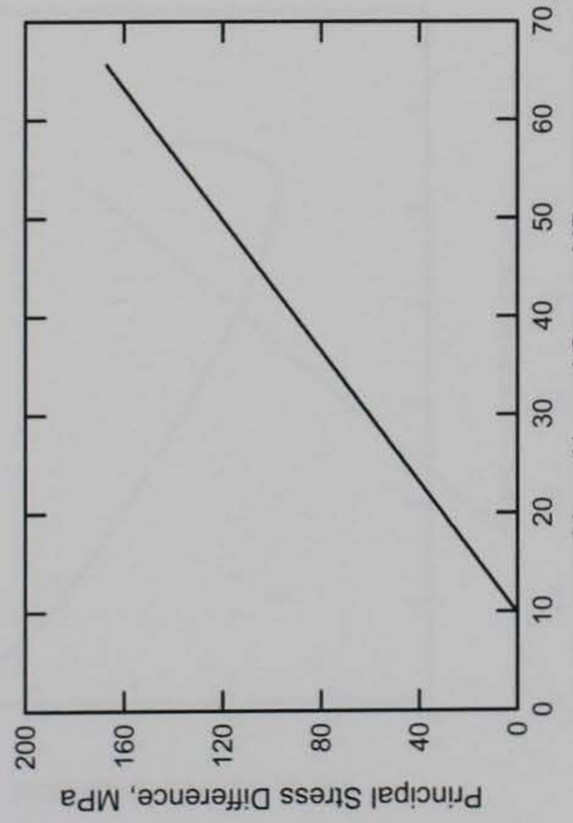


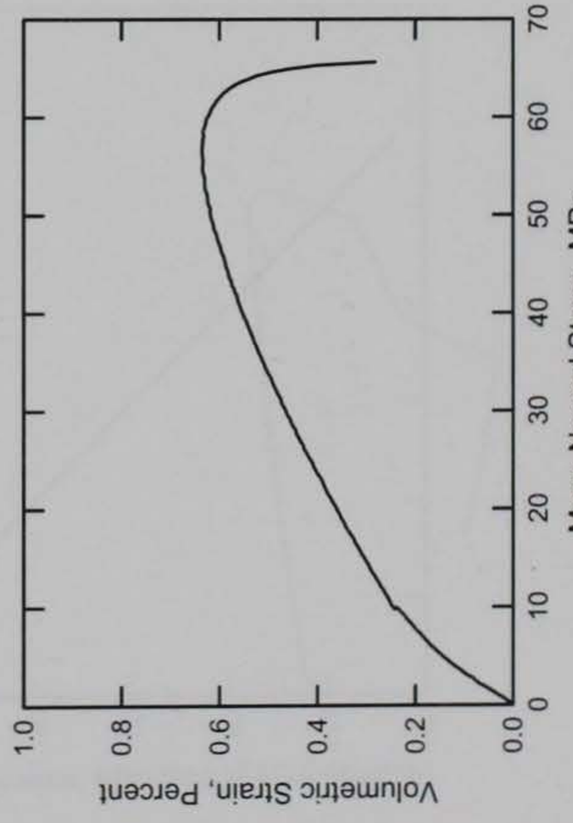


Plate 6

RTTC BRICK
Test No. 10

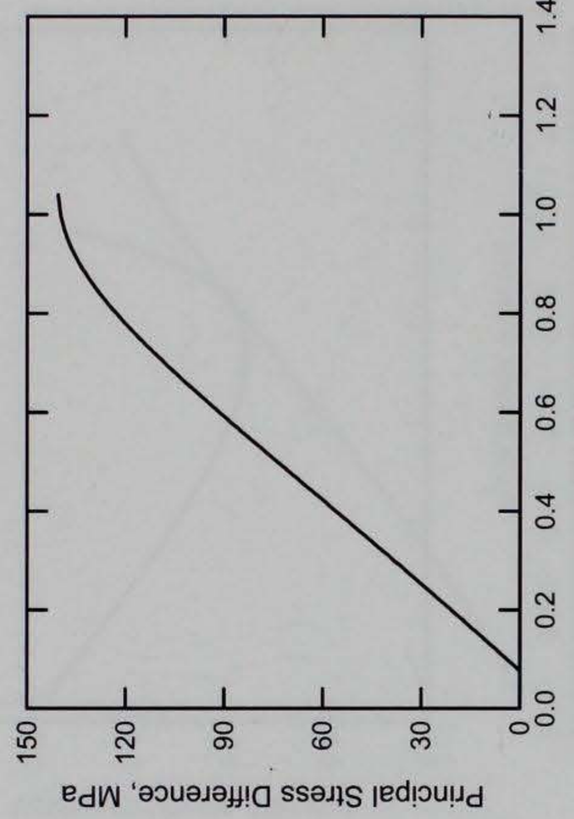





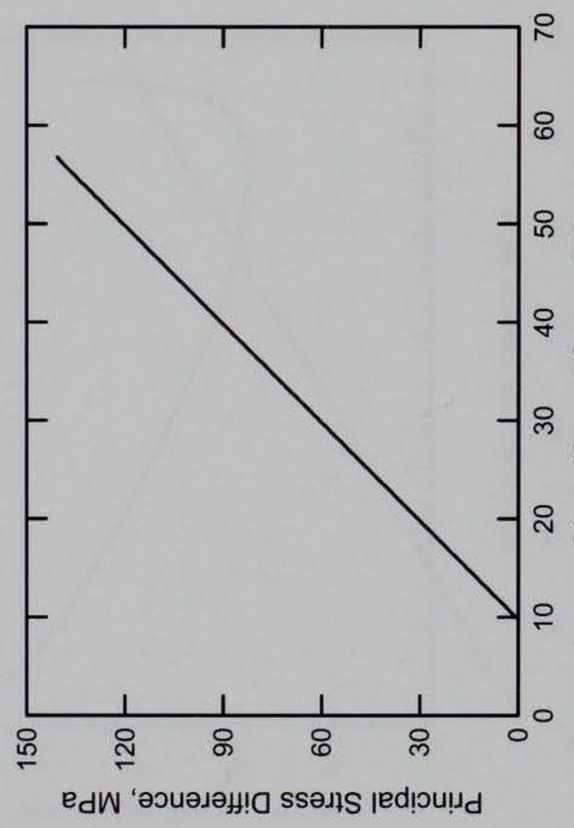





Plate 7

RTTC BRICK
Test No. 11

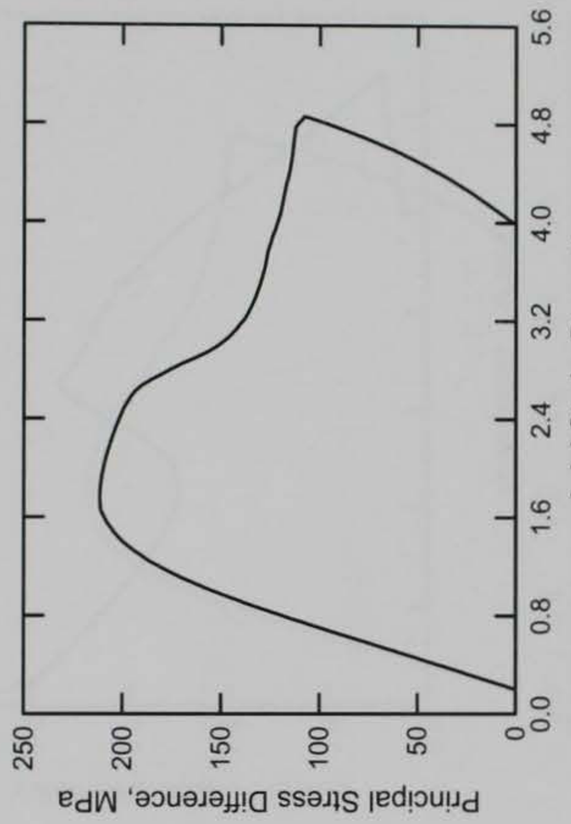


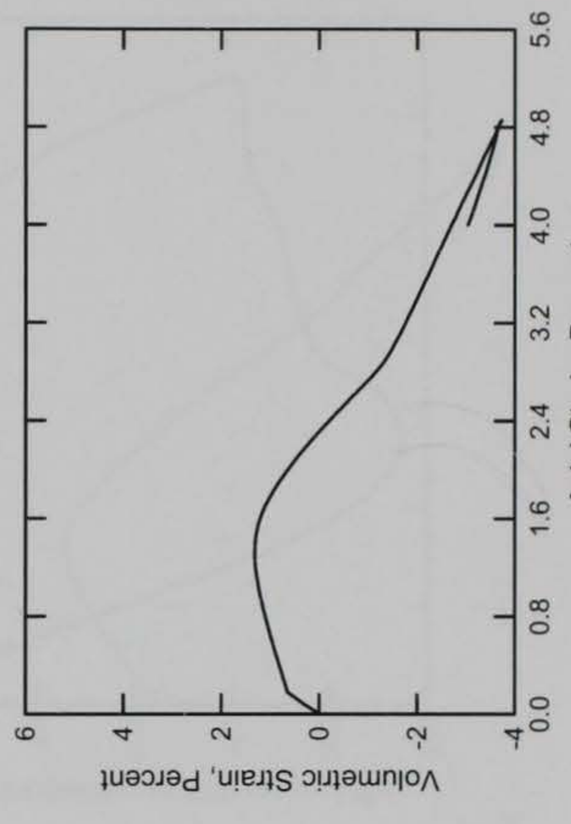


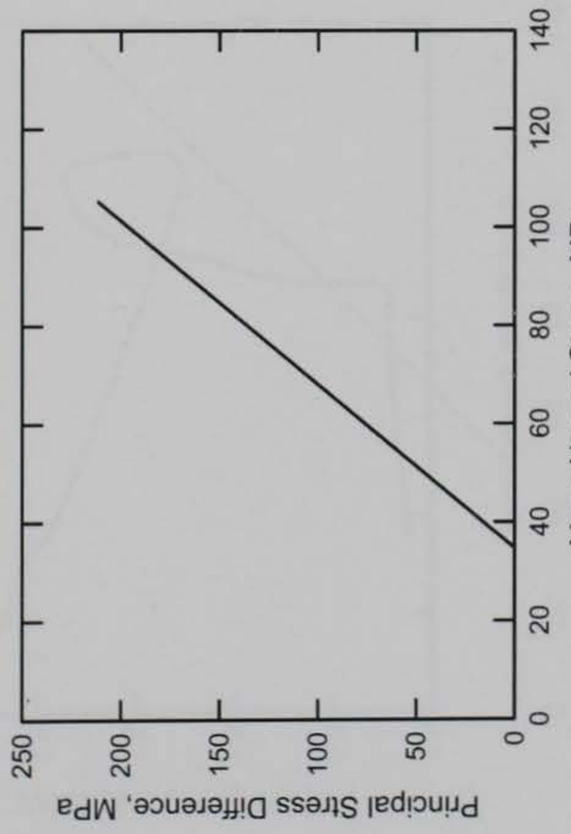


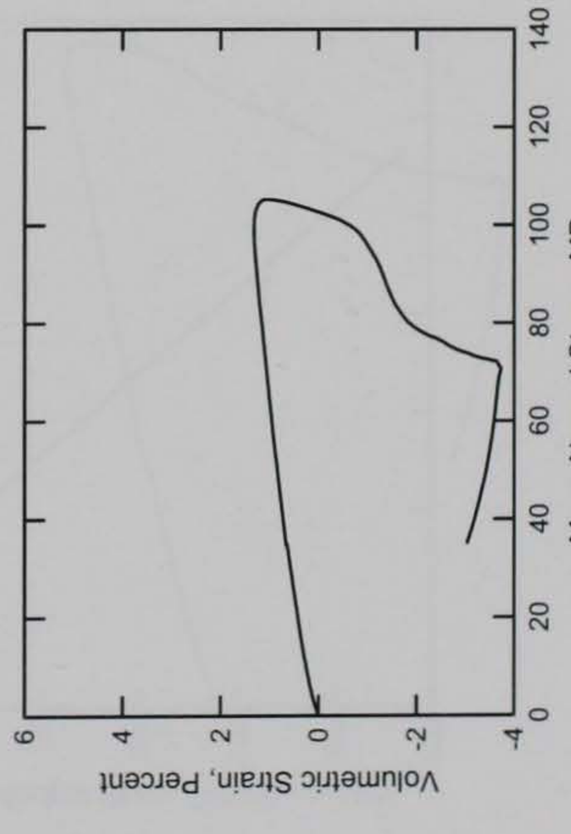


Plate 8

RTTC BRICK
Test No. 12

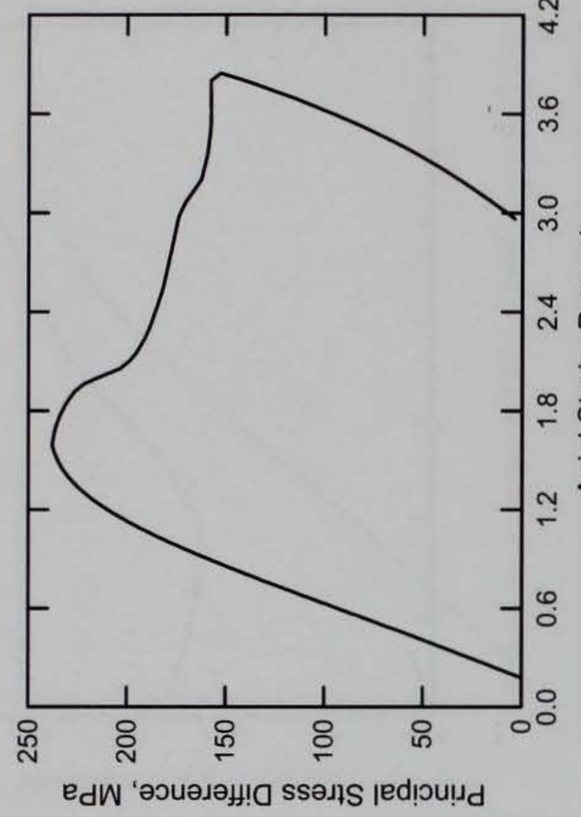


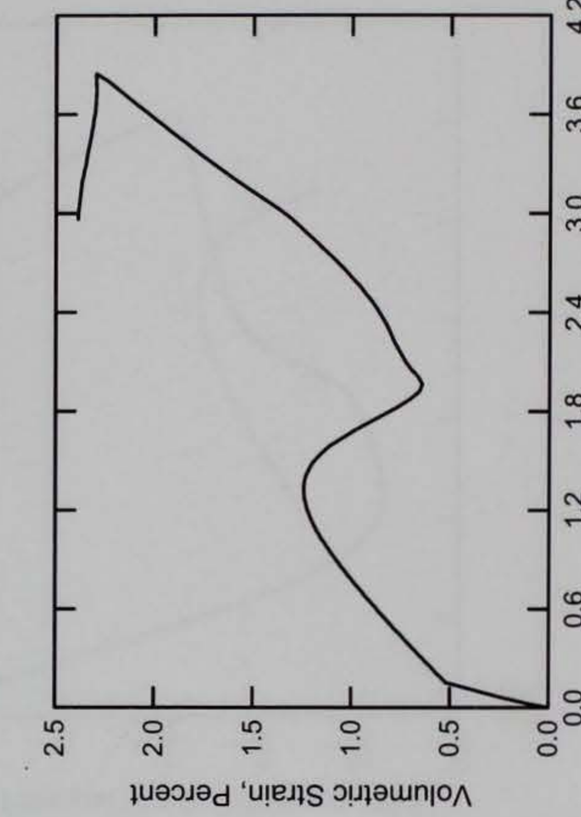


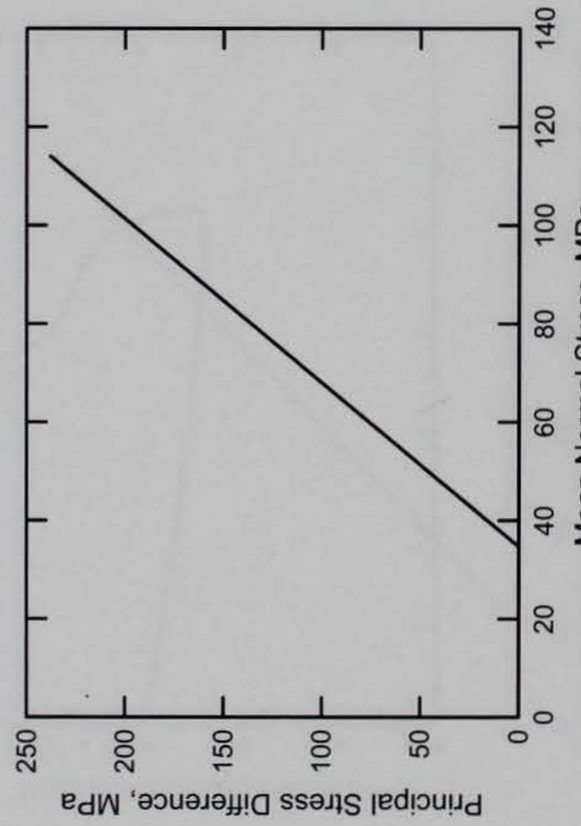


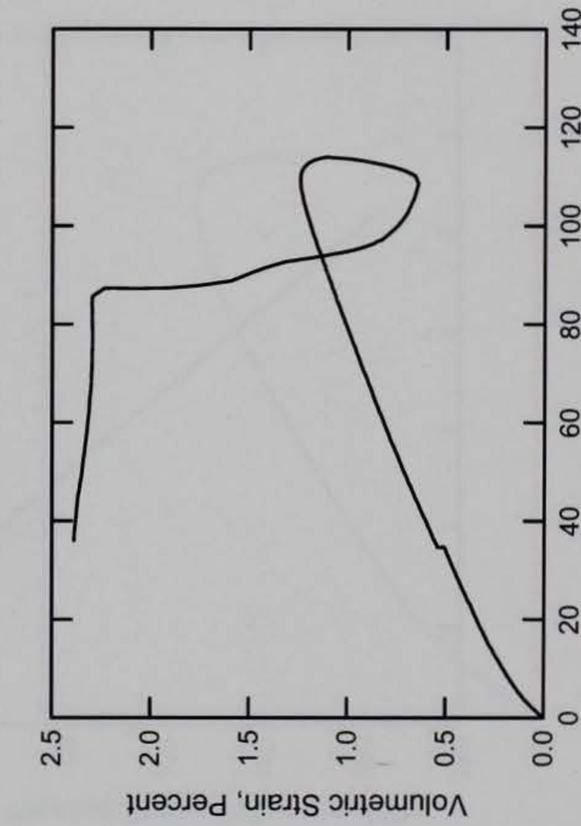


Plate 9

RTTC BRICK
Test No. 13

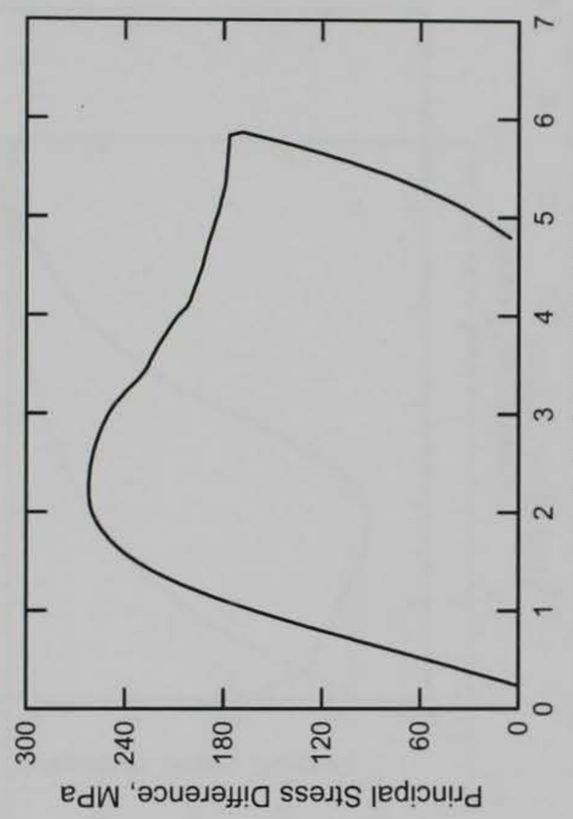





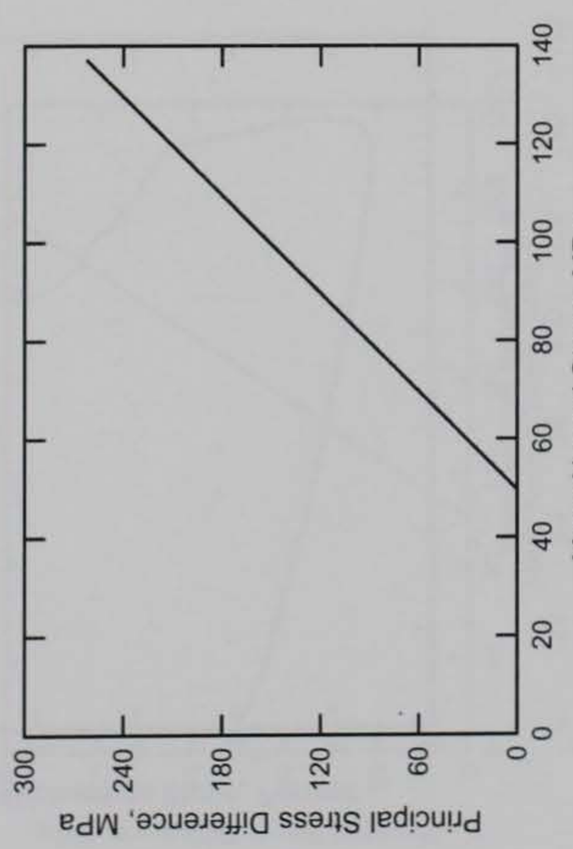





Plate 10

RTTC BRICK
Test No. 14

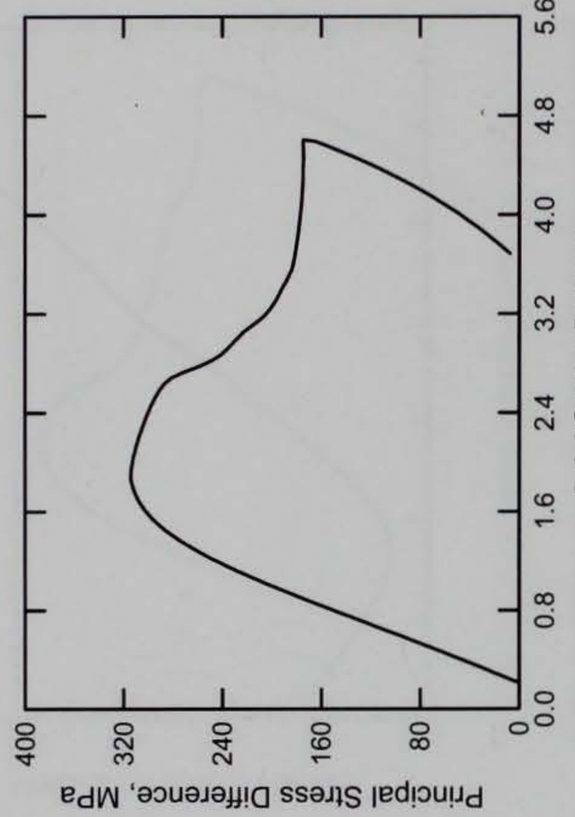


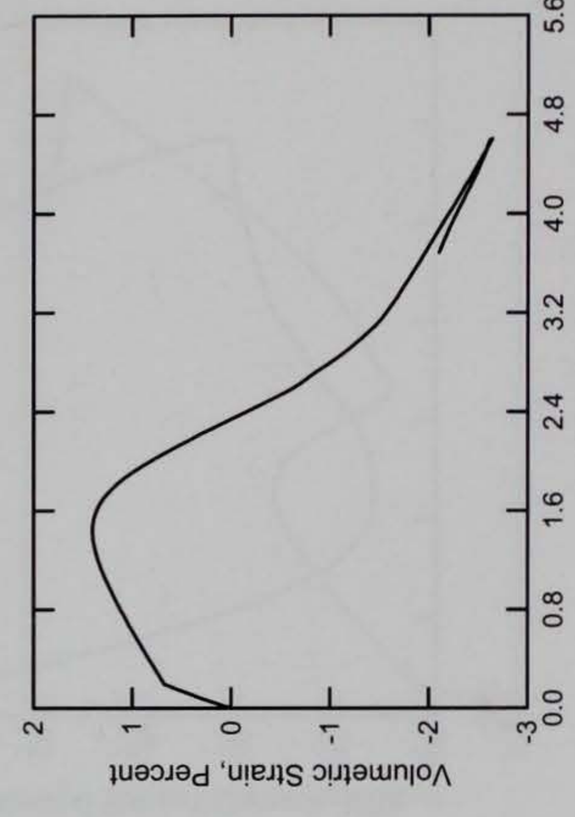


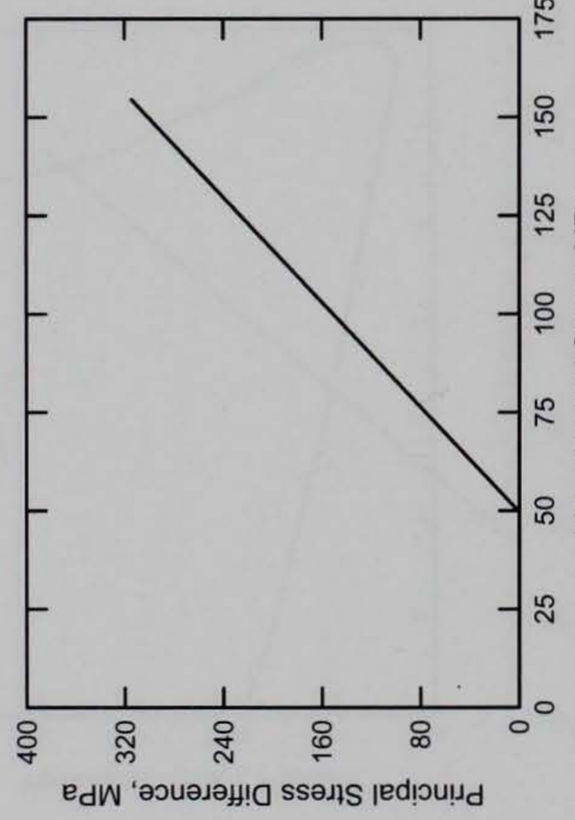


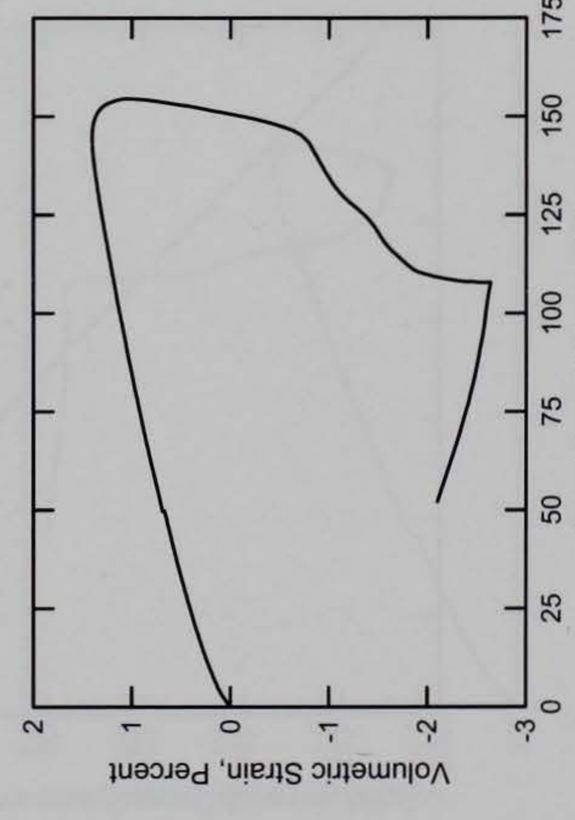


Plate 11

RTTC BRICK
Test No. 15

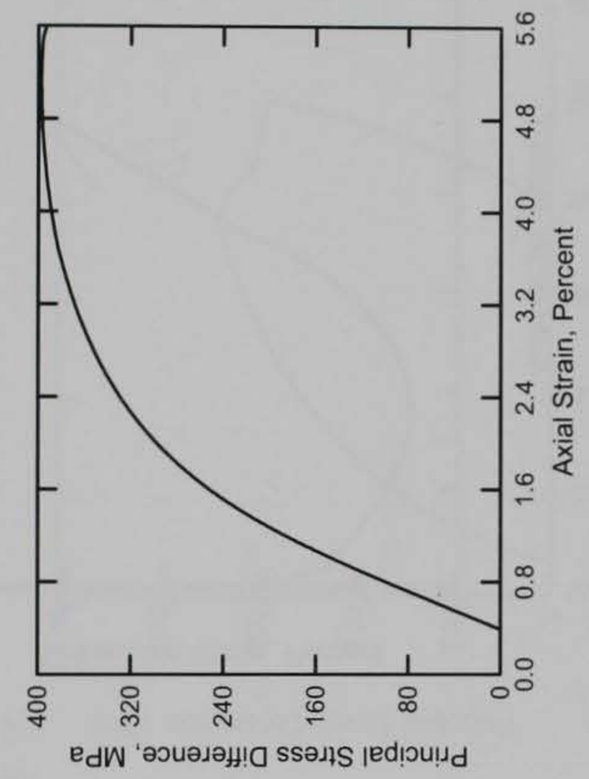


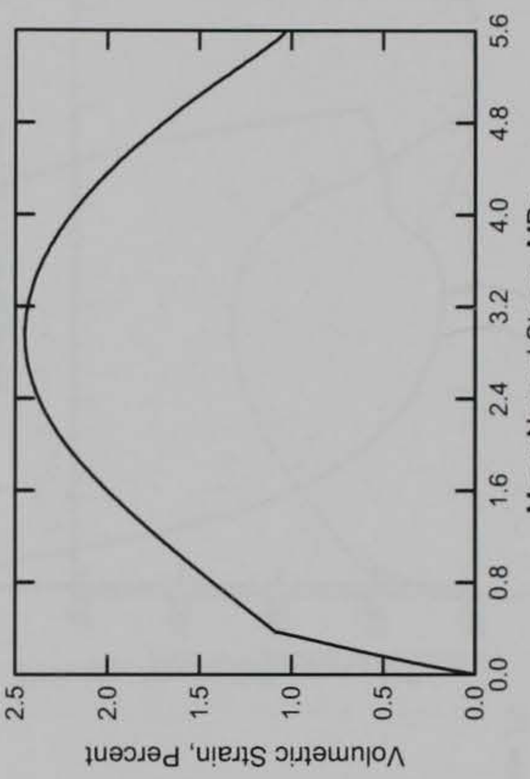


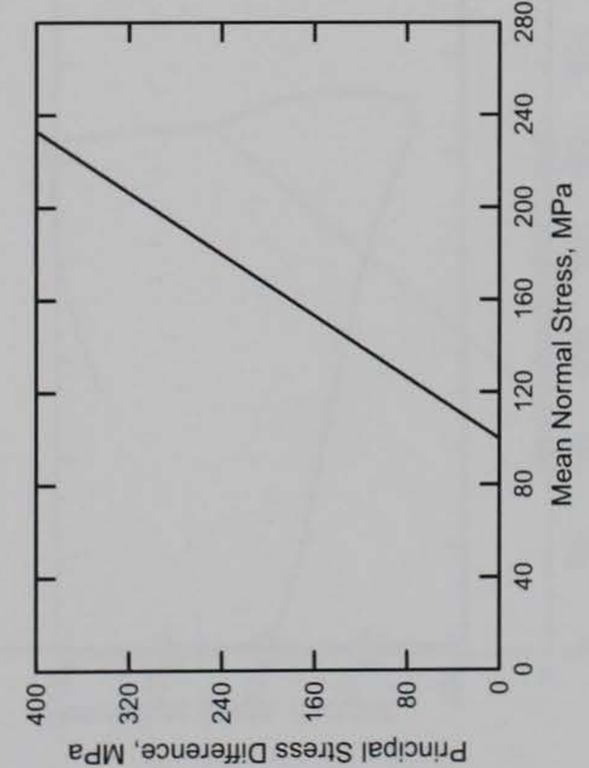


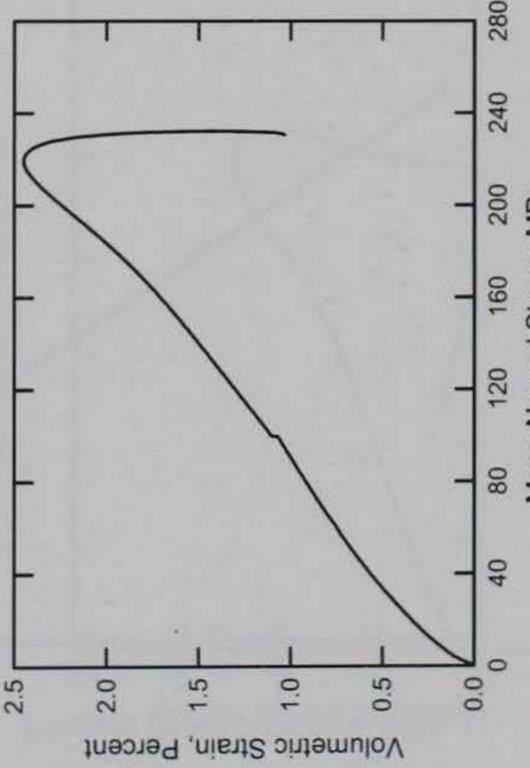


Plate 12

RTTC BRICK
Test No. 16

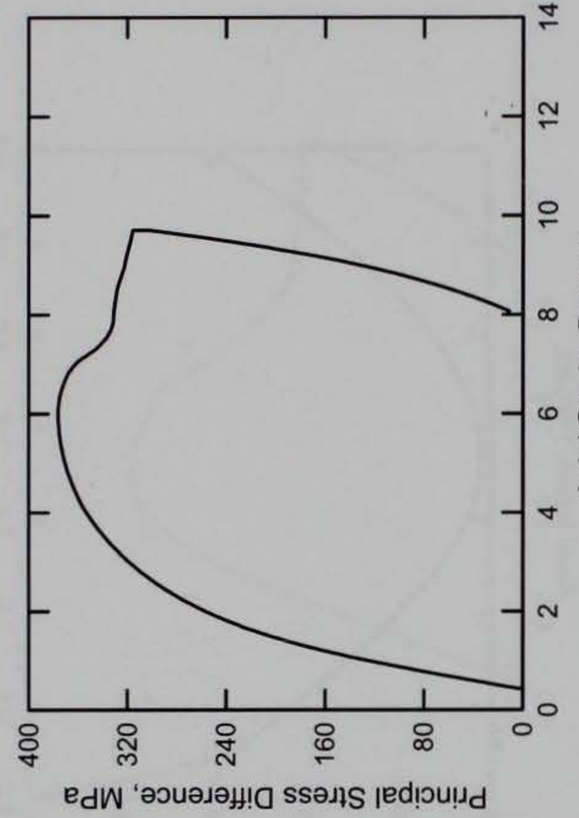


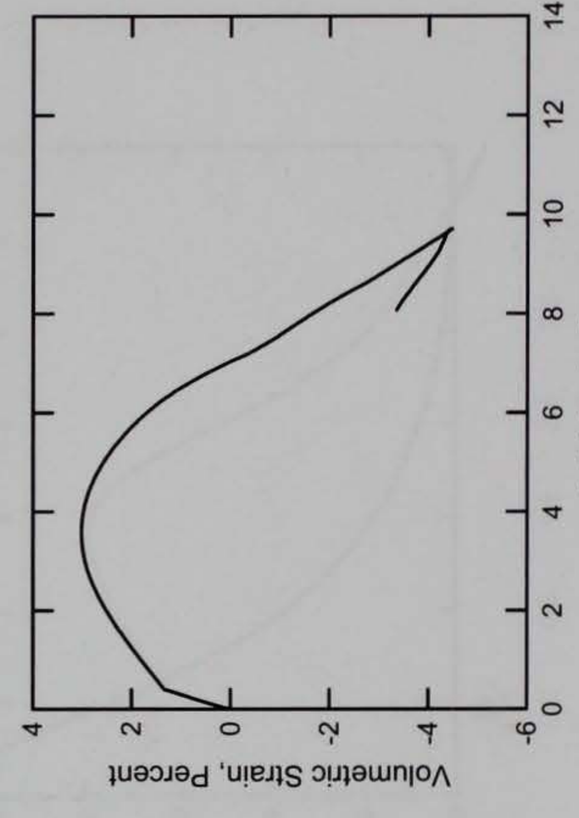


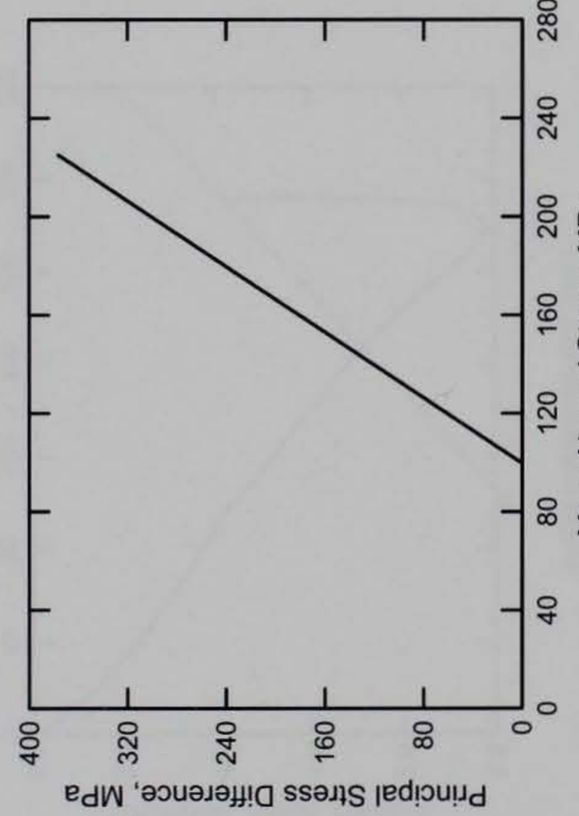


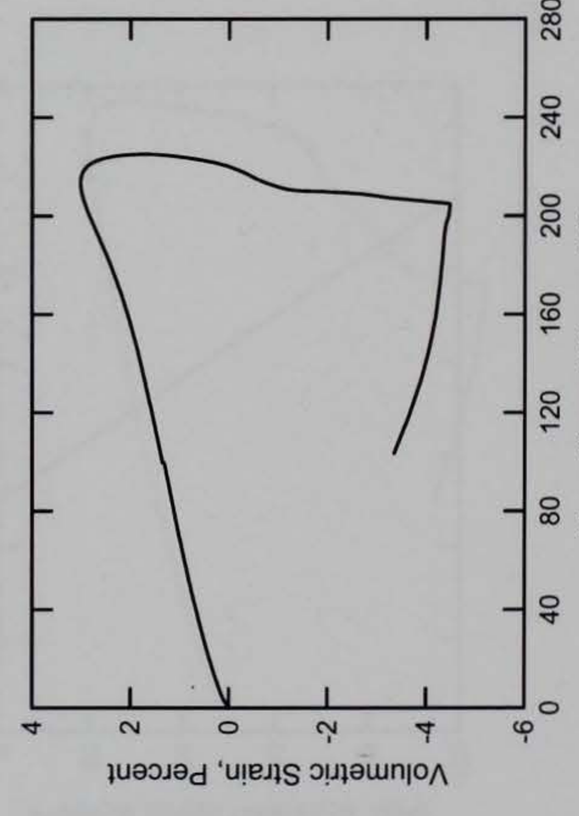


Plate 13

RTTC BRICK
Test No. 17

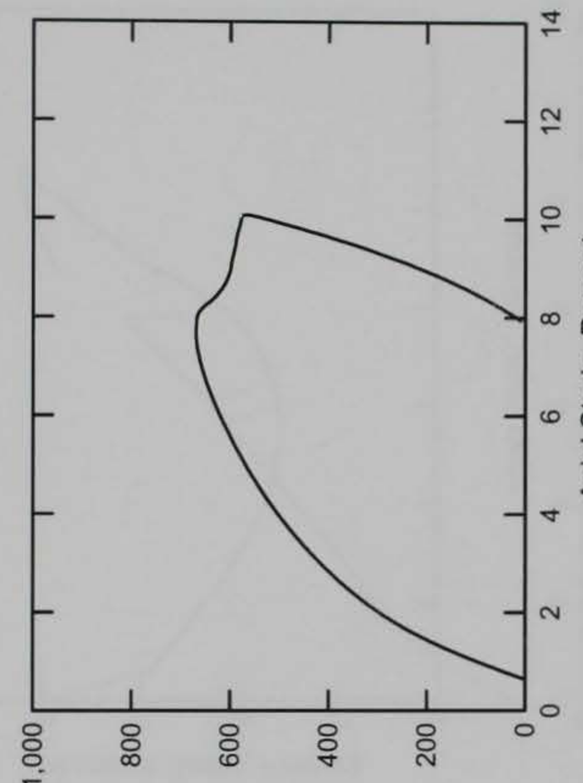





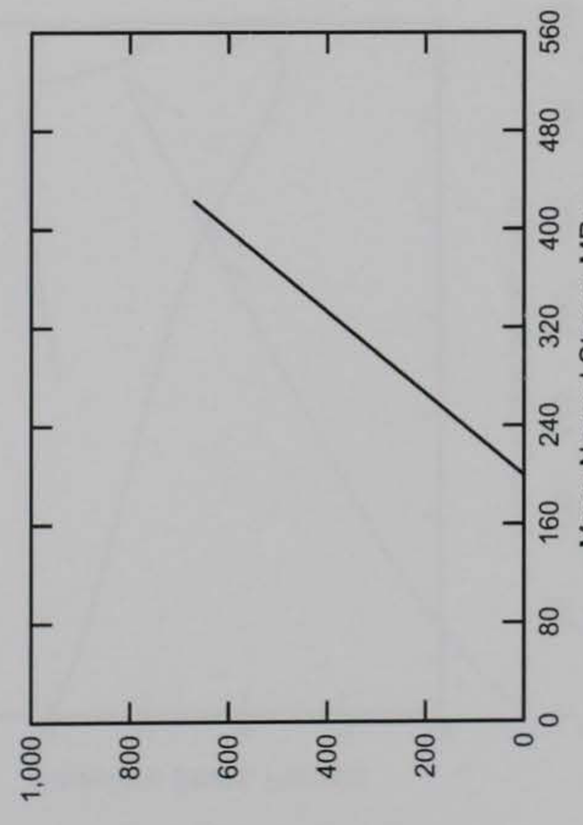





Plate 14

RTTC BRICK
Test No. 18

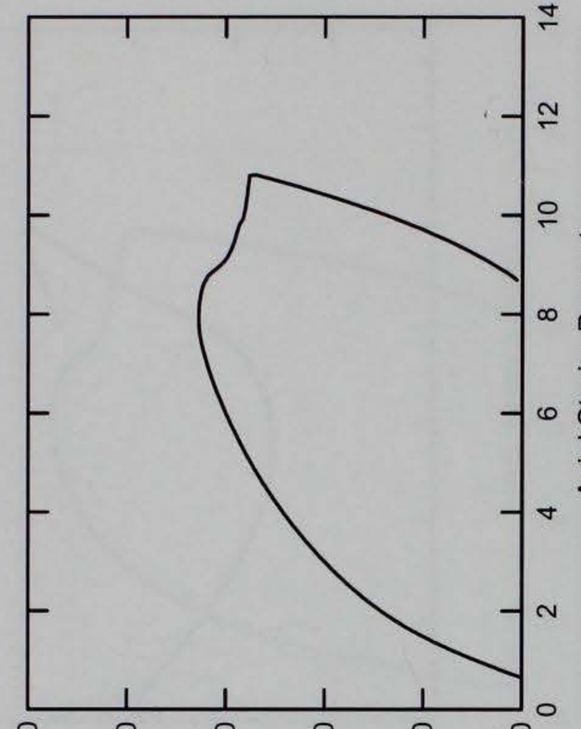


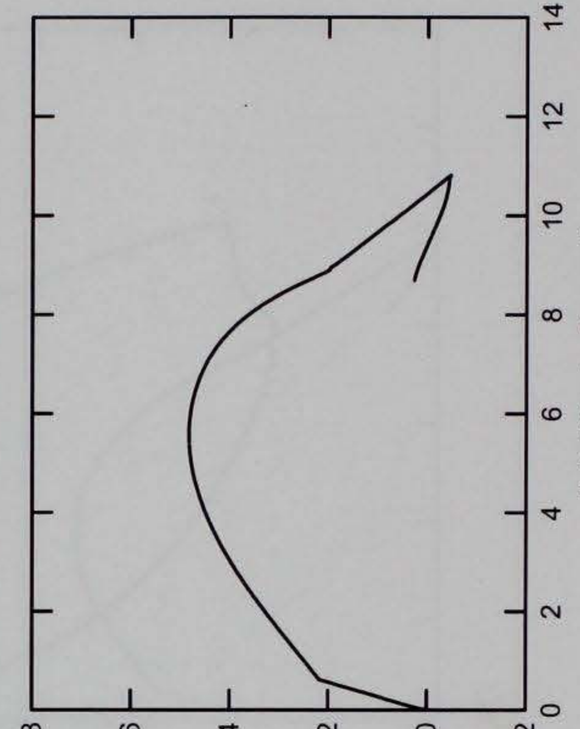


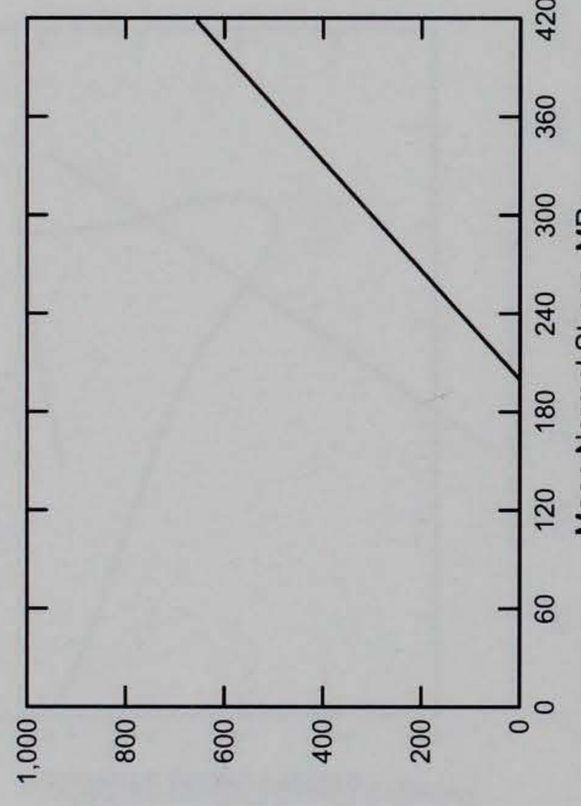


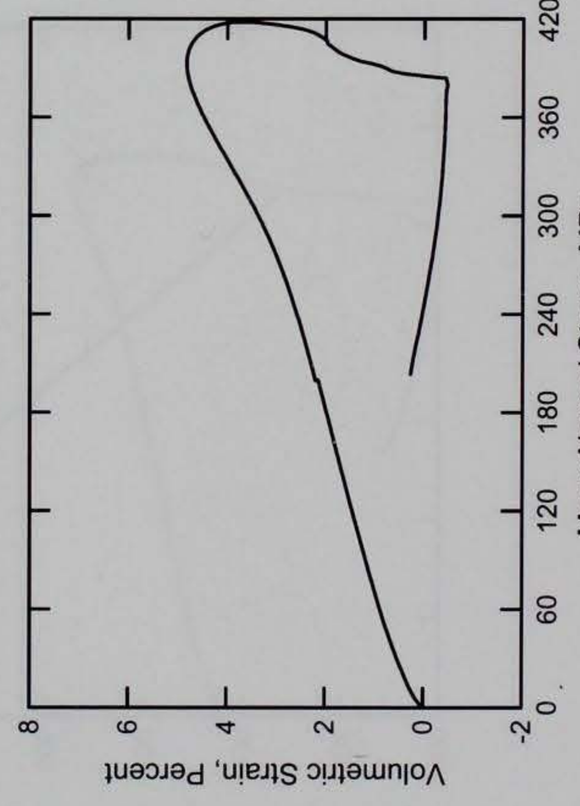


Plate 15

RTTC BRICK
Test No. 6

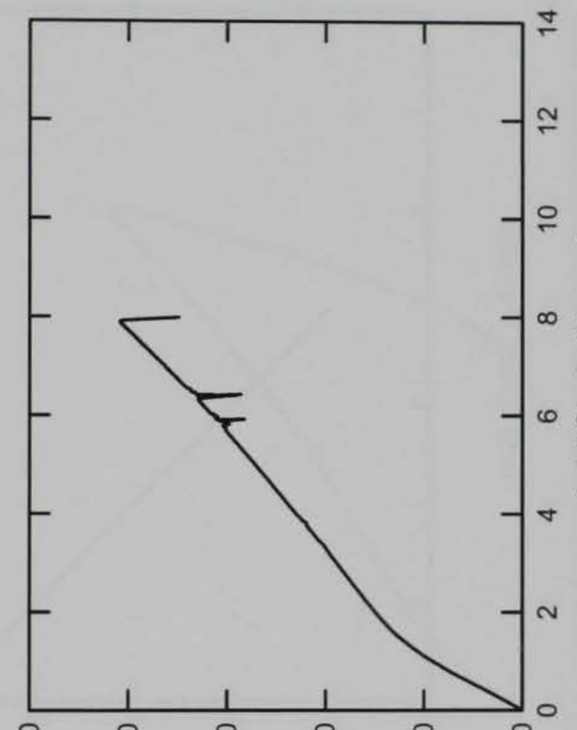


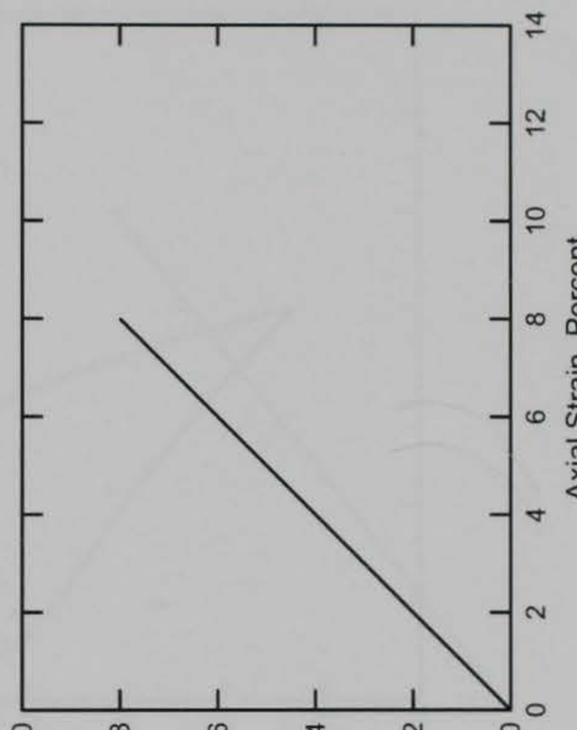


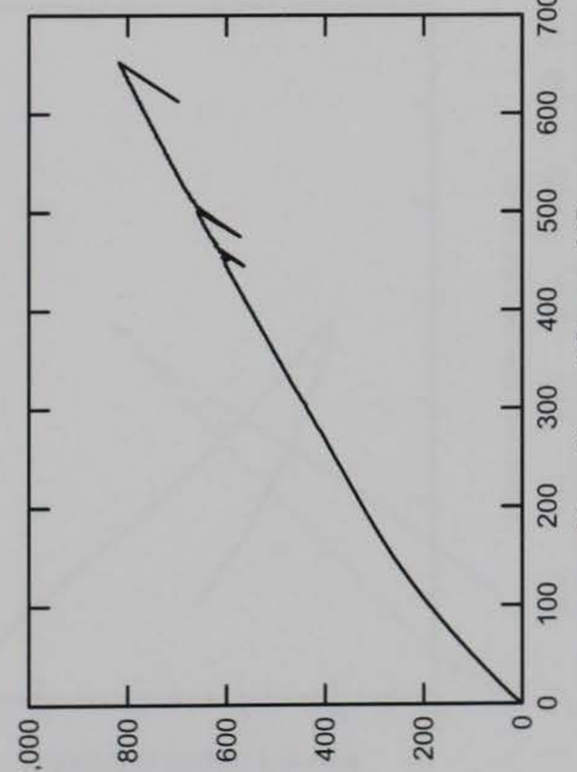


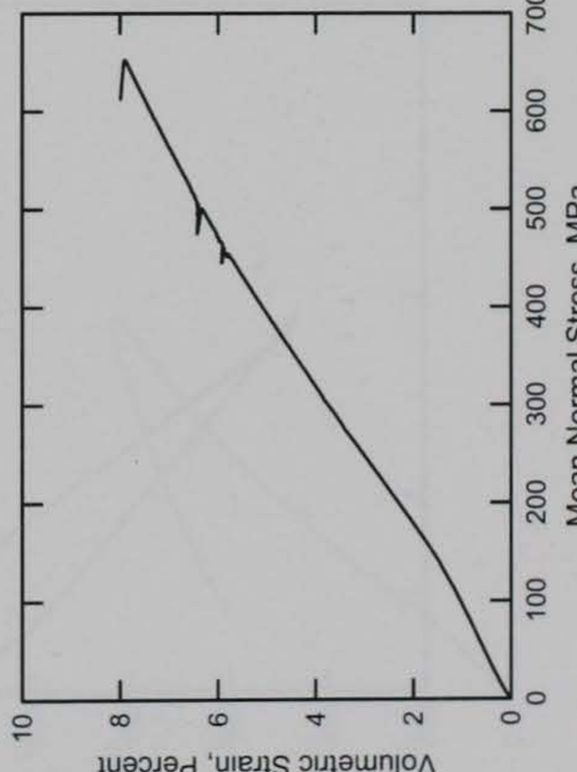


Plate 16

RTTC BRICK
Test No. 7

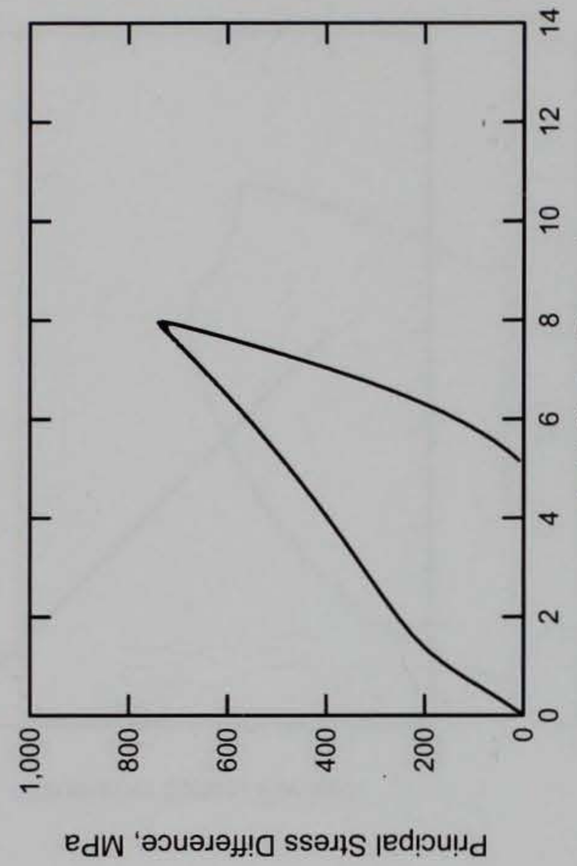


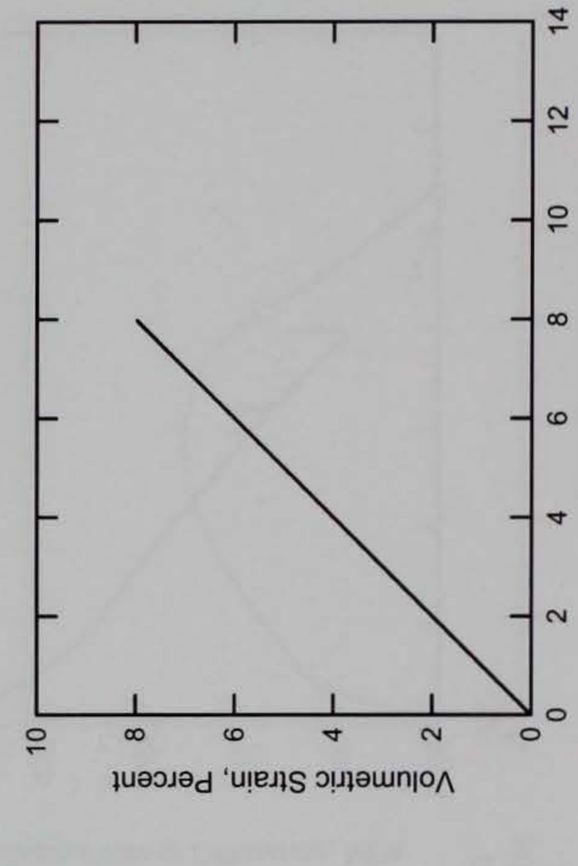


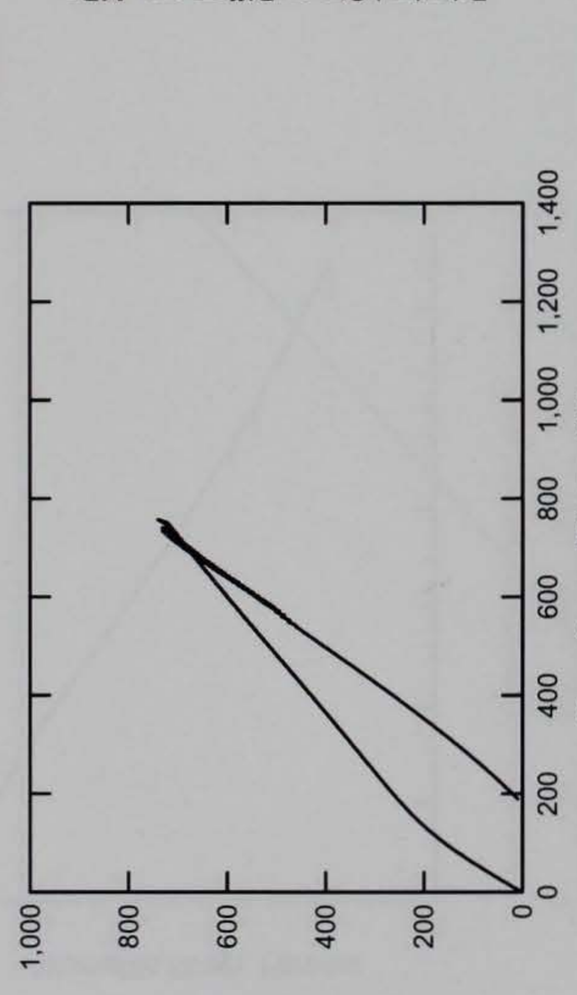


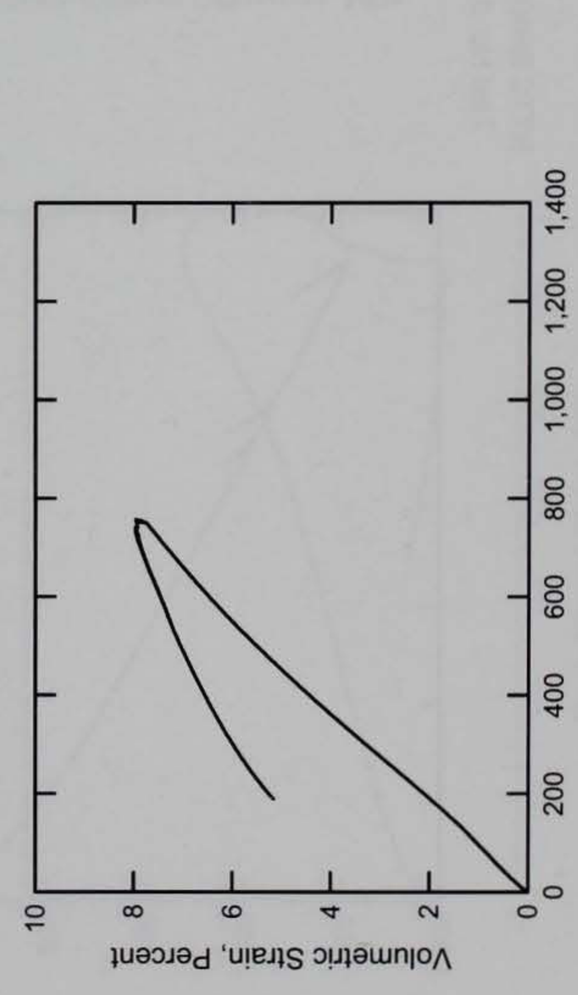


Plate 17

RTTC BRICK
Test No. 8

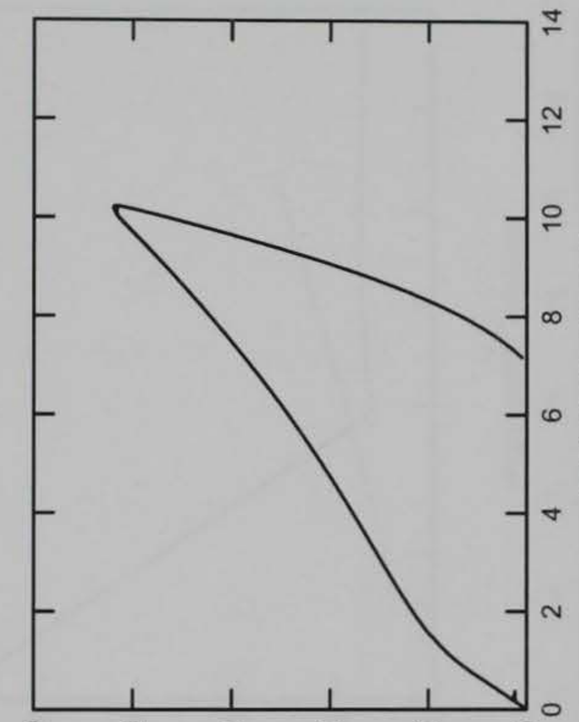


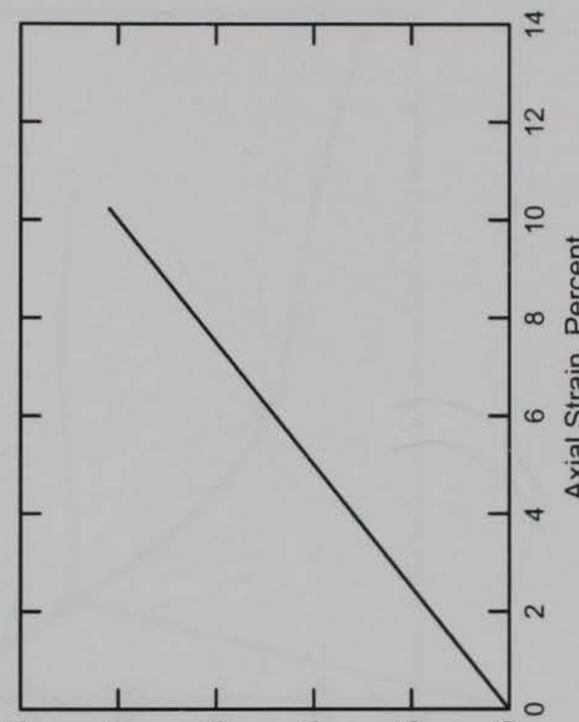


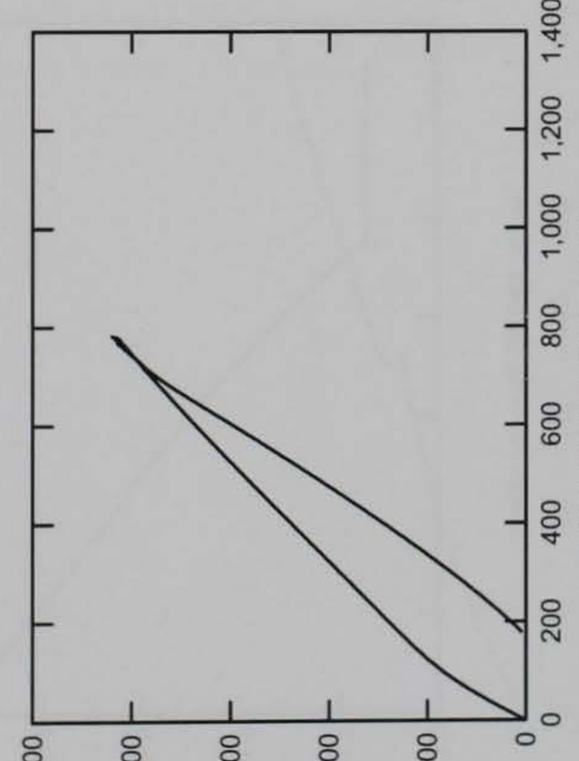


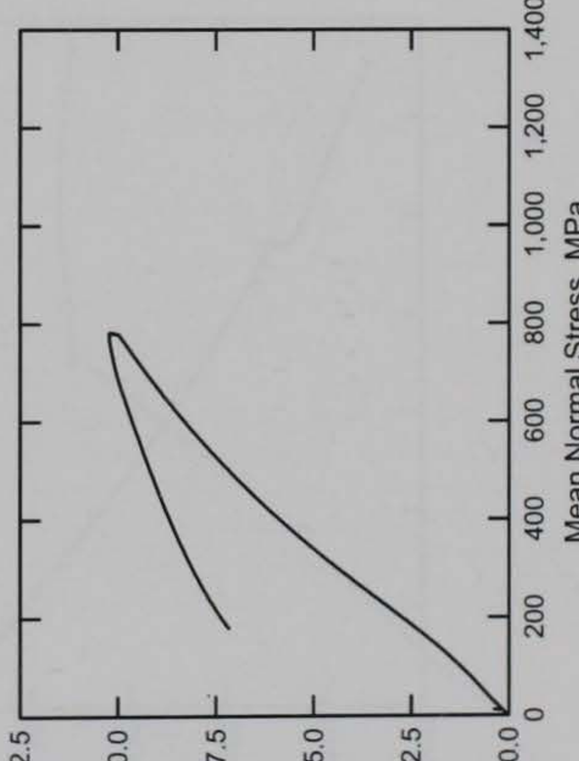


Plate 18

RTTC BRICK
Test No. 20

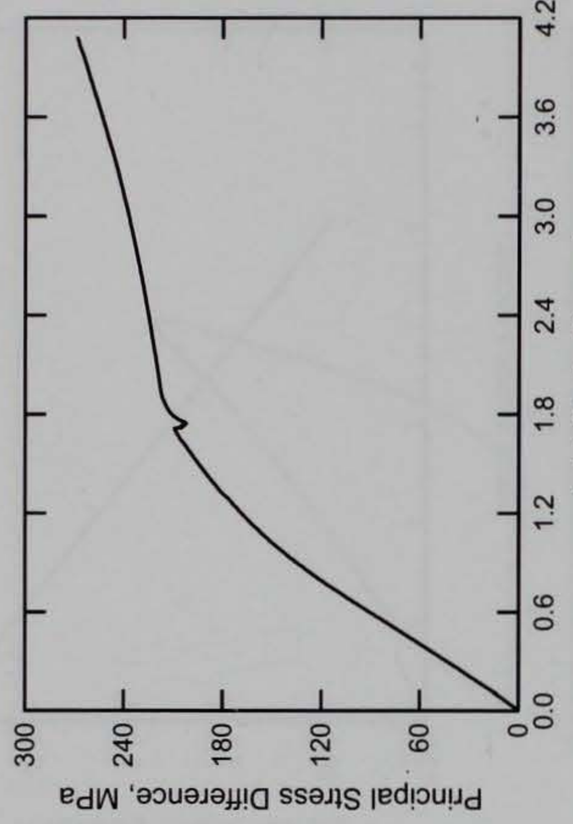


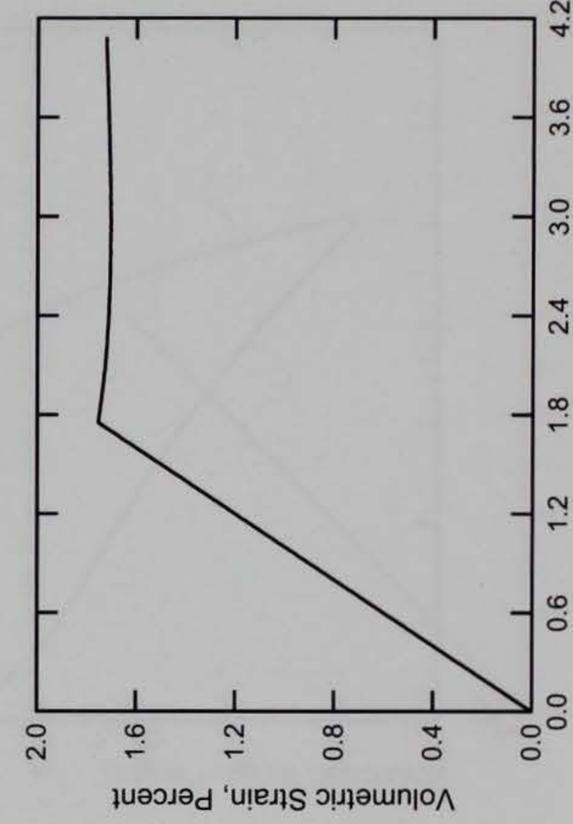


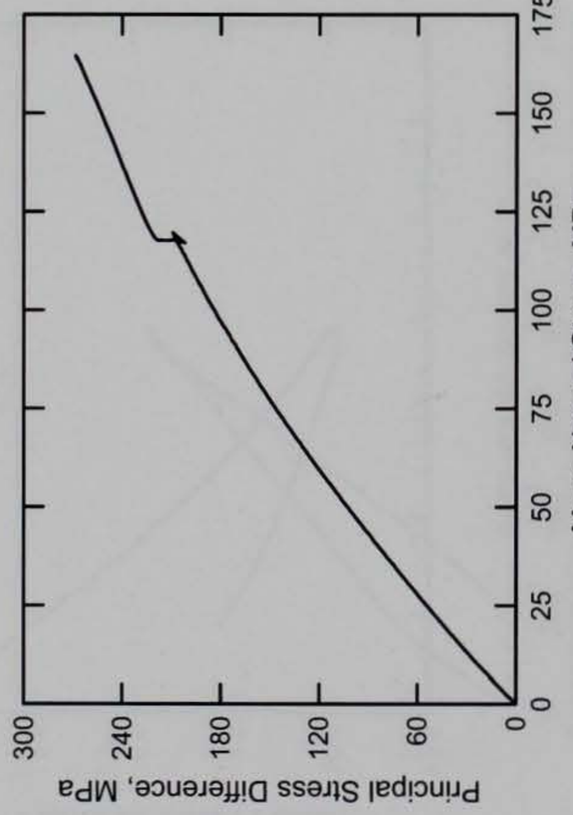


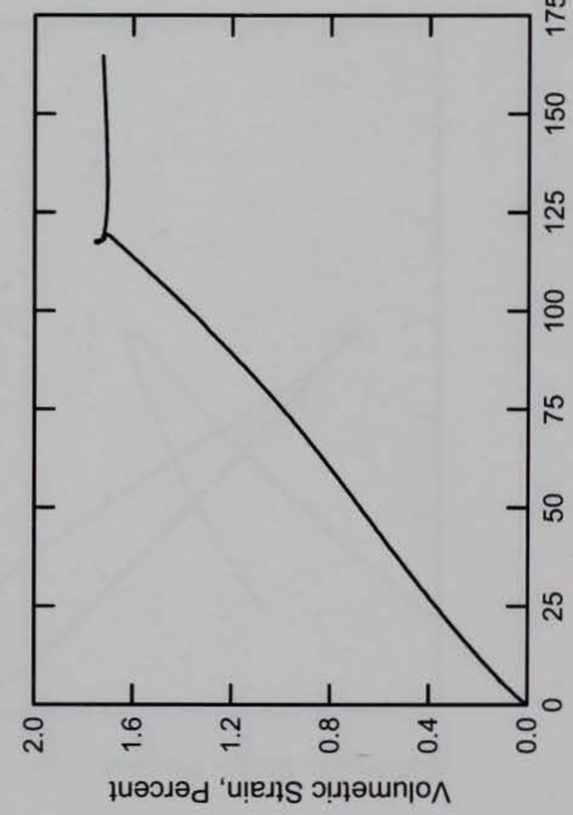


Plate 19

RTTC BRICK
Test No. 21

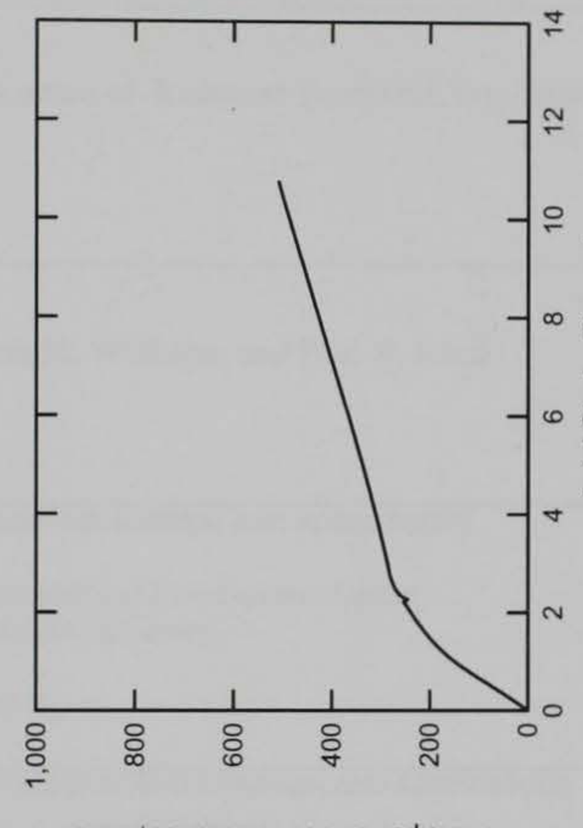





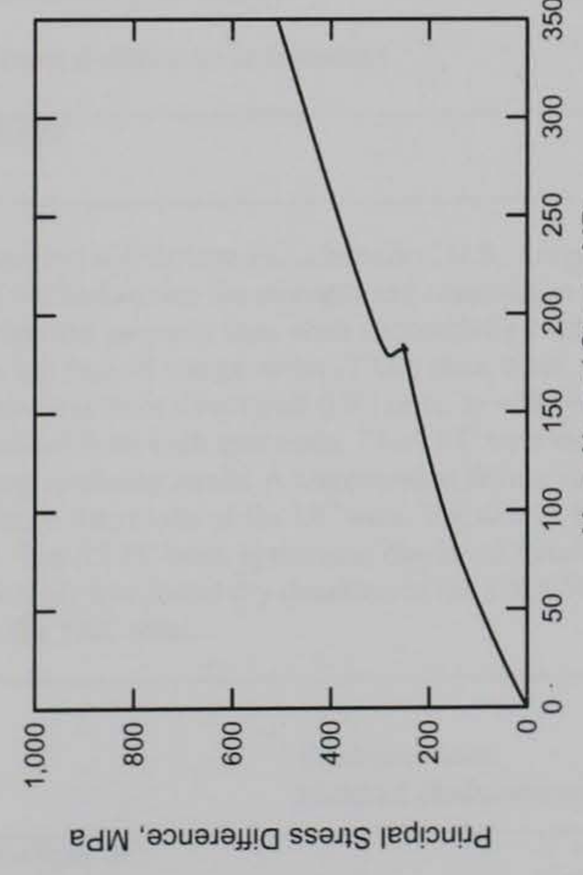





Plate 20

# REPORT DOCUMENTATION PAGE

*Form Approved*
*OMB No. 0704-0188*



| 1. REPORT DATE *(DD-MM-YYYY)* | 2. REPORT TYPE | 3. DATES COVERED *(From - To)* |
|---|---|---|
| June 2009 | Final report | |

**4. TITLE AND SUBTITLE**

Laboratory Characterization of Redstone Technical Test Center Brick

**5a. CONTRACT NUMBER**

**5b. GRANT NUMBER**

**5c. PROGRAM ELEMENT NUMBER**

**6. AUTHOR(S)**

Steven S. Graham, Erin M. Williams, and Paul A. Reed

**5d. PROJECT NUMBER**

**5e. TASK NUMBER**

**5f. WORK UNIT NUMBER**

**7. PERFORMING ORGANIZATION NAME(S) AND ADDRESS(ES)**

U.S. Army Engineer Research and Development Center
Geotechnical and Structures Laboratory
3909 Halls Ferry Road
Vicksburg, MS 39180-6199

**8. PERFORMING ORGANIZATION REPORT NUMBER**

ERDC/GSL TR-09-17

**9. SPONSORING / MONITORING AGENCY NAME(S) AND ADDRESS(ES)**

Headquarters, U.S. Army Corps of Engineers
Washington, DC 20314-1000

**10. SPONSOR/MONITOR'S ACRONYM(S)**

**11. SPONSOR/MONITOR'S REPORT NUMBER(S)**

**12. DISTRIBUTION / AVAILABILITY STATEMENT**

Approved for public release; distribution is unlimited.

**13. SUPPLEMENTARY NOTES**

**14. ABSTRACT**

Personnel of the Geotechnical and Structures Laboratory, U.S. Army Engineer Research and Development Center, conducted a laboratory investigation to characterize the strength and constitutive property behavior of Redstone Technical Test Center (RTTC) brick. A total of 23 mechanical property tests were successfully completed: two hydrostatic compression tests, three unconfined compression (UC) tests, ten triaxial compression (TXC) tests, three uniaxial strain tests, two uniaxial-strain-load/constant-volumetric-strain-load (UX/CV) tests, and three direct-pull (DP) tests. In addition to the mechanical property tests, nondestructive, pulse-velocity measurements were obtained from each specimen. The TXC tests exhibited a continuous increase in maximum principal stress difference with increasing confining stress. A compression failure surface was developed from the TXC test results at six levels of confining pressure and from the results of the UC tests. The results for the DP tests were used to determine the unconfined tensile strength of RTTC brick. The RTTC brick specimens displayed tensile strengths of less than 10 percent of the unconfined compressive strength. Due to the relatively low initial dry densities of the UX/CV test specimens, the stress path data plot just below the failure surface developed from the TXC tests.

**15. SUBJECT TERMS**

Brick
Compression tests
Extension tests
Material characterization
Material properties

| 16. SECURITY CLASSIFICATION OF: | | | 17. LIMITATION OF ABSTRACT | 18. NUMBER OF PAGES | 19a. NAME OF RESPONSIBLE PERSON |
|---|---|---|---|---|---|
| a. REPORT | b. ABSTRACT | c. THIS PAGE | | | 19b. TELEPHONE NUMBER *(include area code)* |
| UNCLASSIFIED | UNCLASSIFIED | UNCLASSIFIED | | 66 | |